

Static Internal Performance of a Two-Dimensional Convergent-Divergent Nozzle With External Shelf

*Milton Lamb and John G. Taylor
Langley Research Center • Hampton, Virginia*

*Mark C. Frassinelli
Air Force Wright Research and Development Center •
Wright-Patterson Air Force Base, Ohio*

Acknowledgments

The research presented in this report is the result of the cooperative effort of General Electric Aircraft Engines and Langley Research Center. The design and development of the nozzle concept were accomplished by General Electric Aircraft Engines. The test was conducted by the staff of the former Propulsion Aerodynamic Branch at Langley Research Center.

Available electronically at the following URL address: <http://techreports.larc.nasa.gov/ltrs/ltrs.html>

Printed copies available from the following:

NASA Center for AeroSpace Information
800 Elkridge Landing Road
Linthicum Heights, MD 21090-2934
(301) 621-0390

National Technical Information Service (NTIS)
5285 Port Royal Road
Springfield, VA 22161-2171
(703) 487-4650

Contents

Summary	1
Introduction	1
Symbols	2
Apparatus and Methods	2
Static Test Facility	2
Single-Engine Propulsion Simulation System	3
Model Description	3
Instrumentation	4
Data Reduction	4
Presentation of Results	5
Results and Discussion	5
Pressure Data	5
Performance Data	6
Shelf Surface Oil Flow Visualization	6
Conclusions	7
References	7
Tables	9
Figures	54

Summary

An investigation was conducted in the static test facility of the Langley 16-Foot Transonic Tunnel to determine the internal performance of a two-dimensional convergent-divergent (2-D C-D) nozzle. The nozzle design was tested with dry and afterburning throat areas which represent different power settings and three expansion ratios (subsonic cruise, subsonic acceleration, and supersonic cruise).

For each configuration, three trailing-edge geometries were tested. The baseline geometry had a straight trailing edge. Two different shaping techniques were applied to the baseline nozzle design to reduce radar observables: the scarfed design and the sawtooth design. A flat plate extended downstream of the lower divergent flap trailing edge parallel to the model centerline to form a shelflike expansion surface. This shelf was designed to shield the plume from ground observation (infrared radiation (IR) signature suppression). The shelf represents the part of the aircraft structure that might be present in an installed configuration. These configurations were tested at nozzle pressure ratios (NPR) from 2.0 to 12.0.

Results indicated that discharge coefficient and peak resultant thrust ratio were not significantly affected by the addition of the shelf or by changes to the upper divergent flap and shelf geometry. Discharge coefficient for these 2-D C-D shelf nozzles was lower than typical 2-D C-D nozzles due to the sharp corner at the nozzle geometric throat. Resultant pitch vector angles were typically nonzero and varied with increasing NPR. In addition to nozzle internal asymmetry, the shelf significantly affected the pitch vector angle by producing a surface on which the shock-cell pressure variation could act. Only the asymmetrical scarfed nozzle produced resultant yaw thrust vector angles.

Introduction

Aircraft survivability has always been an important consideration in the airplane design process. In World War I, the issue of survivability was primarily concerned with the avoidance of visual detection by patrolling aircraft or ground observers. With the introduction of ground-based radar in World War II, aircraft became vulnerable to long-range detection and tracking that allowed adversaries to concentrate forces to intercept them along their route. Once intercepted, precise maneuvering was required at close range to shoot down the enemy with machine guns. During the Vietnam War and more recent conflicts in the Middle East, the combat environment included new weapons such as heat-seeking and radar-guided air-to-air and surface-to-air missiles capable of targeting and destroying aircraft beyond visual range.

Advances in sensors and microprocessors will continue to increase the risk of high-threat environments in the future. Thus, advanced aircraft designs will require visible, infrared, and radar cross-section (RCS) signature shaping and reduction techniques to increase aircraft survivability. (See ref. 1.) Technologies to reduce observables are currently being incorporated into the design of the aircraft structure as well as into the propulsion system.

The capabilities that are necessary to reduce observables require careful integration of the propulsion system into an aircraft because inlets and nozzles are typically large contributors to the overall aircraft infrared and RCS signature. Infrared signature suppression techniques include cooling of the exhaust plume and hot engine and aircraft components as well as shielding of these hot parts from view. The RCS signature shaping techniques include internal and external shaping of leading and trailing edges and elimination of 90° angles between adjacent surfaces. Incorporating technologies that reduce observables can affect nozzle performance as a result of more complex internal and external geometry. (See ref. 2.) To produce acceptable levels of survivability and performance, a compromise must be reached between aircraft aerodynamics and signature-suppression designs. These concerns are addressed in this paper for the design of a two-dimensional convergent-divergent (2-D C-D) nozzle with a flat plate (herein called a shelf) extending downstream of the lower divergent flap trailing edge.

An investigation has been conducted in the static test facility of the Langley 16-Foot Transonic Tunnel to determine the internal performance of this 2-D C-D shelf nozzle design. The nozzle design was tested with dry and afterburning throat areas which represent different power settings and three expansion ratios (subsonic cruise, subsonic acceleration, and supersonic cruise). For each of these configurations, three trailing-edge geometries were tested. The baseline geometry had a straight trailing edge. Two different shaping techniques were applied to the baseline nozzle design to reduce radar observables, henceforth called the scarfed design and the sawtooth design. A flat plate (shelf) extended downstream of the lower divergent flap trailing edge parallel to the model centerline. This shelf was designed to shield the plume from ground observation (IR signature shaping). The shelf also simulated installation of the nozzles on an aircraft surface. These configurations were tested at nozzle pressure ratios (NPR) from 2.0 to 12.0.

The results of this investigation are presented as nozzle internal performance data (discharge coefficient, internal thrust ratio, resultant thrust ratio, resultant pitch thrust vector angle, and resultant yaw thrust vector angle) and internal static pressure ratio data on the divergent

flaps and shelf. Surface oil flow visualization photographs of the shelf are also presented to gain a qualitative understanding of the flow phenomena.

Symbols

All forces and resultant vector angles are referenced to the model body axis (measured from the model centerline). A detailed discussion of the data reduction, calibration procedures, and propulsion relations used in this report is presented in references 3 and 4.

A,B,C,D	represent model stations and dimensions in figures 3–6, in.
A_e	nozzle exit area, in ²
A_e/A_t	nozzle expansion ratio
A_t	nozzle throat area, in ²
F	measured thrust along body axis, positive in upstream direction, lbf
F_i	ideal isentropic gross thrust, $w_p \sqrt{\frac{2\gamma R_j}{(\gamma-1)g}} \sqrt{(T_{t,j} + 459.67) \left[1 - \left(\frac{1}{\text{NPR}} \right)^{\frac{\gamma-1}{\gamma}} \right]}$, lbf
F_N	measured normal force, lbf
F_r	resultant gross thrust, $\sqrt{F^2 + F_N^2 + F_S^2}$, lbf
F_S	measured side force, lbf
g	acceleration due to gravity, 32.174 ft/sec ²
h_e	exit height of nozzle (see fig. 3), in.
h_t	throat height of nozzle (see fig. 3(a)), in.
L_{flap}	reference length of upper and lower divergent flaps (see fig. 2), 4.000 in.
L_{shelf}	reference length of shelf (see fig. 2), 6.600 in.
NPR	nozzle pressure ratio, $\frac{P_{t,j}}{P_a}$
$(\text{NPR})_d$	design nozzle pressure ratio (NPR for fully isentropic expanded flow at nozzle exit)
p	local static pressure, psi
p_a	ambient pressure, psi
$p_{t,j}$	jet total pressure, psi
$p/p_{t,j}$	static pressure ratio
R_j	gas constant for air, 1716 ft ² /sec ² -°R
$T_{t,j}$	jet total temperature, °R
w	width of nozzle at throat (see fig. 2), 4.000 in.

w_i	ideal weight-flow rate, $A_{t,j} \left(\frac{2}{\gamma+1} \right)^{\frac{\gamma+1}{2(\gamma-1)}} \sqrt{\frac{\gamma g}{R_j (T_{t,j} + 459.67)}}$, lbf/sec
w_p	measured weight-flow rate, lbf/sec
x	distance along nozzle surface for tap locations (positive downstream), in.
y	spanwise distance for tap locations (positive to right, see fig. 5), in.
α_l	divergence angle for lower divergent flap (see fig. 3), deg
α_u	divergence angle for upper divergent flap (see fig. 3), deg
β	convergence angle for convergent flaps (see figs. 3(a) and 4), deg
γ	ratio of specific heats for air, 1.3997
δ_p	resultant pitch thrust-vector angle, $\tan^{-1} \frac{F_N}{F}$, deg
δ_y	resultant yaw thrust vector angle, $\tan^{-1} \frac{F_S}{F}$, deg
$\delta_{v,p}$	geometric pitch thrust vector angle, measured from model centerline (positive angle produces positive normal force), $0.5(\alpha_u + \alpha_l)$, deg
ϕ	cutback angle on upper convergent flap (see fig. 6), deg

Abbreviations:

A/B	afterburner
2-D	two-dimensional
Config	configuration
C-D	convergent-divergent
IR	infrared radiation
MS	model station, in.
RCS	radar cross section

Apparatus and Methods

Static Test Facility

This investigation was conducted in the static test facility of the Langley 16-Foot Transonic Tunnel. Tests were performed in a large room with high-pressure air directed through a single-engine propulsion simulation system and exhausted to the atmosphere. The static test facility uses the same clean, dry-air supply as the 16-Foot

Transonic Tunnel (ref. 3) and a similar air control system that features a heat exchanger to maintain a constant jet flow stagnation temperature (approximately room temperature). The static test facility has been instrumental in the development of innovative nonaxisymmetric nozzle concepts through the detailed evaluation of nozzle internal performance. (See refs. 5 and 6.)

Single-Engine Propulsion Simulation System

During this investigation, nozzle configurations were tested on the single-engine, air-powered jet simulation system. Figure 1 shows a schematic of the propulsion simulation system with the 2-D instrumentation section and a typical test nozzle. An external high-pressure air system provided a continuous flow of clean, dry air at a controlled temperature of about 540°R as jet total pressure was varied up to approximately 175 psi in the nozzle. High-pressure air was directed through a dolly-mounted support strut containing six tubes which connect to a high-pressure plenum chamber. As indicated in figure 1, the air was then discharged perpendicularly into the low-pressure plenum through eight multiple-hole nozzles equally spaced around the high-pressure plenum. This arrangement was designed to minimize the forces imposed by the transfer of axial momentum as the air passes from the nonmetric high-pressure plenum to the metric low-pressure plenum (mounted to the force balance). Two flexible metal bellows were used as seals and compensated for axial forces caused by pressurization. The air then passed from the low-pressure plenum through a transition section, choke plate and instrumentation section. The transition section provided a smooth flow path from the circular cross-section low-pressure plenum to the rectangular cross-section choke plate, instrumentation section, and nozzle. The nozzle model was attached at model station 41.845.

Model Description

The basic design parameters for the present nozzle were power settings, expansion ratios, and trailing-edge designs. Throat areas were chosen to represent dry and afterburner (A/B) power settings. Three expansion ratios (same for both dry and A/B configurations) were selected to represent subsonic cruise ($A_e/A_t = 1.100$), subsonic acceleration ($A_e/A_t = 1.750$), and supersonic cruise ($A_e/A_t = 2.500$) operating modes. Typically 2-D C-D nozzles have divergent flaps that are equal in length, but for the present investigation an extension (shelf) was added to the lower divergent flap to provide IR shielding from below. (See fig. 2.) Three trailing-edge geometries were investigated. The baseline configurations (fig. 2(a)) had trailing edges that were normal to the airflow and internal surfaces that are at right angles to each other. The other two planform geometries (scarfed

and sawtooth) were designed to have the same throat areas and expansion ratios.

The scarfed configurations (fig. 2(b)) had trailing edges (upper divergent flap and shelf) that were swept (scarfed) 30° to the sidewall normal. The sawtooth configurations (fig. 2(c)) had double scarfed surfaces (swept 45°) extending from the vertical centerline which resulted in a sawtooth appearance. The internal surface of the upper divergent flap consisted of two planar surfaces extending from the vertical centerline.

The throat areas were rectangular as shown in figure 2. The lengths of the flap ($L_{\text{flap}} = 4.000$ in.) and shelf ($L_{\text{shelf}} = 6.600$ in.) were constant among the three designs and represented the average lengths for the scarfed and sawtooth configurations. For the baseline and scarfed configurations, these lengths were measured along the surface at the vertical centerline. For the sawtooth configurations, the lengths were measured at $(y/w)/2 = -0.500$. (See fig. 2(c).) These dimensions provided configurations that had constant planform areas at each expansion ratio.

Typically, exit area or expansion ratio of 2-D C-D nozzles is varied by changing the waterline location of the trailing edge of both upper and lower divergent flaps. Thus the divergent flap surfaces remain symmetric about the nozzle centerline, which results in a change in A_e , whereas the geometric pitch vector angle $\delta_{v,p}$ remains zero. However for the present investigation, the lower divergent flap and shelf remained stationary and the expansion ratio was varied by moving only the upper divergent flap trailing edge. (See fig. 3.) This geometry produced nozzle asymmetry about the nozzle centerline, which results in nonzero geometric pitch thrust vector angles for all configurations tested. This angle $\delta_{v,p}$ is in figures 3(b)–3(d) and table 1 and is the average of the upper and lower divergent flap divergence angles α_u and α_l .

The design parameters that are common to all configurations are shown in figure 3(a). All test configurations were attached to the 2-D instrumentation section at MS A (41.845) as shown in figures 1 and 3(a). A summary of the test configurations is provided in table 1. The width of all nozzles at the throat was 4.000 in. Thus changing from a dry power to A/B power configuration required an increase in throat height (h_t) from 1.000 to 1.200 in. The changes in throat height resulted in changes in the convergence angle (β) as shown in figure 3(a). Note that MS B has shifted downstream slightly for the A/B configurations. The nozzle geometric throat (minimum internal cross-sectional area) occurred at the juncture of the convergent and divergent flaps. This juncture formed a sharp corner. All dry power configurations used

the same convergent flap geometry which was symmetrical about the model centerline between MS A (41.845) and MS B (44.296). Likewise all A/B configurations used the same convergent flap geometry as shown in figure 3(a).

As mentioned previously, the lengths of the divergent flaps were a constant 4.000 in., and these lengths were measured along the surfaces of the flaps. Changing from a dry power to A/B power configuration resulted in an increase in divergence angle (α_l) on the lower divergent surface and a slight reduction in the length between MS B and MS C. Therefore as shown in figures 3(b)–3(d), slight overall differences in length existed for dry and A/B configurations (MS D) as shown in figures 3(b)–3(d). Figures 3(b)–3(d) also show the parameters that pertain to a particular type of nozzle.

Details of the individual parts (including pressure tap locations) are given in figures 4–9. The sidewalls for baseline configurations 1–6 were mirror images as shown in figure 9(a). The sidewalls for scarfed configurations 7–12 were different as shown in figure 9(b). The sidewalls for sawtooth configurations 13–18 were mirror images as shown in figure 9(c).

To help understand the flow physics, static pressure taps were utilized on the nozzle lower divergent flap and shelf for all configurations and on the upper divergent flap for the sawtooth configurations. The dry power configurations had 9 static pressure taps on the lower divergent flap, whereas the A/B power configurations had 27 taps as shown in figure 5. These taps were arranged in three rows, one along the flap centerline and the other two on either side of the centerline halfway to the sidewall. The sawtooth configurations had a row of 9 taps on the upper divergent flap ($(y/w)/2 = -0.500$) as shown in figure 7(c). The baseline nozzle shelf had 7 taps placed along the shelf centerline. (See fig. 8(a).) The scarfed nozzle shelf had 21 taps in three rows, one row along the centerline and one on either side halfway to the edge. (See fig. 8(b).) The sawtooth nozzle shelf had a row of 7 taps at $(y/w)/2 = -0.500$ as shown in figure 8(c).

Instrumentation

An internally mounted six-component strain-gage balance was used to measure the forces and moments on the model downstream of MS 20.500. (See fig. 1.) Jet total pressure was measured at a fixed station in the instrumentation section by a four-probe rake through the upper surface, a three-probe rake through the side, and a two-probe rake through the corner. Jet total temperature was measured with a thermocouple positioned in the instrumentation section upstream of the nozzle. The weight-flow rate of the high-pressure air supplied to the nozzle was determined by calibrating weight flow as a

function of pressure and temperature measurements in the high-pressure plenum (located on top of the support strut) with standard axisymmetric nozzles of known discharge coefficient in place of the test nozzle. Static pressures were measured with individual transducers.

Data Reduction

All data were recorded on magnetic tape. Each data point is an average of 50 frames of data, acquired at a rate of 10 frames/sec. Data were recorded in ascending order of NPR.

The basic nozzle internal performance parameters presented are internal thrust ratio F/F_i , resultant thrust ratio F_r/F_i , discharge coefficient w_p/w_i , and resultant pitch and yaw vector angles δ_p and δ_y . All data are referenced to the model centerline with the exception of resultant gross thrust F_r . A detailed discussion of the data reduction methodology is presented in reference 4.

The internal thrust ratio F/F_i is the ratio of the measured thrust along the body axis to the ideal isentropic gross thrust. Ideal thrust F_i is computed from the measured weight-flow rate w_p , jet total pressure $p_{t,j}$, and jet total temperature $T_{t,j}$ by assuming isentropic expansion through the nozzle. (See definition of F_i in the section "Symbols.") Nozzle thrust F along the body axis was obtained from the balance axial-force measurement with corrections for model weight tares, balance interactions, and bellow tares. Although the bellows arrangement in the propulsion simulation system was designed to eliminate any pressure and momentum interactions with the balance, small bellows tares on all balance components still existed. These tares resulted from a small pressure difference between the ends of the bellows at high internal velocities and from small differences in the forward and aft bellows spring constants during bellows pressurization. The bellows tares were determined by testing standard axisymmetric calibration nozzles with known performance over a range of loadings expected during the test. These calibration data were used to correct balance force measurements to obtain final forces and moments. (See ref. 4.)

The internal thrust ratio F/F_i provides a measure of the nozzle efficiency in directing the exhaust flow in the axial direction. Axial thrust F is decreased by deflecting the thrust vector away from the axial direction. Axial thrust F and thus internal thrust ratio F/F_i are reduced by actual losses in nozzle efficiency or by thrust vectoring. The resultant thrust ratio F_r/F_i is the resultant gross thrust F_r normalized by the ideal thrust F_i . Resultant thrust is computed from corrected values of axial-, normal-, and side-force balance measurements. By definition, differences between F/F_i and F_r/F_i occur when the exhaust flow is directed (vectored) away from the

axial direction. Decreases in resultant thrust F_r are due to actual losses in nozzle efficiency and turning losses, not to geometric losses as discussed for F .

Nozzle discharge coefficient w_p/w_i is the ratio of measured weight-flow rate to ideal weight-flow rate, where the ideal weight-flow rate is computed from measurements of jet total temperature, jet total pressure, and measured nozzle throat area (the minimum internal cross-sectional flow area in the nozzle). The nozzle discharge coefficient reflects the nozzle efficiency in passing weight flow. This performance parameter is reduced by momentum and vena contracta losses; this results in a decrease in the effective flow (throat) area. (See ref. 7.)

Resultant thrust vector angles δ_p and δ_y are effective angles at which the thrust-vectoring mechanism turns the exhaust flow from the axial direction. As indicated in the section "Symbols," determination of these angles requires the measurements of axial, normal, and side forces on the model.

In addition to force and pressure data, surface oil flow visualization photographs were obtained to qualitatively gain a better understanding of the flow phenomena. A mixture of fine black grit particles and oil was spread on the upper surface of the shelf. The nozzle pressure ratio was held at the desired test conditions for approximately 5 min or until all excess oil was blown out of the nozzle and the oil flow patterns were fully developed. At this point, the high-pressure air was quickly reduced to atmospheric pressure so that the flow patterns were not disturbed. The oil flow patterns were closely observed during this process with a video camera to insure that patterns did not change from those observed at the test NPR. No changes in oil flow patterns were observed during the reduction in NPR from test conditions to jet off.

Presentation of Results

A configuration summary is provided in table 1, which describes the different nozzle designs, power settings, and expansion ratios of each configuration tested in this investigation. In addition, the design nozzle pressure ratio (NPR)_d for fully expanded flow (based on expansion ratio A_e/A_t) and the geometric pitch vector angle are provided. Tabulated nozzle performance data for all configurations are presented in tables 2–4, and the internal static pressure ratio data at all test conditions are presented in tables 5–10. Plots of internal static pressure ratios are presented in figure 10 at selected NPR's for all configurations. Internal performance data are presented in figures 11, 12, and 13 for the baseline, scarfed, and sawtooth configurations, respectively. These plots also show the effect of expansion ratio. Comparison plots for power settings are presented in figures 14, 15, and 16

for the baseline, scarfed, and sawtooth configurations, respectively. Comparison plots for RCS modifications are shown in figures 17 and 18 for the dry power and A/B power configurations, respectively. Also, surface oil flow visualization photographs are presented in figure 19 to aid the researcher in the understanding of the flow phenomena.

Results and Discussion

Pressure Data

Static pressure ratio data along the lower divergent flap and shelf surfaces are presented in figure 10 as a function of NPR. Data are presented on the nozzle centerline for the baseline and scarfed configurations and at a spanwise location of $(y/w)/2 = -0.500$ for the sawtooth configurations. A decision was made to more densely instrument the lower divergent flap of the A/B configurations than the flap for the dry configurations. This decision was based on the likelihood that if flow separation were shown not to occur on the A/B configurations, separation would also be absent on the dry configurations, which have smaller convergence and divergence angles. Because of the limited pressure instrumentation on even the A/B flap, it could not be determined if the flow was attached. As shown in figures 10(b), 10(d), and 10(f), the first tap ($A_e/A_t = 1.100$) downstream of the throat ($x/L_{\text{flap}} = 0.10$) may be in a separation bubble. At low values of NPR, internal shocks are evident. These shocks are characteristic of highly overexpanded nozzle flows and are likely followed by regions of shock-induced separated flow. As NPR is increased and over-expansion of the nozzle is reduced, these shocks move to the nozzle exit. Based on the limited instrumentation, the dry power configurations appear to show the same trends. (See figs. 10(a), 10(c), and 10(e).) Additionally, the configurations with $A_e/A_t = 1.100$ experienced an additional internal shock, evidenced by the pressure rise near the nozzle exit. This shock was likely an impingement of a shock emanating from the downstream end of the throat separation bubble. The impingement occurs for these configurations because the upper flap divergence angle is reduced to obtain the low expansion ratio. (See fig. 3(a).)

However, a change in the static pressure distribution almost always occurred along the shelf as NPR increased. Typically, the size (axial extent) of the shock cells in a supersonic jet increases with increasing NPR. These shock cells indicate the expansion and compression cycles that the exhaust flow undergoes as it adjusts to ambient pressure and are illustrated in the flow visualization photographs discussed later in the paper. The shock cells are evident by the cycling static pressure distributions seen in figure 10. Static pressures on the shelf

surface greater than p_a exert a negative normal force on the nozzle, whereas static pressures on the shelf less than ambient pressure exert a positive normal force on the nozzle. The integrated effect of these shelf loads, as well as similar loads on the divergent flaps, is to influence the magnitude of the thrust vector angles.

Performance Data

The performance data (nozzle internal thrust ratio F/F_i , resultant thrust ratio F_r/F_i , discharge coefficient w_p/w_i , resultant pitch thrust vector angle δ_p , and resultant yaw thrust vector angle δ_y) are presented as functions of NPR in figures 11–18. The data in figures 11, 12, and 13 show the effect of expansion ratio for the baseline, scarfed, and sawtooth configurations, respectively. Comparison plots for power settings are presented in figures 14, 15, and 16 for the baseline, scarfed, and sawtooth configurations, respectively. Comparison plots for RCS modifications are shown in figures 17 and 18 for the dry and A/B power configurations, respectively.

In general, the discharge coefficients for the three shelf nozzle designs (figs. 11–13) were lower than levels typically measured on a 2-D C-D nozzle by approximately 2 percent. (See refs. 7–12.) The lower level of weight-flow efficiency was probably due to the sharp throat corner formed between the convergent and divergent flaps. Sharp throats have been shown to cause separation bubbles immediately downstream; this results in a reduced effective throat area. A separation bubble is indicated by the pressure distribution in figure 10, particularly for A/B configurations with $A_e/A_t = 1.100$, where a sharp pressure rise occurs between the first two pressure taps. As reported in reference 7, a 2-D C-D nozzle with a zero radius (sharp) throat generated a reduced discharge coefficient. In general, increases in expansion ratio produced no significant change in discharge coefficient, the exception being for the baseline configurations with $A_e/A_t = 1.100$. (See figs. 11(a) and 11(b).) The effects were attributed to the more pronounced separation bubble indicated by the pressure distributions. (See fig. 10.) A larger throat area would be more efficient, which is generally shown in the discharge coefficient data of figures 14–16. In general, RCS modifications (figs. 17 and 18) had no effect on discharge coefficient except for the baseline configurations with $A_e/A_t = 1.100$ as discussed earlier.

The internal thrust ratio F/F_i curves are typical of 2-D, C-D nozzles. All C-D nozzles have the same basic thrust curves consisting of internal normal shock flow regime, oblique shock flow regime, and underexpanded flow regime. The first two regimes (normal shock regime at $\text{NPR} < 3$ and oblique shock regime at $\text{NPR} > 3$) can be seen in the data for the configurations with $A_e/A_t = 2.500$

(figs. 11–13), but because $(\text{NPR})_d$ (table 1) is above the NPR range, the underexpanded regime is not seen. Increasing the expansion ratio shifts the curves to the right as expected. The resultant thrust ratio F_r/F_i curves are similar to the internal performance curves—a result of the relatively low levels of thrust vectoring. Peak resultant thrust ratio levels were less than 1.00 due to flow angularity, skin friction, and shock losses. However, despite the additional surface area of the shelf, these levels were comparable peak values typical of 2-D C-D nozzles without shelves. (See refs. 8–12.) The thrust ratio curves are quite similar for the dry and A/B configurations. (See figs. 14–16.) The data in figures 17 and 18 tend to show that RCS modifications have very little effect on peak thrust ratio.

The baseline and sawtooth designs were symmetric about a vertical cut along the nozzle centerline; therefore zero values of resultant yaw vector angles δ_y were expected and are generally shown for those configurations. (See figs. 11–13.) As expected, the asymmetrical scarfed nozzle produced nonzero δ_y values. (See fig. 12.) Resultant pitch thrust vector angles δ_p were typically nonzero and varied with NPR. Nozzle divergent flap geometry (nonzero $\delta_{v,p}$ (table 1)) and the influence of the shelf on the shock-cell pressure variations contributed to these varying pitch thrust vector angles. These nonzero normal forces (δ_p) and side forces (δ_y) would require an exhaustive investigation of any concept considered for integration into a flight vehicle. The vehicle would have to be able to trim these propulsion-induced longitudinal and lateral forces and moments. Since the engines would probably be used in pairs, the nonzero side force would be balanced out by the second engine. The trend for dry and A/B configurations is quite similar as shown in figures 14–16.

Shelf Surface Oil Flow Visualization

Oil flow visualization photographs are presented in figure 19 to illustrate the complex flow patterns on the shelf surface. As previously described, a mixture of fine black grit particles and oil was used to depict flow patterns along the shelf surface. Flow patterns were closely observed with a video camera to ensure that they were fully developed and did not change as the jet was turned off. No changes in oil flow patterns were observed as NPR was reduced from test conditions to jet off. Flow visualization data were obtained only on the dry power configurations with $A_e/A_t = 1.100$ (Config 1, 7, and 13) at NPR near peak F_r/F_i .

All three photographs show what appears to be under-expanded flow although the nozzles are nominally at design or overexpanded conditions. The pressure distributions indicate high pressure at the exit plane as a

result of the compression shock generated by the geometry for $A_e/A_t = 1.100$, as discussed in the pressure discussion. All three nozzle designs—baseline, scarfed, and sawtooth—exhibited flow expansion and recompression along the shelf surface as shown in figure 19. Flow on either side of the centerline expanded away from the centerline just downstream of the nozzle exit plane and then recompressed back toward the centerline farther downstream. Another expansion process was evident downstream of the recompression. The size of these regions of expansion and compression is dependent upon NPR, and they dictate the static pressure distributions along the shelf. These variations in static pressure resulted in variations in δ_p with NPR (as shown in the force data) because normal force was generated on the shelf by static pressure greater or less than p_a .

The scarfed nozzle configuration 7 shown in figure 19(b) also exhibited a compression plane on the shelf that appeared to be parallel to the scarf angle of the upper divergent flap and shelf trailing edge. In addition, the flow on the left side of the shelf (looking upstream) appeared to expand farther away from the nozzle centerline than flow on the right side. These phenomena were a result of nozzle geometry which expanded flow to the left side of the nozzle as well as out the shelf. However, flow at the trailing edge of the scarfed shelf recompressed to travel parallel to the nozzle centerline.

Similar trends appeared for the sawtooth nozzle configuration 13, as shown in figure 19(c). The oil flow photographs highlight the lines formed as the expansion and compression waves impinged on the shelf surface. Downstream of the nozzle exit, flow along the sides expanded away from the centerline and recompressed back toward the centerline further downstream. At the trailing edge of the sawtooth nozzle shelf, the flow patterns were nearly parallel to the nozzle centerline. Weak shock patterns again parallel to the trailing edge can be seen on the shelf surface (one shock nearly intersects orifice 69, as shown).

Conclusions

An investigation was conducted in the static test facility of the Langley 16-Foot Transonic Tunnel to determine the internal performance of a two-dimensional convergent-divergent nozzle. The nozzle design was tested with dry and afterburning throat areas, which represent different power settings and three expansion ratios. For each configuration, three trailing-edge geometries were tested. The baseline geometry had a straight trailing edge. Two different shaping techniques were applied to the baseline nozzle design to reduce radar observables: the scarfed design and the sawtooth design. A flat plate extended downstream of the lower divergent

flap trailing edge parallel to the model centerline to form a shelflike expansion surface. This shelf was designed to shield the plume from observation from the ground (infrared radiation (IR) signature suppression). The shelf represents part of the aircraft structure that might be present in an installed configuration. These configurations were tested at nozzle pressure ratios from 2.0 to 12.0.

Results of this investigation indicated the following conclusions:

1. Discharge coefficient and peak resultant thrust ratio were not significantly affected by the addition of the shelf and changes to the upper divergent flap and shelf geometry. Discharge coefficients for these two-dimensional convergent-divergent shelf nozzles lower than typical two-dimensional convergent-divergent nozzles due to the sharp corner at the nozzle geometric throat.

2. Resultant pitch vector angles were typically non-zero and varied with increasing nozzle pressure ratio. In addition to nozzle internal asymmetry, the shelf significantly affected the pitch vector angle by producing a surface on which the shock-cell pressure variation could act. Only the asymmetrical scarfed nozzle produced resultant yaw thrust vector angles.

NASA Langley Research Center
Hampton, VA 23681-0001
April 4, 1996

References

1. Deitchman, Seymour J.: *Military Power and the Advance of Technology—General Purpose Military Forces for the 1980's and Beyond*. Westview Press, 1983.
2. Leavitt, Laurence D.; and Berrier, Bobby L.: *Static Performance of Nozzles Designed for Low Infrared Radiation and Radar Cross-Section Signatures*. NASA TM-4689, 1995.
3. Staff of the Propulsion Aerodynamics Branch: *A User's Guide to the Langley 16-Foot Transonic Tunnel Complex—Revision 1*. NASA TM-83186, 1990. (Supersedes NASA TM-83186.)
4. Mercer, Charles E.; Berrier, Bobby L.; Capone, Francis J.; and Grayston, Alan M.: *Data Reduction Formulas for the 16-Foot Transonic Tunnel: NASA Langley Research Center—Revision 2*. NASA TM-107646, 1992. (Supersedes NASA TM-86319.)
5. Berrier, Bobby L.: *Results From NASA Langley Experimental Studies of Multi-axis Thrust Vectoring Nozzles*. SAE Paper 881481, Oct. 1988.
6. Leavitt, Laurence D.: *Summary of Nonaxisymmetric Nozzle Internal Performance From the NASA Langley Static Test Facility*. AIAA-85-1347, July 1985.

7. Mason, Mary L.; Putnam, Lawrence E.; and Re, Richard J.: *The Effect of Throat Contouring on Two-Dimensional Converging-Diverging Nozzles at Static Conditions*. NASA TP-1704, 1980.
8. Mason, Mary L.; and Berrier, Bobby L.: *Static Investigation of Several Yaw Vectoring Concepts on Nonaxisymmetric Nozzles*. NASA TP-2432, 1985.
9. Hiley, P. E.; Wallace, H. W.; and Booz, D. E.: *Study of Non-Axisymmetric Nozzles Installed in Advanced Fighter Aircraft*. AIAA-75-1316, Sept.–Oct. 1975.
10. Capone, F. J.: *Nonaxisymmetric Nozzle—It is for Real*. AIAA-79-1810, Aug. 1979.
11. Capone, Francis J.; and Berrier, Bobby L.: *Investigation of Axisymmetric and Nonaxisymmetric Nozzles Installed on a 0.10-Scale F-18 Prototype Airplane Model*. NASA TP-1638, 1980.
12. Taylor, John G.: *Static Investigation of a Two-Dimensional Convergent-Divergent Exhaust Nozzle With Multiaxis Thrust-Vectoring Capability*. NASA TP-2973, 1990.

Table 1. Configuration Summary

Configuration	Design	Power	A_e/A_t	$(NPR)_d$	$\delta_{v, p}$, deg
1	Baseline	Dry	1.100	3.060	6.47
2	Baseline	Dry	1.750	8.371	1.82
3	Baseline	Dry	2.500	15.647	-3.74
4	Baseline	A/B	1.100	3.060	7.80
5	Baseline	A/B	1.750	8.371	2.30
6	Baseline	A/B	2.500	15.647	-4.70
7	Scarfed	Dry	1.100	3.060	5.00
8	Scarfed	Dry	1.750	8.371	0.35
9	Scarfed	Dry	2.500	15.647	-5.21
10	Scarfed	A/B	1.100	3.060	6.33
11	Scarfed	A/B	1.750	8.371	0.83
12	Scarfed	A/B	2.500	15.647	-6.17
13	Sawtooth	Dry	1.100	3.060	5.20
14	Sawtooth	Dry	1.750	8.371	0.55
15	Sawtooth	Dry	2.500	15.647	-5.02
16	Sawtooth	A/B	1.100	3.060	6.53
17	Sawtooth	A/B	1.750	8.371	1.03
18	Sawtooth	A/B	2.500	15.647	-5.98

Table 2. Nozzle Internal Performance Characteristics for Baseline Configurations

(a) Dry power configurations

NPR	w_p/w_i	F/F_i	F_r/F_i	δ_p , deg	δ_y , deg
Configuration 1; $A_e/A_t = 1.100$					
2.003	0.961	0.940	0.940	-0.568	-0.208
2.502	.961	.959	.959	-.316	-.117
3.006	.961	.967	.967	-.574	.013
3.497	.961	.971	.971	1.543	.017
3.996	.962	.972	.972	-.849	-.006
4.502	.962	.971	.971	-1.106	-.002
5.004	.962	.969	.970	-1.026	-.018
6.005	.963	.964	.964	-.010	.017
8.005	.963	.952	.953	-.692	.027
9.996	.963	.945	.952	-7.078	-.213
11.165	.962	.942	.954	-9.279	-.278
Configuration 2; $A_e/A_t = 1.750$					
1.999	0.968	0.871	0.872	-1.510	-0.078
2.999	.966	.907	.907	1.085	-.054
3.999	.966	.940	.940	-.034	-.125
5.003	.967	.961	.961	1.360	-.089
5.996	.968	.974	.974	-.705	-.048
6.998	.968	.980	.981	-1.629	.060
8.000	.968	.984	.985	-1.828	.068
8.503	.967	.986	.986	-1.655	.026
9.011	.967	.987	.987	-1.414	.049
9.497	.967	.987	.988	-1.081	.026
9.995	.967	.988	.988	-.715	-.008
10.572	.967	.988	.988	-.356	-.037
Configuration 3; $A_e/A_t = 2.500$					
2.001	0.964	0.896	0.896	-1.204	-0.541
3.003	.967	.875	.875	1.297	-.122
4.002	.967	.912	.913	1.994	-.025
5.006	.968	.899	.903	-5.785	-.115
6.004	.968	.917	.921	-4.997	-.008
6.997	.968	.936	.937	-3.370	.012
7.995	.968	.951	.954	-4.298	.048
9.000	.967	.963	.967	-5.136	.010
9.998	.968	.971	.976	-5.677	.039
10.793	.967	.976	.981	-5.730	.048
10.994	.967	.977	.982	-5.679	.027

Table 2. Concluded

(b) A/B power configurations

NPR	w_p/w_i	F/F_i	F_r/F_i	δ_p , deg	δ_y , deg
Configuration 4; $A_e/A_t = 1.100$					
2.004	0.958	0.949	0.949	-0.151	-0.075
2.503	.957	.964	.964	.751	-.095
3.007	.957	.972	.973	1.808	-.054
3.504	.957	.975	.975	-.412	-.091
4.003	.957	.975	.976	-1.655	-.119
4.507	.958	.974	.974	-1.020	-.096
5.007	.957	.971	.971	.054	-.043
6.003	.958	.966	.966	1.977	-.043
7.721	.957	.957	.957	-.435	-.004
Configuration 5; $A_e/A_t = 1.750$					
2.003	0.972	0.890	0.890	-0.206	0.068
2.998	.972	.920	.920	1.946	-.064
4.008	.973	.943	.943	-.813	-.073
5.001	.973	.967	.967	1.386	-.014
6.009	.973	.978	.978	-1.226	.008
7.000	.973	.984	.985	-2.013	.033
8.004	.972	.989	.989	-1.431	.038
8.495	.972	.990	.990	-.844	.018
8.996	.972	.991	.991	-.363	-.021
9.565	.971	.991	.991	-.036	-.022
Configuration 6; $A_e/A_t = 2.500$					
2.000	0.963	0.942	0.942	-0.108	-0.248
3.002	.969	.866	.866	1.514	-.093
3.998	.970	.901	.901	-1.092	-1.129
5.007	.970	.918	.920	-3.845	-.035
5.997	.970	.927	.929	-3.864	.046
7.002	.970	.931	.935	-5.717	-.003
8.005	.970	.947	.953	-6.577	.046
9.007	.969	.958	.966	-7.533	.106
9.982	.968	.968	.977	-7.817	.155

Table 3. Nozzle Internal Performance Characteristics for Scarfed Configurations

(a) Dry power configurations

NPR	w_p/w_i	F/F_i	F_r/F_i	δ_p , deg	δ_y , deg
Configuration 7; $A_e/A_t = 1.100$					
2.001	0.970	0.914	0.914	-0.526	0.316
2.504	.969	.935	.935	-.251	-.048
3.001	.968	.954	.954	.375	-.169
3.497	.969	.966	.966	-.057	.390
4.003	.969	.974	.974	-.825	1.523
4.508	.969	.977	.978	-.142	2.346
5.007	.970	.978	.980	.406	3.014
6.002	.970	.978	.980	.505	3.896
6.998	.970	.975	.979	1.608	4.539
8.001	.970	.973	.977	1.481	4.988
9.007	.970	.972	.976	.317	5.186
10.006	.970	.969	.974	-1.115	5.318
10.939	.969	.968	.973	-2.742	5.362
Configuration 8; $A_e/A_t = 1.750$					
2.001	0.971	0.866	0.866	-1.127	0.931
3.005	.969	.911	.911	-.222	.998
4.009	.969	.923	.923	-.718	-1.216
5.000	.969	.945	.947	1.316	-2.384
5.999	.970	.961	.962	-.586	-1.469
7.001	.969	.972	.973	-2.134	.386
7.998	.969	.980	.980	-2.423	.403
8.493	.969	.982	.983	-2.456	.724
9.001	.969	.985	.986	-2.412	1.021
9.493	.969	.986	.987	-2.328	1.239
10.001	.969	.987	.988	-2.172	1.452
11.080	.968	.989	.990	-1.565	1.790
Configuration 9; $A_e/A_t = 2.500$					
1.998	0.962	0.940	0.940	-1.121	0.335
2.998	.967	.870	.870	.759	.560
3.999	.968	.879	.883	-3.894	-4.143
4.997	.968	.910	.912	-2.564	-2.010
6.002	.968	.912	.917	-4.779	-2.841
6.997	.968	.918	.922	-4.918	-2.726
8.009	.968	.934	.938	-4.919	-2.529
9.013	.967	.947	.952	-5.635	-2.207
10.008	.968	.956	.963	-6.504	-1.619
11.474	.966	.967	.975	-7.169	-.815

Table 3. Concluded

(b) A/B power configurations

NPR	w_p/w_i	F/F_i	F_r/F_i	δ_p , deg	δ_y , deg
Configuration 10; $A_e/A_t = 1.100$					
2.005	0.970	0.927	0.927	-0.068	0.893
2.499	.971	.946	.946	.060	-.955
2.998	.971	.962	.962	.668	-.359
3.496	.971	.971	.971	-.371	.552
3.999	.971	.976	.976	-.007	1.678
4.501	.972	.978	.979	.884	2.515
5.010	.972	.978	.980	1.022	3.116
5.995	.972	.977	.980	1.592	4.021
8.010	.971	.972	.976	-.265	4.900
9.848	.970	.968	.973	-2.682	5.156
Configuration 11; $A_e/A_t = 1.750$					
1.999	0.972	0.864	0.864	-0.336	2.074
3.001	.970	.916	.916	-.471	.186
3.993	.971	.929	.931	.503	-3.138
4.991	.971	.951	.952	1.368	-2.612
5.981	.971	.967	.967	-1.444	-1.492
6.994	.971	.977	.978	-2.986	-.349
7.965	.971	.984	.986	-3.119	.407
8.498	.971	.986	.987	-2.952	.757
8.991	.970	.989	.990	-2.616	1.029
9.485	.970	.990	.991	-2.233	1.246
Configuration 12; $A_e/A_t = 2.500$					
2.003	0.964	0.947	0.947	-0.373	0.944
3.006	.970	.905	.905	.238	1.645
3.999	.970	.869	.876	-5.403	-4.972
5.000	.971	.891	.899	-3.500	-6.660
6.002	.971	.914	.919	-5.367	-2.512
7.006	.970	.927	.932	-5.584	-2.540
7.987	.970	.938	.945	-6.280	-2.692
9.009	.969	.947	.957	-7.760	-2.395
10.030	.968	.956	.968	-8.798	-1.755

Table 4. Nozzle Internal Performance Characteristics for Sawtooth Configurations

(a) Dry power configurations

NPR	w_p/w_i	F/F_i	F_r/F_i	δ_p , deg	δ_y , deg
Configuration 13; $A_e/A_t = 1.100$					
2.000	0.972	0.916	0.916	-0.933	0.592
2.501	.970	.941	.941	-1.320	-.139
3.092	.971	.959	.960	-1.247	-.145
3.502	.971	.969	.969	-.741	-.088
3.992	.970	.976	.976	-1.533	-.103
4.500	.972	.977	.977	-.284	-.065
5.004	.971	.978	.978	-.138	-.023
6.002	.972	.977	.977	-.049	.020
7.994	.972	.972	.972	1.636	.116
10.020	.971	.965	.966	2.478	.030
11.315	.971	.961	.961	.853	-.022
Configuration 14; $A_e/A_t = 1.750$					
2.000	0.970	0.866	0.866	-0.880	-0.216
3.007	.969	.890	.894	-5.224	-.218
3.999	.969	.930	.931	-3.134	-.031
5.011	.970	.953	.954	-2.554	-.086
6.002	.970	.968	.968	-.798	-.047
7.017	.970	.977	.977	-2.292	-.007
8.008	.970	.982	.983	-3.118	.005
8.414	.970	.984	.985	-3.103	.040
9.000	.970	.986	.987	-2.658	.009
10.000	.970	.988	.988	-1.696	.016
11.205	.969	.989	.989	-.635	-.044
Configuration 15; $A_e/A_t = 2.500$					
2.003	0.963	0.945	0.945	-0.506	-0.388
3.006	.969	.867	.867	.481	-.192
3.996	.969	.886	.894	-7.704	-.081
6.003	.970	.907	.917	-8.659	.053
8.008	.970	.939	.944	-6.189	.031
9.000	.969	.951	.957	-6.628	.044
10.013	.970	.959	.966	-7.278	.088
11.851	.968	.971	.980	-7.866	.174

Table 4. Concluded

(b) A/B power configurations

NPR	w_p/w_i	F/F_i	F_r/F_i	δ_p , deg	δ_y , deg
Configuration 16; $A_e/A_t = 1.100$					
2.005	0.971	0.935	0.935	-0.363	-0.086
2.501	.969	.955	.955	-.254	-.208
3.003	.970	.967	.967	.112	-.085
3.504	.970	.974	.975	-.924	-.099
4.000	.970	.977	.977	-.672	-.047
4.502	.971	.977	.977	.231	-.002
5.001	.971	.976	.976	.436	.007
5.503	.971	.975	.975	.595	-.003
6.002	.971	.974	.974	.704	.036
8.004	.969	.967	.969	3.268	.057
8.929	.969	.964	.965	3.341	.048
Configuration 17; $A_e/A_t = 1.750$					
NPR	w_p/w_i	F/F_i	F_r/F_i	δ_p , deg	δ_y , deg
1.999	0.971	0.849	0.853	-2.585	-5.188
3.007	.971	.917	.917	1.075	-.080
3.997	.971	.932	.933	-2.450	.013
4.998	.972	.954	.955	-.802	-.052
6.002	.971	.970	.970	-1.666	.014
7.004	.971	.979	.980	-3.180	.085
7.995	.971	.986	.988	-3.701	.072
8.497	.971	.987	.988	-3.152	.071
8.999	.970	.989	.990	-2.559	.085
9.729	.970	.991	.992	-1.817	.080
Configuration 18; $A_e/A_t = 2.500$					
1.996	0.965	0.950	0.950	-0.053	-0.184
3.001	.971	.858	.863	-6.545	-.099
3.999	.971	.888	.896	-7.645	.002
4.999	.972	.896	.909	-9.844	.015
5.997	.971	.919	.928	-8.227	.086
7.000	.971	.931	.940	-7.888	.110
7.999	.970	.942	.950	-7.598	.129
8.998	.970	.952	.963	-8.681	.222
10.017	.969	.960	.973	-9.393	.243
10.119	.969	.961	.974	-9.435	.284

Table 5. Nozzle Internal Static Pressure Ratios for Dry Power Baseline Configurations

(a) Configuration 1; $A_e/A_t = 1.100$

NPR	$p/p_{t,j}$ for lower divergent flap at—								
	$(y/w)/2 = 0.500$ for x/L_{flap} of—			$(y/w)/2 = 0.000$ for x/L_{flap} of—			$(y/w)/2 = -0.500$ for x/L_{flap} of—		
	0.500	0.700	0.900	0.500	0.700	0.900	0.500	0.700	0.900
2.003	0.291	0.358	0.449	0.288	0.362	0.457	0.291	0.359	0.450
2.502	.288	.357	.305	.287	.361	.314	.287	.359	.305
3.006	.286	.356	.304	.286	.360	.308	.286	.359	.305
3.497	.285	.356	.303	.286	.359	.299	.285	.359	.305
3.996	.284	.355	.303	.285	.359	.296	.284	.358	.305
4.502	.283	.355	.302	.285	.358	.294	.283	.358	.304
5.004	.283	.355	.302	.285	.358	.293	.283	.358	.305
6.005	.283	.356	.302	.285	.357	.292	.283	.358	.305
8.005	.283	.356	.302	.284	.358	.292	.282	.358	.305
9.996	.283	.357	.302	.284	.359	.292	.283	.359	.305
11.165	.284	.357	.301	.283	.359	.292	.283	.358	.306

NPR	$p/p_{t,j}$ on shelf at $(y/w)/2 = 0.000$ for x/L_{shelf} of—						
	0.076	0.227	0.379	0.530	0.682	0.833	0.985
2.003	0.558	0.513	0.507	0.506	0.505	0.504	0.501
2.502	.522	.371	.454	.384	.439	.385	.409
3.006	.453	.335	.239	.469	.294	.292	.403
3.497	.435	.363	.180	.298	.400	.268	.230
3.996	.436	.276	.150	.200	.308	.292	.220
4.502	.436	.209	.159	.172	.255	.316	.205
5.004	.437	.203	.165	.154	.184	.263	.223
6.005	.439	.203	.108	.076	.134	.174	.215
8.005	.441	.203	.087	.044	.089	.111	.145
9.996	.442	.203	.087	.042	.091	.093	.096
11.165	.442	.203	.087	.042	.084	.086	.086

Table 5. Continued

(b) Configuration 2; $A_e/A_t = 1.750$

NPR	$p/p_{t,j}$ for lower divergent flap at—								
	$(y/w)/2 = 0.500$ for x/L_{flap} of—			$(y/w)/2 = 0.000$ for x/L_{flap} of—			$(y/w)/2 = -0.500$ for x/L_{flap} of—		
	0.500	0.700	0.900	0.500	0.700	0.900	0.500	0.700	0.900
1.999	0.437	0.498	0.527	0.433	0.500	0.527	0.432	0.497	0.526
2.999	.220	.160	.285	.219	.163	.289	.220	.159	.281
3.999	.219	.159	.118	.218	.163	.137	.219	.158	.118
5.003	.219	.159	.118	.217	.162	.127	.218	.158	.118
5.996	.218	.159	.118	.216	.162	.124	.218	.158	.118
6.998	.218	.159	.117	.216	.162	.122	.217	.158	.118
8.000	.218	.159	.117	.215	.162	.120	.217	.158	.118
8.503	.218	.159	.117	.215	.162	.118	.217	.158	.118
9.011	.218	.159	.117	.215	.162	.117	.217	.158	.118
9.497	.218	.159	.116	.214	.161	.116	.217	.158	.117
9.995	.218	.159	.116	.213	.161	.116	.217	.158	.117
10.572	.218	.158	.116	.213	.161	.116	.217	.158	.117

NPR	$p/p_{t,j}$ on shelf at $(y/w)/2 = 0.000$ for x/L_{shelf} of—						
	0.076	0.227	0.379	0.530	0.682	0.833	0.985
1.999	0.536	0.514	0.510	0.511	0.511	0.510	0.502
2.999	.367	.424	.316	.374	.327	.362	.313
3.999	.249	.315	.248	.265	.265	.292	.206
5.003	.167	.242	.346	.255	.139	.112	.216
5.996	.167	.137	.231	.298	.179	.121	.124
6.998	.167	.138	.110	.242	.224	.126	.112
8.000	.166	.138	.108	.105	.187	.152	.094
8.503	.166	.138	.108	.095	.152	.166	.102
9.011	.166	.138	.108	.092	.088	.160	.110
9.497	.165	.138	.108	.090	.062	.149	.120
9.995	.165	.138	.107	.089	.050	.111	.128
10.572	.165	.138	.107	.089	.047	.048	.127

Table 5. Concluded

(c) Configuration 3; $A_e/A_t = 2.500$

NPR	$p/p_{t,j}$ for lower divergent flap at—								
	$(y/w)/2 = 0.500$ for x/L_{flap} of—			$(y/w)/2 = 0.000$ for x/L_{flap} of—			$(y/w)/2 = -0.500$ for x/L_{flap} of—		
	0.500	0.700	0.900	0.500	0.700	0.900	0.500	0.700	0.900
2.001	0.484	0.484	0.528	0.478	0.486	0.531	0.474	0.489	0.531
3.003	.232	.238	.303	.236	.239	.306	.235	.238	.299
4.002	.109	.196	.193	.111	.206	.212	.110	.195	.192
5.006	.109	.070	.136	.110	.116	.141	.110	.067	.130
6.004	.109	.067	.082	.110	.067	.071	.109	.065	.071
6.997	.109	.067	.065	.110	.067	.068	.109	.065	.065
7.995	.109	.066	.063	.109	.066	.066	.109	.065	.064
9.000	.109	.066	.061	.108	.066	.064	.108	.065	.063
9.998	.109	.066	.060	.108	.066	.062	.108	.065	.062
10.793	.109	.066	.058	.107	.066	.060	.108	.065	.061
10.994	.109	.066	.056	.105	.066	.060	.108	.065	.060

NPR	$p/p_{t,j}$ on shelf at $(y/w)/2 = 0.000$ for x/L_{shelf} of—						
	0.076	0.227	0.379	0.530	0.682	0.833	0.985
2.001	0.531	0.510	0.508	0.508	0.507	0.506	0.501
3.003	.408	.401	.309	.354	.355	.326	.345
4.002	.212	.232	.263	.259	.284	.237	.251
5.006	.180	.224	.223	.214	.229	.203	.190
6.004	.149	.188	.242	.169	.145	.134	.220
6.997	.092	.160	.191	.249	.137	.123	.083
7.995	.091	.071	.150	.199	.227	.111	.084
9.000	.091	.071	.115	.150	.218	.172	.081
9.998	.091	.071	.054	.125	.179	.206	.115
10.793	.091	.071	.054	.079	.146	.189	.155
10.994	.090	.070	.054	.075	.137	.183	.161

Table 6. Nozzle Internal Static Pressure Ratios for A/B Power Baseline Configurations

(a) Configuration 4; $A_e/A_t = 1.100$

NPR	$p/p_{t,j}$ for lower divergent flap at $(y/w)/2 = 0.500$ for x/L_{flap} of—								
	0.100	0.200	0.300	0.400	0.500	0.600	0.700	0.800	0.900
2.004	0.367	0.465	0.445	0.385	0.335	0.287	0.383	0.362	0.482
2.503	.366	.464	.444	.385	.334	.286	.382	.362	.346
3.007	.364	.465	.444	.385	.333	.286	.382	.360	.345
3.504	.362	.465	.444	.385	.333	.285	.382	.359	.345
4.003	.361	.465	.444	.385	.332	.285	.382	.359	.345
4.507	.361	.465	.444	.385	.332	.285	.383	.359	.345
5.007	.360	.465	.443	.385	.332	.286	.383	.359	.345
6.003	.360	.465	.443	.385	.332	.285	.383	.359	.344
7.721	.359	.465	.443	.385	.332	.287	.383	.359	.344

NPR	$p/p_{t,j}$ for lower divergent flap at $(y/w)/2 = 0.000$ for x/L_{flap} of—								
	0.100	0.200	0.300	0.400	0.500	0.600	0.700	0.800	0.900
2.004	0.359	0.464	0.448	0.392	0.332	0.285	0.389	0.368	0.487
2.503	.358	.462	.447	.392	.332	.285	.388	.368	.344
3.007	.356	.461	.447	.392	.332	.285	.387	.368	.343
3.504	.355	.460	.447	.392	.332	.285	.388	.368	.343
4.003	.354	.459	.447	.391	.332	.285	.388	.368	.343
4.507	.354	.459	.446	.391	.332	.284	.388	.368	.343
5.007	.354	.458	.446	.391	.333	.284	.388	.369	.342
6.003	.354	.458	.446	.391	.332	.284	.389	.369	.342
7.721	.353	.457	.446	.391	.333	.284	.390	.369	.343

Table 6. Continued

(a) Concluded

NPR	$p/p_{t,j}$ for lower divergent flap at $(y/w)/2 = -0.500$ for x/L_{flap} of—								
	0.100	0.200	0.300	0.400	0.500	0.600	0.700	0.800	0.900
2.004	0.350	0.473	0.441	0.390	0.334	0.289	0.380	0.365	0.478
2.503	.349	.470	.441	.389	.334	.288	.380	.365	.345
3.007	.348	.469	.441	.390	.334	.287	.379	.364	.345
3.504	.348	.468	.441	.392	.333	.286	.379	.364	.344
4.003	.347	.467	.441	.392	.331	.286	.379	.364	.344
4.507	.347	.466	.441	.392	.330	.286	.379	.364	.344
5.007	.347	.465	.441	.393	.329	.285	.379	.364	.344
6.003	.346	.465	.442	.393	.328	.285	.380	.364	.344
7.721	.345	.464	.443	.394	.327	.285	.381	.365	.345

NPR	$p/p_{t,j}$ on shelf at $(y/w)/2 = 0.000$ for x/L_{shelf} of—						
	0.076	0.227	0.379	0.530	0.682	0.833	0.985
2.004	0.577	0.514	0.508	0.507	0.506	0.505	0.498
2.503	.544	.379	.423	.416	.379	.421	.387
3.007	.441	.415	.228	.311	.425	.281	.286
3.504	.431	.323	.226	.197	.306	.352	.256
4.003	.428	.253	.214	.131	.328	.310	.272
4.507	.426	.248	.170	.102	.211	.302	.293
5.007	.425	.249	.138	.103	.168	.228	.266
6.003	.424	.249	.110	.076	.120	.137	.203
7.721	.423	.250	.110	.053	.066	.104	.132

Table 6. Continued

(b) Configuration 5; $A_e/A_t = 1.750$

NPR	$p/p_{t,j}$ for lower divergent flap at $(y/w)/2 = 0.500$ for x/L_{flap} of—								
	0.100	0.200	0.300	0.400	0.500	0.600	0.700	0.800	0.900
2.003	0.316	0.308	0.238	0.369	0.390	0.453	0.514	0.534	0.549
2.998	.315	.308	.238	.180	.228	.203	.180	.287	.307
4.008	.313	.308	.238	.180	.228	.203	.180	.159	.140
5.001	.312	.308	.238	.180	.227	.204	.180	.159	.140
6.009	.312	.308	.238	.180	.227	.204	.180	.159	.140
7.000	.311	.308	.238	.180	.227	.204	.180	.158	.140
8.004	.311	.307	.238	.180	.226	.204	.179	.158	.140
8.495	.311	.308	.239	.180	.226	.204	.179	.158	.140
8.996	.311	.307	.239	.180	.226	.204	.179	.158	.140
9.565	.310	.307	.239	.180	.226	.204	.179	.158	.140

NPR	$p/p_{t,j}$ for lower divergent flap at $(y/w)/2 = 0.000$ for x/L_{flap} of—								
	0.100	0.200	0.300	0.400	0.500	0.600	0.700	0.800	0.900
2.003	0.311	0.313	0.245	0.369	0.391	0.455	0.513	0.537	0.556
2.998	.309	.310	.241	.180	.219	.201	.185	.291	.310
4.008	.308	.309	.240	.180	.218	.202	.185	.163	.141
5.001	.308	.309	.237	.180	.217	.201	.185	.163	.142
6.009	.308	.308	.236	.180	.217	.200	.185	.163	.142
7.000	.308	.308	.236	.179	.217	.199	.184	.162	.142
8.004	.307	.308	.236	.179	.217	.199	.184	.162	.142
8.495	.307	.308	.236	.179	.216	.200	.184	.162	.142
8.996	.307	.308	.236	.179	.216	.200	.185	.162	.142
9.565	.307	.308	.235	.178	.216	.200	.185	.162	.142

Table 6. Continued

(b) Concluded

NPR	$p/p_{t,j}$ for lower divergent flap at $(y/w)/2 = -0.500$ for x/L_{flap} of—								
	0.100	0.200	0.300	0.400	0.500	0.600	0.700	0.800	0.900
2.003	0.307	0.310	0.241	0.371	0.388	0.450	0.510	0.534	0.550
2.998	.307	.309	.241	.181	.226	.205	.180	.289	.307
4.008	.307	.308	.241	.181	.226	.206	.180	.158	.140
5.001	.306	.308	.240	.180	.225	.205	.180	.158	.140
6.009	.305	.307	.240	.180	.225	.205	.180	.158	.140
7.000	.305	.307	.240	.180	.224	.205	.179	.158	.140
8.004	.305	.307	.240	.180	.224	.205	.179	.158	.140
8.495	.304	.307	.240	.180	.224	.205	.179	.158	.140
8.996	.304	.307	.240	.180	.224	.205	.179	.158	.140
9.565	.304	.307	.240	.180	.224	.205	.179	.158	.140

NPR	$p/p_{t,j}$ on shelf at $(y/w)/2 = 0.000$ for x/L_{shelf} of—						
	0.076	0.227	0.379	0.530	0.682	0.833	0.985
2.003	0.552	0.513	0.508	0.508	0.507	0.506	0.499
2.998	.421	.471	.306	.306	.387	.294	.370
4.008	.216	.350	.318	.196	.163	.279	.312
5.001	.165	.221	.318	.310	.186	.110	.134
6.009	.165	.123	.214	.279	.226	.155	.124
7.000	.164	.122	.135	.242	.186	.189	.121
8.004	.165	.122	.133	.117	.161	.140	.144
8.495	.165	.122	.133	.108	.119	.120	.151
8.996	.165	.123	.133	.103	.077	.105	.142
9.565	.165	.123	.133	.101	.071	.085	.111

Table 6. Continued

(c) Configuration 6; $A_e/A_t = 2.500$

NPR	$p/p_{t,j}$ for lower divergent flap at $(y/w)/2 = 0.500$ for x/L_{flap} of—								
	0.100	0.200	0.300	0.400	0.500	0.600	0.700	0.800	0.900
2.000	0.333	0.354	0.548	0.555	0.515	0.497	0.499	0.509	0.549
3.002	.316	.305	.235	.178	.148	.247	.249	.252	.264
3.998	.313	.305	.235	.178	.135	.110	.200	.202	.205
5.007	.312	.305	.235	.178	.135	.105	.085	.133	.144
5.997	.311	.305	.235	.178	.135	.105	.085	.070	.058
7.002	.311	.305	.235	.178	.135	.106	.085	.070	.058
8.005	.311	.305	.235	.178	.135	.106	.085	.070	.059
9.007	.310	.305	.235	.178	.135	.106	.085	.070	.059
9.982	.310	.305	.235	.178	.135	.106	.085	.070	.059

NPR	$p/p_{t,j}$ for lower divergent flap at $(y/w)/2 = 0.000$ for x/L_{flap} of—								
	0.100	0.200	0.300	0.400	0.500	0.600	0.700	0.800	0.900
2.000	0.325	0.360	0.545	0.556	0.516	0.499	0.499	0.511	0.559
3.002	.308	.306	.237	.176	.253	.267	.264	.262	.270
3.998	.307	.305	.236	.177	.135	.107	.187	.187	.190
5.007	.307	.305	.233	.177	.135	.107	.086	.153	.156
5.997	.307	.304	.232	.176	.135	.107	.086	.071	.059
7.002	.307	.304	.232	.176	.135	.107	.086	.071	.059
8.005	.306	.304	.232	.175	.135	.107	.086	.071	.059
9.007	.306	.304	.232	.175	.135	.107	.086	.071	.059
9.982	.306	.304	.231	.175	.135	.106	.086	.071	.059

Table 6. Concluded

(c) Concluded

NPR	$p/p_{t,j}$ for lower divergent flap at $(y/w)/2 = -0.500$ for x/L_{flap} of—								
	0.100	0.200	0.300	0.400	0.500	0.600	0.700	0.800	0.900
2.000	0.322	0.355	0.548	0.556	0.516	0.503	0.499	0.509	0.552
3.002	.305	.304	.237	.177	.154	.250	.250	.253	.263
3.998	.305	.303	.237	.177	.134	.107	.127	.168	.180
5.007	.304	.303	.236	.177	.134	.107	.084	.113	.141
5.997	.303	.303	.236	.177	.134	.107	.084	.069	.058
7.002	.303	.302	.236	.177	.135	.107	.084	.069	.058
8.005	.303	.302	.236	.177	.135	.107	.084	.069	.058
9.007	.302	.302	.235	.177	.134	.106	.084	.069	.058
9.982	.302	.302	.235	.177	.134	.106	.084	.069	.058

NPR	$p/p_{t,j}$ on shelf at $(y/w)/2 = 0.000$ for x/L_{shelf} of—						
	0.076	0.227	0.379	0.530	0.682	0.833	0.985
2.000	0.555	0.510	0.508	0.507	0.507	0.507	0.500
3.002	.312	.372	.375	.358	.344	.335	.337
3.998	.220	.285	.289	.277	.229	.319	.248
5.007	.184	.226	.242	.200	.223	.220	.179
5.997	.130	.197	.223	.186	.153	.134	.183
7.002	.069	.138	.220	.242	.125	.104	.104
8.005	.069	.072	.141	.211	.248	.111	.109
9.007	.069	.063	.112	.140	.204	.206	.090
9.982	.069	.062	.090	.112	.139	.203	.148

Table 7. Nozzle Internal Static Pressure Ratios for Dry Power Scarfed Configurations

(a) Configuration 7; $A_e/A_t = 1.100$

NPR	$p/p_{t,j}$ for lower divergent flap at—								
	$(y/w)/2 = 0.500$ for x/L_{flap} of—			$(y/w)/2 = 0.000$ for x/L_{flap} of—			$(y/w)/2 = -0.500$ for x/L_{flap} of—		
	0.500	0.700	0.900	0.500	0.700	0.900	0.500	0.700	0.900
2.001	0.261	0.420	0.504	0.260	0.427	0.523	0.263	0.470	0.548
2.504	.261	.272	.331	.259	.230	.390	.262	.189	.373
3.001	.261	.272	.227	.259	.225	.243	.262	.189	.331
3.497	.261	.272	.227	.259	.220	.239	.261	.189	.229
4.003	.261	.271	.227	.259	.215	.236	.261	.189	.227
4.508	.261	.271	.226	.259	.210	.230	.260	.189	.226
5.007	.261	.271	.226	.259	.206	.227	.260	.189	.226
6.002	.260	.270	.226	.259	.199	.225	.260	.189	.226
6.998	.260	.270	.226	.259	.193	.224	.260	.188	.226
8.001	.260	.270	.226	.259	.189	.224	.260	.188	.226
9.007	.260	.270	.226	.259	.186	.224	.260	.188	.226
10.006	.261	.270	.226	.259	.184	.224	.260	.188	.226
10.939	.261	.270	.225	.259	.182	.224	.260	.189	.226

NPR	$p/p_{t,j}$ on shelf at $(y/w)/2 = 0.500$ for x/L_{shelf} of—							
	0.076	0.227	0.379	0.530	0.682	0.833	0.985	1.061
2.001	0.561	0.514	0.505	0.505	0.504	0.505	0.502	0.501
2.504	.457	.383	.400	.406	.407	.409	.400	.402
3.001	.329	.358	.333	.367	.319	.365	.324	.354
3.497	.254	.426	.223	.289	.361	.285	.256	.298
4.003	.254	.298	.260	.181	.259	.332	.261	.211
4.508	.254	.222	.255	.240	.149	.230	.280	.253
5.007	.253	.222	.246	.186	.190	.214	.213	.253
6.002	.253	.221	.175	.101	.146	.198	.193	.204
6.998	.253	.221	.135	.087	.120	.121	.166	.181
8.001	.254	.220	.135	.076	.080	.102	.111	.123
9.007	.254	.220	.135	.053	.069	.075	.094	.098
10.006	.254	.220	.135	.051	.062	.049	.084	.089
10.939	.254	.220	.135	.051	.055	.043	.080	.105

Table 7. Continued

(a) Concluded

NPR	$p/p_{t,j}$ on shelf at $(y/w)/2 = 0.000$ for x/L_{shelf} of—						
	0.076	0.227	0.379	0.530	0.682	0.833	0.985
2.001	0.554	0.519	0.510	0.510	0.505	0.505	0.500
2.504	.446	.410	.417	.409	.407	.411	.396
3.001	.415	.361	.291	.390	.332	.330	.342
3.497	.256	.418	.235	.218	.405	.292	.248
4.003	.252	.389	.244	.201	.180	.354	.263
4.508	.252	.312	.289	.164	.169	.266	.296
5.007	.252	.216	.248	.150	.172	.187	.237
6.002	.252	.210	.166	.130	.108	.156	.234
6.998	.252	.209	.130	.119	.060	.125	.182
8.001	.253	.209	.119	.087	.059	.074	.128
9.007	.253	.209	.118	.068	.058	.068	.109
10.006	.253	.209	.118	.061	.046	.050	.098
10.939	.253	.209	.118	.060	.038	.075	.088

NPR	$p/p_{t,j}$ on shelf at $(y/w)/2 = -0.500$ for x/L_{shelf} of—					
	0.076	0.227	0.379	0.530	0.682	0.833
2.001	0.543	0.512	0.520	0.507	0.507	0.503
2.504	.481	.395	.429	.397	.403	.407
3.001	.431	.326	.358	.357	.361	.300
3.497	.371	.356	.231	.268	.339	.326
4.003	.326	.346	.241	.226	.222	.338
4.508	.317	.300	.274	.148	.225	.193
5.007	.298	.190	.245	.149	.203	.192
6.002	.277	.176	.164	.179	.103	.187
6.998	.275	.167	.089	.153	.111	.084
8.001	.274	.156	.086	.068	.117	.073
9.007	.275	.153	.080	.052	.084	.070
10.006	.275	.153	.077	.046	.065	.068
10.939	.275	.153	.076	.044	.063	.065

Table 7. Continued

(b) Configuration 8; $A_e/A_t = 1.750$

NPR	$p/p_{t,j}$ for lower divergent flap at—								
	$(y/w)/2 = 0.500$ for x/L_{flap} of—			$(y/w)/2 = 0.000$ for x/L_{flap} of—			$(y/w)/2 = -0.500$ for x/L_{flap} of—		
	0.500	0.700	0.900	0.500	0.700	0.900	0.500	0.700	0.900
2.001	0.458	0.515	0.532	0.441	0.517	0.532	0.413	0.514	0.535
3.005	.201	.279	.359	.242	.269	.310	.258	.268	.299
4.009	.201	.146	.202	.183	.144	.127	.109	.134	.174
5.000	.201	.146	.105	.182	.144	.115	.109	.134	.106
5.999	.201	.145	.104	.181	.144	.112	.109	.134	.106
7.001	.201	.145	.104	.181	.144	.110	.109	.134	.106
7.998	.201	.145	.104	.181	.144	.108	.109	.134	.105
8.493	.201	.145	.104	.181	.143	.107	.109	.134	.105
9.001	.201	.145	.104	.181	.143	.106	.109	.134	.105
9.493	.201	.145	.104	.181	.143	.105	.109	.133	.105
10.001	.201	.145	.104	.181	.143	.103	.108	.133	.105
11.080	.201	.145	.104	.181	.143	.102	.108	.133	.105

NPR	$p/p_{t,j}$ on shelf at $(y/w)/2 = 0.500$ for x/L_{shelf} of—							
	0.076	0.227	0.379	0.530	0.682	0.833	0.985	1.061
2.001	0.529	0.504	0.504	0.506	0.505	0.505	0.502	0.501
3.005	.443	.321	.376	.315	.335	.351	.340	.346
4.009	.230	.284	.254	.265	.292	.260	.227	.244
5.000	.113	.246	.294	.200	.189	.174	.179	.262
5.999	.113	.106	.218	.274	.147	.108	.198	.155
7.001	.113	.105	.129	.224	.195	.109	.116	.132
7.998	.113	.105	.086	.167	.202	.140	.087	.086
8.493	.113	.105	.085	.099	.193	.159	.094	.084
9.001	.113	.105	.085	.091	.166	.168	.106	.088
9.493	.113	.105	.085	.084	.139	.160	.114	.098
10.001	.113	.105	.085	.077	.124	.135	.122	.107
11.080	.113	.105	.085	.064	.079	.100	.108	.111

Table 7. Continued

(b) Concluded

NPR	$p/p_{t,j}$ on shelf at $(y/w)/2 = 0.000$ for x/L shelf of—						
	0.076	0.227	0.379	0.530	0.682	0.833	0.985
2.001	0.521	0.510	0.509	0.509	0.505	0.504	0.500
3.005	.393	.359	.342	.353	.355	.325	.334
4.009	.238	.393	.217	.344	.233	.254	.239
5.000	.111	.257	.339	.220	.126	.169	.219
5.999	.111	.129	.256	.278	.180	.123	.154
7.001	.111	.112	.133	.243	.214	.134	.119
7.998	.111	.112	.112	.175	.210	.155	.107
8.493	.111	.112	.099	.096	.200	.161	.105
9.001	.111	.112	.095	.093	.181	.161	.109
9.493	.111	.112	.094	.090	.113	.165	.115
10.001	.111	.112	.093	.084	.091	.161	.120
11.080	.111	.112	.093	.072	.065	.092	.131

NPR	$p/p_{t,j}$ on shelf at $(y/w)/2 = -0.500$ for x/L shelf of—					
	0.076	0.227	0.379	0.530	0.682	0.833
2.001	0.528	0.509	0.515	0.506	0.504	0.502
3.005	.359	.373	.340	.336	.346	.333
4.009	.320	.293	.249	.257	.234	.245
5.000	.181	.232	.279	.253	.138	.185
5.999	.163	.194	.206	.186	.231	.122
7.001	.134	.168	.148	.179	.170	.174
7.998	.124	.119	.133	.146	.131	.178
8.493	.123	.112	.126	.125	.129	.152
9.001	.123	.105	.122	.098	.128	.131
9.493	.123	.099	.118	.093	.128	.111
10.001	.123	.093	.116	.089	.119	.102
11.080	.122	.082	.111	.081	.066	.095

Table 7. Continued

(c) Configuration 9; $A_e/A_t = 2.500$

NPR	$p/p_{t,j}$ for lower divergent flap at—								
	$(y/w)/2 = 0.500$ for x/L_{flap} of—			$(y/w)/2 = 0.000$ for x/L_{flap} of—			$(y/w)/2 = -0.500$ for x/L_{flap} of—		
	0.500	0.700	0.900	0.500	0.700	0.900	0.500	0.700	0.900
1.998	0.497	0.500	0.544	0.495	0.497	0.541	0.492	0.498	0.539
2.998	.256	.260	.299	.262	.260	.299	.240	.245	.305
3.999	.108	.198	.196	.110	.169	.190	.110	.158	.267
4.997	.109	.157	.154	.110	.123	.135	.110	.066	.118
6.002	.109	.067	.095	.110	.067	.103	.110	.066	.084
6.997	.109	.067	.045	.110	.067	.054	.110	.066	.045
8.009	.109	.067	.045	.110	.067	.053	.110	.066	.045
9.013	.109	.067	.045	.110	.067	.052	.109	.066	.045
10.008	.109	.067	.045	.110	.067	.051	.109	.066	.045
11.474	.109	.067	.045	.110	.067	.050	.109	.066	.045

NPR	$p/p_{t,j}$ on shelf at $(y/w)/2 = 0.500$ for x/L shelf of—							
	0.076	0.227	0.379	0.530	0.682	0.833	0.985	1.061
1.998	0.535	0.503	0.505	0.507	0.505	0.506	0.503	0.501
2.998	.368	.384	.363	.341	.328	.336	.338	.335
3.999	.210	.246	.277	.257	.296	.257	.238	.279
4.997	.162	.196	.213	.214	.234	.184	.184	.218
6.002	.145	.187	.149	.161	.164	.199	.190	.146
6.997	.082	.162	.223	.144	.103	.100	.162	.188
8.009	.082	.062	.165	.201	.122	.099	.077	.110
9.013	.082	.062	.108	.167	.170	.100	.079	.071
10.008	.082	.062	.069	.105	.182	.125	.081	.077
11.474	.082	.062	.049	.069	.103	.149	.110	.082

Table 7. Concluded

(c) Concluded

NPR	$p/p_{t,j}$ on shelf at $(y/w)/2 = 0.000$ for x/L shelf of—						
	0.076	0.227	0.379	0.530	0.682	0.833	0.985
1.998	0.523	0.510	0.509	0.511	0.506	0.506	0.501
2.998	.357	.388	.362	.344	.331	.338	.335
3.999	.247	.297	.382	.216	.271	.247	.245
4.997	.158	.246	.234	.190	.313	.164	.176
6.002	.108	.177	.254	.198	.139	.189	.177
6.997	.106	.081	.280	.167	.114	.130	.118
8.009	.078	.102	.117	.277	.128	.087	.109
9.013	.074	.096	.078	.161	.241	.096	.068
10.008	.074	.073	.080	.066	.194	.158	.070
11.474	.074	.060	.072	.066	.072	.222	.130

NPR	$p/p_{t,j}$ on shelf at $(y/w)/2 = -0.500$ for x/L shelf of—					
	0.076	0.227	0.379	0.530	0.682	0.833
1.998	0.528	0.507	0.518	0.506	0.506	0.503
2.998	.391	.384	.376	.351	.338	.341
3.999	.272	.260	.269	.253	.254	.252
4.997	.219	.213	.208	.203	.204	.200
6.002	.231	.174	.172	.168	.168	.167
6.997	.081	.155	.153	.144	.143	.143
8.009	.076	.148	.135	.131	.125	.124
9.013	.074	.136	.118	.116	.116	.110
10.008	.072	.123	.105	.104	.105	.102
11.474	.067	.101	.092	.090	.091	.092

Table 8. Nozzle Internal Static Pressure Ratios for A/B Power Scarfed Configurations

(a) Configuration 10; $A_e/A_t = 1.100$

NPR	$p/p_{t,j}$ for lower divergent flap at $(y/w)/2 = 0.500$ for x/L_{flap} of—								
	0.100	0.200	0.300	0.400	0.500	0.600	0.700	0.800	0.900
2.005	0.348	0.412	0.406	0.355	0.301	0.300	0.431	0.467	0.516
2.499	.347	.412	.406	.355	.301	.260	.223	.267	.348
2.998	.345	.412	.406	.355	.301	.260	.222	.266	.250
3.496	.344	.412	.406	.354	.300	.259	.222	.266	.250
3.999	.343	.412	.406	.354	.300	.259	.222	.265	.249
4.501	.342	.411	.406	.354	.300	.259	.221	.264	.249
5.010	.342	.412	.406	.354	.300	.259	.221	.264	.249
5.995	.341	.411	.406	.355	.301	.258	.221	.263	.249
8.010	.341	.412	.406	.355	.301	.258	.220	.263	.248
9.848	.340	.412	.406	.356	.302	.258	.221	.262	.246

NPR	$p/p_{t,j}$ for lower divergent flap at $(y/w)/2 = 0.000$ for x/L_{flap} of—								
	0.100	0.200	0.300	0.400	0.500	0.600	0.700	0.800	0.900
2.005	0.329	0.390	0.380	0.348	0.304	0.291	0.442	0.497	0.552
2.499	.329	.388	.381	.348	.304	.264	.226	.328	.368
2.998	.327	.387	.381	.348	.304	.263	.225	.194	.284
3.496	.326	.386	.380	.347	.304	.263	.225	.194	.249
3.999	.325	.386	.380	.346	.304	.262	.225	.193	.248
4.501	.325	.385	.379	.346	.304	.262	.224	.193	.248
5.010	.325	.384	.379	.346	.304	.261	.224	.193	.247
5.995	.325	.384	.378	.345	.304	.260	.224	.192	.247
8.010	.324	.384	.378	.345	.303	.260	.224	.191	.247
9.848	.324	.384	.378	.345	.303	.261	.225	.191	.247

Table 8. Continued

(a) Continued

NPR	$p/p_{t,j}$ for lower divergent flap at $(y/w)/2 = -0.500$ for x/L_{flap} of—								
	0.100	0.200	0.300	0.400	0.500	0.600	0.700	0.800	0.900
2.005	0.309	0.345	0.363	0.343	0.304	0.360	0.471	0.525	0.559
2.499	.309	.345	.363	.342	.304	.264	.229	.217	.365
2.998	.309	.344	.362	.342	.305	.264	.229	.201	.307
3.496	.308	.344	.361	.342	.305	.263	.229	.200	.181
3.999	.308	.343	.361	.342	.304	.263	.229	.200	.176
4.501	.307	.343	.360	.341	.304	.262	.229	.200	.176
5.010	.307	.342	.360	.341	.304	.262	.229	.200	.176
5.995	.306	.342	.360	.341	.303	.262	.228	.200	.175
8.010	.305	.342	.360	.341	.303	.263	.228	.200	.175
9.848	.305	.342	.359	.341	.303	.263	.228	.199	.175

NPR	$p/p_{t,j}$ on shelf at $(y/w)/2 = 0.500$ for x/L shelf of—							
	0.076	0.227	0.379	0.530	0.682	0.833	0.985	1.061
2.005	0.583	0.520	0.505	0.506	0.505	0.505	0.501	0.500
2.499	.445	.448	.396	.400	.398	.420	.397	.404
2.998	.337	.410	.250	.348	.364	.304	.362	.340
3.496	.313	.460	.249	.203	.320	.355	.245	.241
3.999	.313	.258	.298	.195	.179	.300	.318	.286
4.501	.312	.256	.297	.144	.207	.231	.255	.267
5.010	.312	.256	.231	.135	.182	.187	.238	.229
5.995	.312	.256	.169	.119	.105	.144	.194	.195
8.010	.312	.255	.165	.073	.076	.068	.123	.139
9.848	.312	.255	.165	.064	.053	.052	.075	.108

Table 8. Continued

(a) Concluded

NPR	$p/p_{t,j}$ on shelf at $(y/w)/2 = 0.000$ for x/L shelf of—						
	0.076	0.227	0.379	0.530	0.682	0.833	0.985
2.005	0.570	0.515	0.511	0.509	0.506	0.502	0.499
2.499	.418	.459	.399	.429	.393	.421	.390
2.998	.409	.400	.297	.355	.373	.317	.316
3.496	.326	.450	.264	.207	.319	.393	.250
3.999	.314	.353	.298	.174	.179	.327	.329
4.501	.309	.282	.325	.158	.150	.190	.295
5.010	.308	.277	.262	.167	.113	.210	.240
5.995	.308	.267	.149	.157	.083	.133	.215
8.010	.308	.266	.140	.079	.068	.091	.109
9.848	.309	.266	.140	.074	.046	.067	.096

NPR	$p/p_{t,j}$ on shelf at $(y/w)/2 = -0.500$ for x/L shelf of—					
	0.076	0.227	0.379	0.530	0.682	0.833
2.005	0.564	0.514	0.521	0.506	0.512	0.501
2.499	.525	.435	.407	.423	.390	.410
2.998	.452	.378	.319	.318	.399	.311
3.496	.383	.411	.264	.204	.290	.389
3.999	.364	.321	.303	.166	.255	.235
4.501	.362	.229	.336	.173	.150	.219
5.010	.353	.223	.275	.191	.118	.210
5.995	.327	.215	.119	.223	.128	.089
8.010	.324	.186	.112	.062	.120	.078
9.848	.324	.182	.099	.060	.046	.073

Table 8. Continued

(b) Configuration 11; $A_e/A_t = 1.750$

NPR	$p/p_{t,j}$ for lower divergent flap at $(y/w)/2 = 0.500$ for x/L_{flap} of—								
	0.100	0.200	0.300	0.400	0.500	0.600	0.700	0.800	0.900
1.999	0.315	0.306	0.240	0.375	0.400	0.470	0.529	0.542	0.559
3.001	.314	.306	.240	.181	.147	.269	.298	.309	.325
3.993	.311	.306	.241	.181	.138	.182	.161	.143	.123
4.991	.310	.306	.240	.181	.137	.183	.160	.143	.123
5.981	.310	.305	.240	.181	.137	.183	.160	.143	.123
6.994	.309	.305	.240	.180	.136	.183	.160	.143	.123
7.965	.309	.305	.240	.180	.136	.183	.160	.143	.123
8.498	.309	.305	.240	.180	.136	.183	.160	.143	.123
8.991	.309	.305	.240	.180	.136	.184	.160	.143	.123
9.485	.309	.305	.240	.180	.136	.184	.160	.142	.123

NPR	$p/p_{t,j}$ for lower divergent flap at $(y/w)/2 = 0.000$ for x/L_{flap} of—								
	0.100	0.200	0.300	0.400	0.500	0.600	0.700	0.800	0.900
1.999	0.310	0.312	0.238	0.384	0.398	0.442	0.500	0.536	0.559
3.001	.309	.310	.239	.181	.192	.255	.277	.297	.311
3.993	.308	.309	.239	.181	.138	.153	.157	.140	.122
4.991	.308	.308	.239	.181	.138	.151	.156	.140	.122
5.981	.308	.308	.239	.180	.138	.148	.156	.140	.122
6.994	.308	.308	.239	.180	.137	.145	.156	.140	.122
7.965	.308	.308	.239	.180	.137	.143	.156	.140	.122
8.498	.308	.308	.239	.179	.137	.142	.156	.140	.122
8.991	.307	.308	.239	.179	.137	.140	.155	.140	.122
9.485	.307	.308	.239	.179	.137	.139	.155	.140	.122

Table 8. Continued

(b) Continued

NPR	$p/p_{t,j}$ for lower divergent flap at $(y/w)/2 = -0.500$ for x/L_{flap} of—								
	0.100	0.200	0.300	0.400	0.500	0.600	0.700	0.800	0.900
1.999	0.306	0.310	0.241	0.382	0.393	0.434	0.484	0.522	0.543
3.001	.308	.310	.240	.181	.136	.223	.256	.335	.387
3.993	.307	.309	.239	.181	.137	.108	.119	.177	.175
4.991	.306	.308	.239	.181	.137	.108	.100	.127	.124
5.981	.305	.308	.239	.181	.137	.108	.098	.127	.119
6.994	.305	.307	.240	.181	.137	.108	.096	.127	.119
7.965	.304	.307	.239	.181	.137	.108	.095	.127	.119
8.498	.304	.307	.239	.181	.137	.108	.094	.126	.119
8.991	.304	.307	.239	.181	.137	.108	.094	.126	.119
9.485	.304	.307	.239	.181	.136	.108	.093	.126	.119

NPR	$p/p_{t,j}$ on shelf at $(y/w)/2 = 0.500$ for x/L shelf of—							
	0.076	0.227	0.379	0.530	0.682	0.833	0.985	1.061
1.999	0.552	0.512	0.506	0.506	0.506	0.505	0.502	0.501
3.001	.384	.390	.351	.348	.330	.348	.334	.324
3.993	.270	.315	.251	.271	.250	.296	.254	.234
4.991	.146	.207	.283	.251	.168	.181	.165	.173
5.981	.146	.106	.203	.255	.198	.134	.121	.164
6.994	.146	.106	.111	.213	.224	.157	.093	.093
7.965	.146	.106	.092	.113	.210	.180	.117	.093
8.498	.146	.106	.090	.104	.166	.176	.136	.104
8.991	.146	.106	.089	.097	.103	.157	.151	.121
9.485	.146	.106	.089	.091	.095	.125	.148	.135

Table 8. Continued

(b) Concluded

NPR	$p/p_{t,j}$ on shelf at $(y/w)/2 = 0.000$ for x/L shelf of—						
	0.076	0.227	0.379	0.530	0.682	0.833	0.985
1.999	0.545	0.514	0.511	0.509	0.507	0.504	0.501
3.001	.385	.401	.309	.371	.316	.360	.334
3.993	.258	.360	.272	.193	.320	.276	.257
4.991	.140	.178	.330	.289	.161	.104	.214
5.981	.140	.119	.202	.288	.238	.145	.151
6.994	.140	.110	.110	.221	.246	.182	.117
7.965	.140	.109	.096	.117	.220	.193	.139
8.498	.140	.109	.091	.107	.166	.189	.150
8.991	.140	.109	.089	.101	.099	.181	.159
9.485	.140	.109	.088	.095	.089	.170	.156

NPR	$p/p_{t,j}$ on shelf at $(y/w)/2 = -0.500$ for x/L shelf of—					
	0.076	0.227	0.379	0.530	0.682	0.833
1.999	0.547	0.516	0.518	0.507	0.511	0.502
3.001	.370	.353	.339	.358	.324	.355
3.993	.277	.314	.261	.241	.266	.294
4.991	.213	.208	.242	.236	.184	.164
5.981	.197	.173	.165	.210	.230	.133
6.994	.178	.152	.135	.155	.206	.190
7.965	.164	.139	.116	.136	.147	.184
8.498	.161	.132	.109	.133	.127	.168
8.991	.160	.127	.102	.111	.108	.140
9.485	.159	.121	.097	.087	.100	.123

Table 8. Continued

(c) Configuration 12; $A_e/A_t = 2.500$

NPR	$p/p_{t,j}$ for lower divergent flap at $(y/w)/2 = 0.500$ for x/L_{flap} of—								
	0.100	0.200	0.300	0.400	0.500	0.600	0.700	0.800	0.900
2.003	0.330	0.353	0.555	0.556	0.517	0.500	0.504	0.520	0.563
3.006	.312	.303	.237	.183	.157	.266	.280	.325	.382
3.999	.311	.303	.236	.178	.135	.147	.200	.201	.199
5.000	.310	.303	.236	.178	.135	.105	.085	.070	.112
6.002	.310	.303	.236	.178	.135	.105	.085	.070	.058
7.006	.309	.303	.236	.178	.135	.105	.085	.070	.058
7.987	.309	.303	.236	.178	.135	.106	.085	.070	.058
9.009	.309	.303	.236	.178	.134	.106	.085	.070	.058
10.030	.308	.303	.236	.178	.134	.106	.085	.069	.056

NPR	$p/p_{t,j}$ for lower divergent flap at $(y/w)/2 = 0.000$ for x/L_{flap} of—								
	0.100	0.200	0.300	0.400	0.500	0.600	0.700	0.800	0.900
2.003	0.325	0.358	0.554	0.559	0.516	0.502	0.504	0.518	0.563
3.006	.306	.305	.240	.193	.166	.275	.283	.313	.363
3.999	.305	.305	.235	.177	.135	.107	.168	.169	.175
5.000	.305	.304	.234	.177	.135	.107	.086	.071	.060
6.002	.306	.303	.234	.176	.134	.107	.086	.071	.059
7.006	.306	.303	.234	.176	.134	.107	.086	.071	.059
7.987	.305	.303	.234	.176	.134	.107	.086	.071	.059
9.009	.305	.303	.234	.175	.134	.106	.086	.071	.059
10.030	.305	.303	.234	.175	.134	.106	.085	.070	.059

Table 8. Continued

(c) Continued

NPR	$p/p_{t,j}$ for lower divergent flap at $(y/w)/2 = -0.500$ for x/L_{flap} of—								
	0.100	0.200	0.300	0.400	0.500	0.600	0.700	0.800	0.900
2.003	0.318	0.354	0.554	0.556	0.516	0.500	0.501	0.513	0.552
3.006	.302	.303	.242	.193	.159	.272	.280	.310	.353
3.999	.302	.302	.237	.177	.134	.105	.084	.160	.206
5.000	.301	.302	.236	.177	.134	.105	.084	.068	.106
6.002	.301	.302	.236	.177	.134	.106	.084	.069	.058
7.006	.301	.301	.236	.177	.134	.106	.084	.069	.058
7.987	.301	.301	.235	.177	.134	.106	.084	.069	.058
9.009	.301	.301	.235	.177	.134	.106	.084	.069	.058
10.030	.301	.301	.235	.177	.134	.106	.084	.069	.058

NPR	$p/p_{t,j}$ on shelf at $(y/w)/2 = 0.500$ for x/L_{shelf} of—							
	0.076	0.227	0.379	0.530	0.682	0.833	0.985	1.061
2.003	0.557	0.505	0.503	0.505	0.505	0.504	0.501	0.500
3.006	.451	.356	.333	.363	.319	.353	.330	.330
3.999	.215	.250	.272	.274	.252	.298	.229	.239
5.000	.125	.182	.292	.210	.161	.268	.230	.185
6.002	.133	.208	.191	.170	.154	.153	.218	.201
7.006	.070	.142	.194	.160	.133	.117	.132	.148
7.987	.070	.064	.147	.190	.141	.107	.079	.107
9.009	.070	.049	.081	.154	.189	.136	.071	.096
10.030	.070	.049	.075	.089	.161	.117	.121	.081

Table 8. Concluded

(c) Concluded

NPR	$p/p_{t,j}$ on shelf at $(y/w)/2 = 0.000$ for x/L_{shelf} of—						
	0.076	0.227	0.379	0.530	0.682	0.833	0.985
2.003	0.542	0.504	0.509	0.508	0.505	0.502	0.499
3.006	.448	.358	.324	.372	.322	.348	.327
3.999	.224	.336	.254	.308	.227	.305	.232
5.000	.116	.296	.269	.218	.175	.190	.208
6.002	.132	.186	.240	.211	.150	.132	.198
7.006	.068	.140	.197	.218	.135	.118	.126
7.987	.068	.075	.135	.235	.182	.082	.092
9.009	.068	.049	.102	.116	.230	.130	.060
10.030	.067	.048	.070	.093	.155	.210	.093

NPR	$p/p_{t,j}$ on shelf at $(y/w)/2 = -0.500$ for x/L_{shelf} of—					
	0.076	0.227	0.379	0.530	0.682	0.833
2.003	0.553	0.508	0.518	0.505	0.510	0.501
3.006	.444	.349	.371	.358	.335	.347
3.999	.336	.281	.261	.269	.258	.254
5.000	.257	.219	.211	.206	.206	.203
6.002	.116	.194	.184	.172	.170	.167
7.006	.104	.149	.159	.150	.146	.143
7.987	.098	.127	.137	.132	.128	.124
9.009	.095	.101	.119	.118	.117	.111
10.030	.085	.083	.101	.107	.107	.106

Table 9. Nozzle Internal Static Pressure Ratios for Dry Power Sawtooth Configurations

(a) Configuration 13; $A_e/A_t = 1.100$

NPR	$p/p_{t,j}$ for upper divergent flap at $(y/w)/2 = -0.500$ for x/L_{flap} of—								
	0.100	0.200	0.300	0.400	0.500	0.600	0.700	0.800	0.900
2.000	0.502	0.370	0.251	0.323	0.315	0.293	0.407	0.486	0.504
2.501	.502	.370	.252	.321	.314	.293	.262	.250	.372
3.092	.501	.370	.252	.320	.313	.293	.261	.251	.213
3.502	.501	.370	.252	.319	.312	.293	.261	.252	.213
3.992	.500	.370	.252	.318	.312	.293	.260	.252	.212
4.500	.500	.370	.252	.317	.312	.293	.260	.253	.212
5.004	.500	.370	.252	.316	.312	.292	.260	.253	.211
6.002	.501	.371	.251	.316	.312	.292	.260	.253	.211
7.994	.501	.372	.251	.314	.311	.292	.259	.253	.210
10.020	.501	.372	.251	.314	.311	.293	.259	.253	.210
11.315	.500	.373	.252	.313	.311	.293	.259	.253	.211

NPR	$p/p_{t,j}$ for lower divergent flap at—								
	$(y/w)/2 = 0.500$ for x/L_{flap} of—			$(y/w)/2 = 0.000$ for x/L_{flap} of—			$(y/w)/2 = -0.500$ for x/L_{flap} of—		
	0.500	0.700	0.900	0.500	0.700	0.900	0.500	0.700	0.900
2.000	0.264	0.410	0.503	0.259	0.417	0.474	0.269	0.415	0.479
2.501	.265	.258	.415	.259	.258	.408	.269	.261	.415
3.092	.265	.257	.249	.259	.257	.245	.268	.259	.253
3.502	.265	.255	.248	.259	.257	.242	.268	.257	.251
3.992	.265	.254	.248	.259	.256	.238	.267	.255	.251
4.500	.265	.252	.247	.258	.255	.232	.267	.253	.250
5.004	.264	.250	.247	.258	.254	.230	.267	.250	.250
6.002	.264	.245	.246	.258	.253	.229	.267	.246	.250
7.994	.264	.237	.246	.258	.252	.228	.266	.236	.250
10.020	.264	.229	.245	.258	.251	.227	.267	.227	.250
11.315	.265	.224	.246	.258	.251	.227	.267	.221	.250

Table 9. Continued

(a) Concluded

NPR	$p/p_{t,j}$ on shelf at $(y/w)/2 = -0.500$ for x/L_{shelf} of—						
	0.076	0.227	0.379	0.530	0.682	0.833	0.985
2.000	0.554	0.522	0.518	0.506	0.506	0.506	0.498
2.501	.470	.384	.435	.392	.407	.411	.395
3.092	.464	.325	.343	.348	.355	.321	.323
3.502	.339	.373	.234	.270	.353	.316	.259
3.992	.300	.313	.244	.236	.237	.297	.241
4.500	.275	.300	.256	.205	.199	.281	.246
5.004	.264	.203	.214	.134	.209	.213	.215
6.002	.261	.175	.204	.106	.128	.207	.234
7.994	.262	.151	.094	.084	.059	.141	.180
10.020	.264	.151	.090	.038	.045	.061	.105
11.315	.264	.151	.090	.038	.048	.049	.083

Table 9. Continued

(b) Configuration 14; $A_e/A_t = 1.750$

NPR	$p/p_{t,j}$ for upper divergent flap at $(y/w)/2 = -0.500$ for x/L_{flap} of—								
	0.100	0.200	0.300	0.400	0.500	0.600	0.700	0.800	0.900
2.000	0.363	0.301	0.443	0.442	0.442	0.446	0.454	0.464	0.476
3.007	.364	.301	.210	.146	.176	.165	.148	.269	.362
3.999	.362	.302	.211	.146	.175	.165	.142	.130	.222
5.011	.361	.301	.211	.146	.175	.165	.141	.128	.112
6.002	.360	.302	.211	.146	.174	.165	.141	.129	.105
7.017	.359	.302	.210	.146	.174	.164	.141	.129	.105
8.008	.359	.302	.210	.146	.173	.164	.140	.129	.105
8.414	.359	.302	.210	.146	.173	.164	.141	.129	.105
9.000	.359	.302	.210	.146	.173	.164	.141	.129	.105
10.000	.359	.302	.210	.146	.172	.164	.141	.129	.105
11.205	.359	.302	.210	.146	.171	.164	.141	.129	.104

NPR	$p/p_{t,j}$ for lower divergent flap at—								
	$(y/w)/2 = 0.500$ for x/L_{flap} of—			$(y/w)/2 = 0.000$ for x/L_{flap} of—			$(y/w)/2 = -0.500$ for x/L_{flap} of—		
	0.500	0.700	0.900	0.500	0.700	0.900	0.500	0.700	0.900
2.000	0.419	0.515	0.525	0.454	0.512	0.523	0.423	0.516	0.527
3.007	.179	.242	.315	.187	.272	.296	.180	.264	.309
3.999	.180	.140	.206	.187	.135	.220	.180	.137	.195
5.011	.180	.140	.108	.187	.135	.109	.180	.138	.108
6.002	.180	.140	.108	.187	.135	.107	.180	.138	.108
7.017	.180	.140	.108	.187	.135	.104	.179	.138	.108
8.008	.179	.140	.108	.187	.134	.103	.179	.138	.108
8.414	.179	.140	.108	.187	.134	.102	.179	.138	.108
9.000	.179	.139	.108	.186	.134	.101	.179	.138	.108
10.000	.179	.139	.108	.186	.134	.099	.179	.138	.108
11.205	.179	.139	.108	.186	.134	.097	.179	.138	.108

Table 9. Continued

(b) Concluded

NPR	$p/p_{t,j}$ on shelf at $(y/w)/2 = -0.500$ for x/L_{shelf} of—						
	0.076	0.227	0.379	0.530	0.682	0.833	0.985
2.000	0.521	0.508	0.515	0.505	0.504	0.504	0.497
3.007	.381	.341	.356	.353	.339	.339	.334
3.999	.307	.250	.259	.306	.223	.257	.262
5.011	.169	.260	.234	.205	.173	.192	.248
6.002	.145	.171	.257	.264	.134	.122	.145
7.017	.123	.152	.135	.215	.210	.104	.119
8.008	.119	.143	.116	.151	.198	.156	.092
8.414	.118	.138	.109	.139	.159	.161	.105
9.000	.118	.124	.103	.097	.132	.165	.107
10.000	.118	.101	.093	.085	.111	.125	.114
11.205	.118	.092	.087	.072	.070	.092	.109

Table 9. Concluded

(c) Configuration 15; $A_e/A_t = 2.500$

NPR	$p/p_{t,j}$ for upper divergent flap at $(y/w)/2 = -0.500$ for x/L_{flap} of—								
	0.100	0.200	0.300	0.400	0.500	0.600	0.700	0.800	0.900
2.003	0.490	0.488	0.487	0.486	0.486	0.486	0.489	0.491	0.490
3.006	.202	.200	.303	.313	.312	.312	.315	.316	.319
3.996	.202	.199	.150	.111	.093	.176	.247	.321	.253
6.003	.200	.199	.150	.110	.083	.066	.095	.091	.149
8.008	.199	.198	.150	.110	.083	.066	.094	.092	.076
9.000	.199	.198	.150	.110	.083	.066	.094	.092	.076
10.013	.198	.198	.150	.110	.083	.066	.094	.092	.076
11.851	.199	.198	.150	.110	.083	.066	.094	.092	.076

NPR	$p/p_{t,j}$ for lower divergent flap at—								
	$(y/w)/2 = 0.500$ for x/L_{flap} of—			$(y/w)/2 = 0.000$ for x/L_{flap} of—			$(y/w)/2 = -0.500$ for x/L_{flap} of—		
	0.500	0.700	0.900	0.500	0.700	0.900	0.500	0.700	0.900
2.003	0.492	0.498	0.535	0.492	0.498	0.538	0.492	0.496	0.538
3.006	.248	.252	.295	.270	.265	.299	.249	.252	.295
3.996	.109	.181	.229	.110	.201	.221	.110	.181	.231
6.003	.110	.067	.106	.110	.067	.115	.110	.067	.108
8.008	.110	.067	.045	.110	.067	.053	.110	.067	.046
9.000	.110	.067	.045	.110	.067	.052	.109	.067	.046
10.013	.110	.067	.045	.110	.067	.051	.109	.067	.046
11.851	.109	.067	.045	.110	.067	.050	.109	.067	.046

NPR	$p/p_{t,j}$ on shelf at $(y/w)/2 = -0.500$ for x/L_{shelf} of—							
	0.076	0.227	0.379	0.530	0.682	0.833	0.985	
2.003	0.524	0.507	0.515	0.504	0.504	0.504	0.496	
3.006	.371	.377	.371	.358	.347	.339	.330	
3.996	.277	.277	.260	.255	.254	.252	.250	
6.003	.207	.184	.170	.168	.170	.173	.165	
8.008	.102	.129	.134	.130	.132	.113	.122	
9.000	.102	.116	.116	.123	.112	.108	.105	
10.013	.101	.099	.100	.104	.107	.100	.093	
11.851	.096	.082	.079	.081	.091	.094	.089	

Table 10. Nozzle Internal Static Pressure Ratios for A/B Power Sawtooth Configurations

(a) Configuration 16; $A_e/A_t = 1.100$

NPR	$p/p_{t,j}$ for upper divergent flap at $(y/w)/2 = -0.500$ for x/L_{flap} of—								
	0.100	0.200	0.300	0.400	0.500	0.600	0.700	0.800	0.900
2.005	0.531	0.431	0.313	0.226	0.334	0.323	0.337	0.500	0.515
2.501	.529	.430	.313	.225	.332	.323	.297	.291	.331
3.003	.529	.430	.314	.225	.330	.323	.296	.292	.256
3.504	.528	.430	.313	.225	.329	.323	.296	.293	.255
4.000	.528	.430	.313	.225	.328	.323	.295	.293	.254
4.502	.527	.430	.313	.225	.327	.322	.295	.293	.254
5.001	.527	.430	.313	.225	.326	.322	.294	.293	.254
5.503	.527	.431	.313	.225	.325	.322	.294	.293	.253
6.002	.527	.431	.313	.225	.325	.322	.294	.293	.253
8.004	.527	.431	.313	.225	.324	.322	.293	.293	.253
8.929	.527	.432	.313	.224	.323	.322	.293	.293	.253

NPR	$p/p_{t,j}$ for lower divergent flap at $(y/w)/2 = 0.500$ for x/L_{flap} of—								
	0.100	0.200	0.300	0.400	0.500	0.600	0.700	0.800	0.900
2.005	0.339	0.392	0.393	0.359	0.312	0.267	0.430	0.464	0.508
2.501	.338	.392	.393	.358	.312	.267	.230	.348	.399
3.003	.337	.391	.393	.358	.311	.267	.230	.199	.282
3.504	.335	.391	.393	.358	.311	.267	.230	.199	.253
4.000	.335	.391	.394	.358	.311	.267	.229	.198	.252
4.502	.334	.391	.394	.358	.311	.267	.229	.198	.251
5.001	.334	.390	.394	.358	.310	.267	.229	.198	.251
5.503	.333	.390	.394	.358	.310	.267	.229	.198	.251
6.002	.333	.390	.394	.358	.310	.267	.228	.198	.251
8.004	.332	.390	.394	.358	.310	.267	.228	.197	.250
8.929	.332	.390	.394	.358	.310	.267	.228	.197	.250

Table 10. Continued

(a) Continued

NPR	$p/p_{t,j}$ for lower divergent flap at $(y/w)/2 = 0.000$ for x/L_{flap} of—								
	0.100	0.200	0.300	0.400	0.500	0.600	0.700	0.800	0.900
2.005	0.341	0.415	0.396	0.349	0.305	0.359	0.438	0.453	0.484
2.501	.340	.413	.394	.349	.304	.264	.226	.357	.408
3.003	.338	.412	.391	.349	.304	.264	.225	.258	.265
3.504	.337	.411	.390	.349	.304	.264	.225	.256	.265
4.000	.337	.411	.390	.348	.304	.263	.225	.254	.265
4.502	.337	.410	.389	.348	.304	.263	.225	.251	.265
5.001	.337	.410	.389	.347	.304	.262	.224	.249	.265
5.503	.337	.409	.389	.347	.304	.262	.224	.248	.264
6.002	.337	.409	.388	.347	.304	.262	.224	.246	.264
8.004	.336	.408	.388	.346	.304	.261	.224	.237	.264
8.929	.336	.408	.388	.347	.304	.261	.224	.234	.264

NPR	$p/p_{t,j}$ for lower divergent flap at $(y/w)/2 = -0.500$ for x/L_{flap} of—								
	0.100	0.200	0.300	0.400	0.500	0.600	0.700	0.800	0.900
2.005	0.327	0.397	0.402	0.360	0.310	0.269	0.428	0.459	0.501
2.501	.327	.396	.400	.359	.310	.269	.227	.352	.398
3.003	.327	.395	.399	.359	.310	.268	.227	.197	.297
3.504	.326	.394	.399	.358	.310	.268	.227	.198	.257
4.000	.325	.394	.398	.358	.310	.268	.227	.198	.256
4.502	.324	.393	.398	.358	.309	.268	.227	.198	.256
5.001	.324	.393	.398	.358	.309	.267	.227	.198	.256
5.503	.324	.392	.397	.358	.309	.267	.227	.197	.256
6.002	.324	.392	.397	.358	.309	.267	.227	.197	.255
8.004	.323	.391	.397	.358	.309	.267	.227	.197	.255
8.929	.323	.391	.397	.358	.309	.267	.227	.197	.255

Table 10. Continued

(a) Concluded

NPR	$p/p_{t,j}$ on shelf at $(y/w)/2 = 0.000$ for x/L_{shelf} of—						
	0.076	0.227	0.379	0.530	0.682	0.833	0.985
2.005	0.563	0.522	0.509	0.506	0.506	0.504	0.496
2.501	.486	.445	.408	.432	.396	.423	.395
3.003	.462	.367	.281	.331	.403	.271	.331
3.504	.373	.422	.236	.246	.320	.373	.247
4.000	.346	.337	.251	.184	.205	.342	.288
4.502	.325	.248	.259	.137	.235	.222	.259
5.001	.313	.232	.248	.123	.211	.204	.256
5.503	.308	.219	.254	.127	.105	.223	.235
6.002	.304	.207	.127	.132	.082	.217	.225
8.004	.303	.188	.110	.056	.068	.077	.144
8.929	.304	.184	.107	.051	.056	.042	.110

Table 10. Continued

(b) Configuration 17; $A_e/A_t = 1.750$

NPR	$p/p_{t,j}$ for upper divergent flap at $(y/w)/2 = -0.500$ for x/L_{flap} of—								
	0.100	0.200	0.300	0.400	0.500	0.600	0.700	0.800	0.900
1.999	0.341	0.326	0.247	0.343	0.499	0.498	0.500	0.522	0.504
3.007	.340	.325	.248	.182	.293	.294	.300	.307	.310
3.997	.338	.325	.248	.182	.135	.110	.153	.164	.225
4.998	.336	.326	.248	.182	.135	.110	.152	.149	.126
6.002	.335	.326	.248	.181	.135	.110	.152	.150	.122
7.004	.335	.326	.248	.181	.135	.110	.151	.150	.122
7.995	.335	.326	.248	.181	.134	.110	.151	.151	.122
8.497	.335	.326	.248	.181	.134	.110	.151	.151	.122
8.999	.335	.327	.248	.181	.134	.110	.151	.151	.122
9.729	.335	.327	.248	.181	.134	.110	.150	.151	.122

NPR	$p/p_{t,j}$ for lower divergent flap at $(y/w)/2 = 0.500$ for x/L_{flap} of—								
	0.100	0.200	0.300	0.400	0.500	0.600	0.700	0.800	0.900
1.999	0.316	0.306	0.323	0.406	0.407	0.416	0.432	0.452	0.474
3.007	.315	.306	.237	.179	.145	.251	.273	.290	.310
3.997	.313	.305	.237	.179	.137	.162	.154	.139	.189
4.998	.312	.305	.237	.179	.137	.162	.153	.139	.126
6.002	.312	.305	.237	.179	.137	.162	.153	.139	.126
7.004	.311	.305	.237	.179	.136	.162	.153	.139	.125
7.995	.311	.305	.237	.179	.136	.162	.153	.139	.125
8.497	.310	.305	.237	.179	.136	.162	.153	.139	.125
8.999	.310	.305	.237	.179	.136	.162	.153	.139	.125
9.729	.310	.305	.237	.179	.136	.162	.153	.139	.125

Table 10. Continued

(b) Continued

NPR	$p/p_{t,j}$ for lower divergent flap at $(y/w)/2 = 0.000$ for x/L_{flap} of—								
	0.100	0.200	0.300	0.400	0.500	0.600	0.700	0.800	0.900
1.999	0.309	0.310	0.245	0.382	0.390	0.412	0.452	0.485	0.514
3.007	.308	.309	.240	.179	.146	.183	.284	.295	.326
3.997	.308	.308	.239	.180	.143	.169	.149	.131	.229
4.998	.308	.308	.237	.179	.141	.169	.149	.131	.116
6.002	.308	.307	.236	.179	.140	.169	.148	.131	.116
7.004	.308	.307	.236	.179	.139	.168	.148	.131	.116
7.995	.307	.307	.236	.179	.139	.168	.148	.131	.115
8.497	.307	.307	.236	.178	.139	.167	.148	.131	.115
8.999	.307	.307	.236	.178	.138	.167	.148	.131	.115
9.729	.307	.307	.236	.178	.138	.167	.147	.131	.115

NPR	$p/p_{t,j}$ for lower divergent flap at $(y/w)/2 = -0.500$ for x/L_{flap} of—								
	0.100	0.200	0.300	0.400	0.500	0.600	0.700	0.800	0.900
1.999	0.306	0.311	0.241	0.371	0.505	0.495	0.496	0.504	0.511
3.007	.306	.310	.241	.182	.152	.257	.275	.290	.306
3.997	.306	.309	.241	.181	.137	.160	.148	.135	.196
4.998	.305	.309	.240	.181	.137	.160	.148	.135	.124
6.002	.304	.309	.240	.181	.138	.159	.148	.135	.124
7.004	.304	.309	.240	.181	.138	.159	.148	.135	.123
7.995	.303	.308	.240	.181	.137	.158	.148	.135	.123
8.497	.303	.308	.240	.181	.137	.158	.148	.135	.123
8.999	.303	.308	.240	.181	.137	.158	.148	.135	.123
9.729	.303	.308	.240	.181	.137	.158	.148	.135	.123

Table 10. Continued

(b) Concluded

NPR	$p/p_{t,j}$ on shelf at $(y/w)/2 = 0.000$ for x/L_{shelf} of—						
	0.076	0.227	0.379	0.530	0.682	0.833	0.985
1.999	0.514	0.509	0.504	0.504	0.504	0.503	0.500
3.007	.370	.373	.364	.340	.331	.343	.332
3.997	.276	.312	.275	.239	.312	.235	.242
4.998	.203	.205	.336	.174	.173	.152	.201
6.002	.175	.165	.177	.304	.141	.153	.138
7.004	.154	.142	.156	.150	.227	.128	.107
7.995	.151	.123	.107	.125	.201	.164	.124
8.497	.151	.115	.099	.118	.142	.166	.139
8.999	.151	.107	.093	.112	.111	.157	.130
9.729	.151	.098	.085	.108	.093	.119	.126

Table 10. Continued

(c) Configuration 18; $A_e/A_t = 2.500$

NPR	$p/p_{t,j}$ for upper divergent flap at $(y/w)/2 = -0.500$ for x/L_{flap} of—								
	0.100	0.200	0.300	0.400	0.500	0.600	0.700	0.800	0.900
1.996	0.496	0.493	0.493	0.493	0.492	0.492	0.494	0.495	0.494
3.001	.157	.182	.165	.231	.258	.331	.351	.365	.341
3.999	.157	.182	.153	.124	.128	.185	.252	.311	.243
4.999	.156	.181	.153	.124	.095	.079	.103	.165	.253
5.997	.156	.181	.153	.123	.095	.079	.132	.136	.149
7.000	.156	.181	.153	.123	.095	.079	.064	.110	.124
7.999	.156	.181	.153	.123	.095	.079	.064	.057	.105
8.998	.156	.181	.153	.123	.095	.079	.064	.057	.091
10.017	.156	.181	.153	.123	.095	.079	.064	.057	.052
10.119	.155	.181	.153	.123	.095	.079	.064	.057	.048

NPR	$p/p_{t,j}$ for lower divergent flap at $(y/w)/2 = 0.500$ for x/L_{flap} of—								
	0.100	0.200	0.300	0.400	0.500	0.600	0.700	0.800	0.900
1.996	0.331	0.356	0.564	0.553	0.515	0.499	0.503	0.514	0.549
3.001	.312	.304	.236	.177	.245	.267	.309	.330	.380
3.999	.310	.303	.237	.178	.135	.110	.195	.203	.227
4.999	.310	.303	.236	.178	.135	.105	.085	.153	.157
5.997	.310	.303	.236	.178	.135	.106	.085	.070	.108
7.000	.310	.303	.236	.178	.135	.106	.085	.070	.059
7.999	.309	.303	.236	.178	.135	.106	.085	.070	.059
8.998	.309	.303	.236	.178	.135	.106	.085	.070	.059
10.017	.309	.303	.236	.178	.135	.106	.085	.070	.058
10.119	.309	.303	.236	.178	.135	.106	.085	.070	.058

Table 10. Continued

(c) Continued

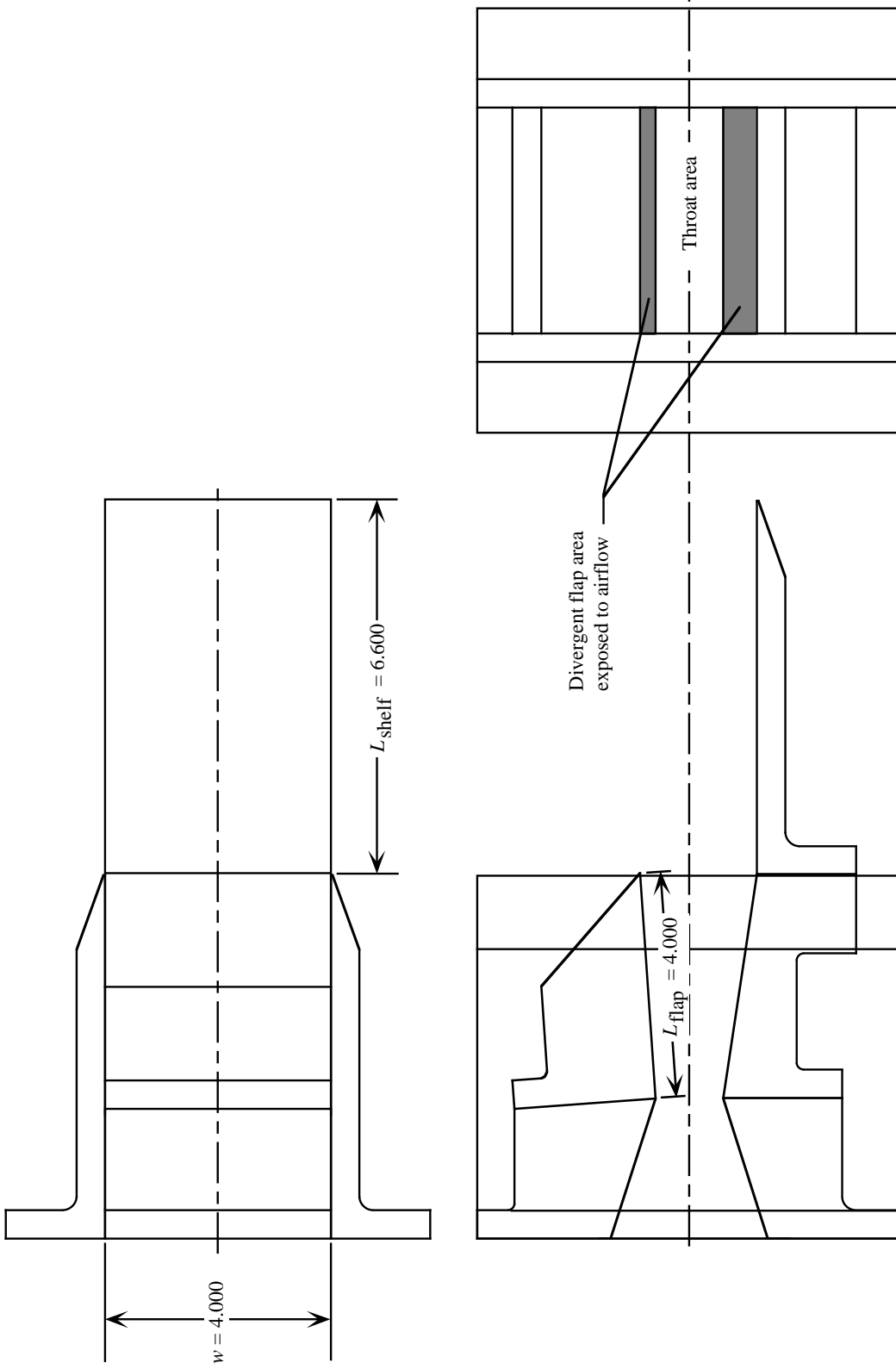
NPR	$p/p_{t,j}$ for lower divergent flap at $(y/w)/2 = 0.000$ for x/L_{flap} of—								
	0.100	0.200	0.300	0.400	0.500	0.600	0.700	0.800	0.900
1.996	0.325	0.361	0.560	0.555	0.516	0.503	0.504	0.516	0.560
3.001	.308	.306	.237	.176	.284	.289	.296	.307	.326
3.999	.307	.305	.235	.176	.135	.191	.212	.216	.225
4.999	.308	.305	.233	.176	.135	.107	.092	.164	.166
5.997	.308	.305	.232	.176	.135	.107	.086	.071	.126
7.000	.307	.304	.232	.176	.135	.107	.086	.071	.059
7.999	.307	.304	.231	.175	.134	.107	.086	.071	.059
8.998	.307	.305	.231	.175	.134	.106	.085	.071	.059
10.017	.307	.305	.231	.175	.134	.106	.085	.070	.059
10.119	.307	.305	.231	.175	.134	.106	.085	.070	.059

NPR	$p/p_{t,j}$ for lower divergent flap at $(y/w)/2 = -0.500$ for x/L_{flap} of—								
	0.100	0.200	0.300	0.400	0.500	0.600	0.700	0.800	0.900
1.996	0.322	0.356	0.564	0.554	0.516	0.503	0.503	0.513	0.551
3.001	.306	.304	.238	.178	.224	.265	.314	.336	.391
3.999	.305	.303	.237	.178	.134	.107	.189	.197	.228
4.999	.304	.303	.237	.177	.135	.107	.084	.146	.151
5.997	.304	.302	.236	.177	.135	.107	.084	.069	.106
7.000	.304	.302	.236	.177	.135	.106	.084	.069	.058
7.999	.303	.302	.236	.177	.135	.106	.084	.069	.058
8.998	.303	.302	.236	.177	.134	.106	.084	.069	.058
10.017	.303	.302	.236	.177	.134	.106	.084	.069	.058
10.119	.303	.302	.236	.177	.134	.106	.084	.069	.058

Table 10. Concluded

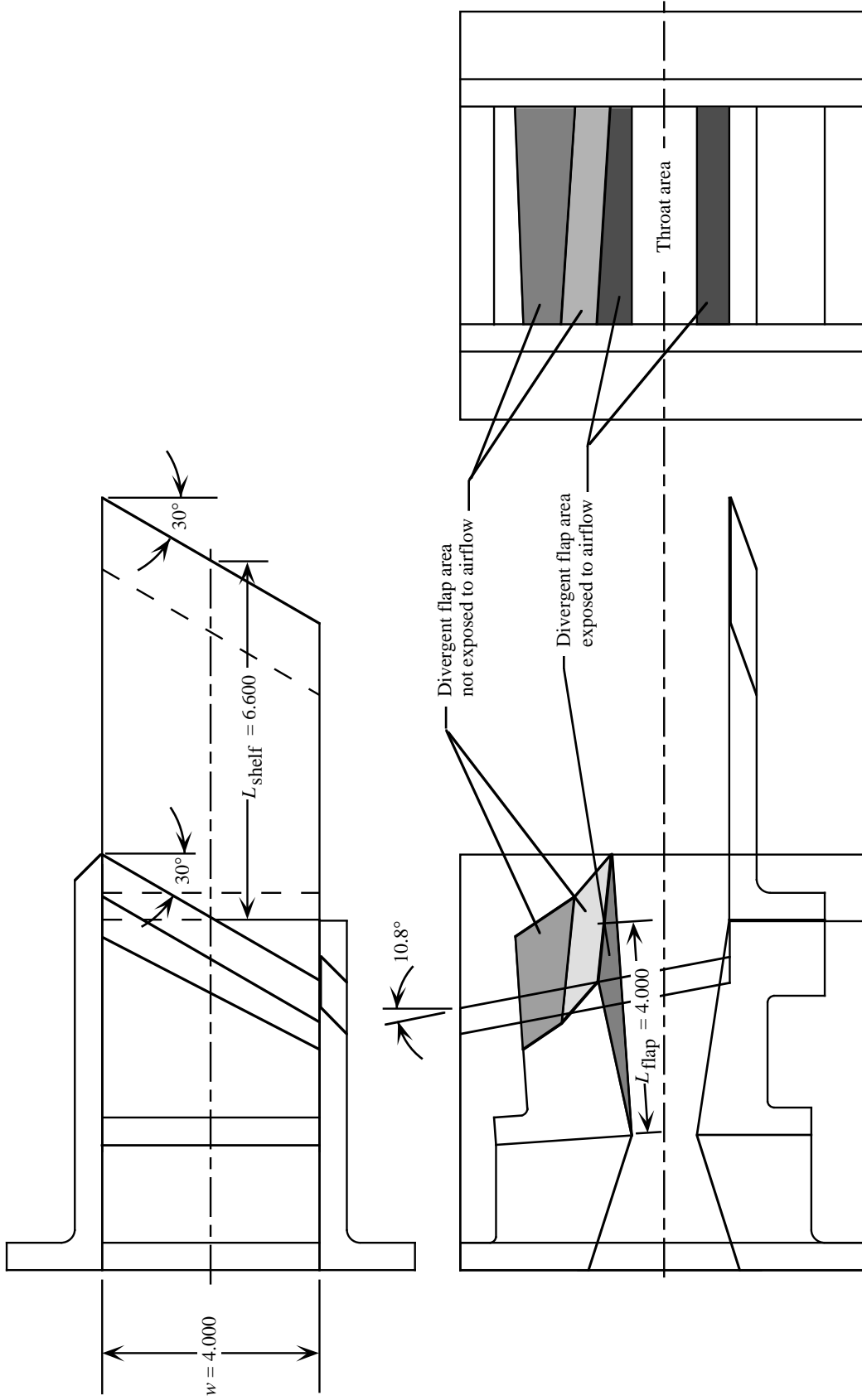
(c) Concluded

NPR	$p/p_{t,j}$ on shelf at $(y/w)/2 = 0.000$ for x/L_{shelf} of—						
	0.076	0.227	0.379	0.530	0.682	0.833	0.985
1.996	0.545	0.511	0.505	0.507	0.507	0.506	0.498
3.001	.370	.353	.338	.337	.335	.333	.331
3.999	.300	.285	.279	.248	.273	.245	.251
4.999	.222	.255	.236	.202	.216	.192	.202
5.997	.139	.198	.155	.173	.168	.172	.171
7.000	.100	.184	.160	.130	.137	.135	.144
7.999	.095	.128	.130	.143	.120	.115	.122
8.998	.090	.101	.117	.118	.119	.111	.105
10.017	.086	.085	.106	.102	.112	.107	.096
10.119	.085	.083	.105	.101	.119	.107	.098



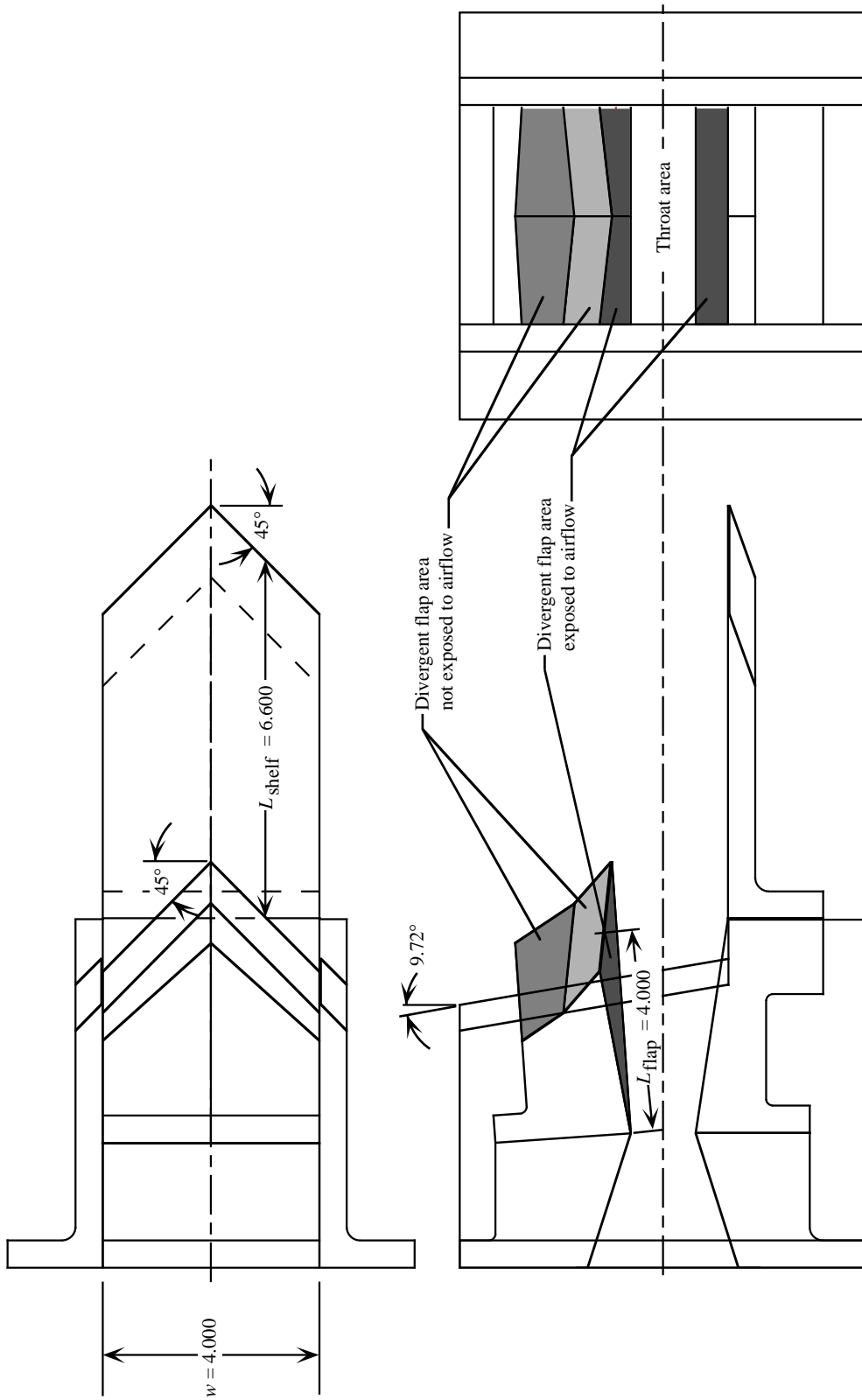
(a) Baseline configurations (dry subsonic acceleration).

Figure 2. Three planview sketches of configurations. Left sidewall shown as transparent with some hidden lines excluded for clarity; linear dimensions are in inches.



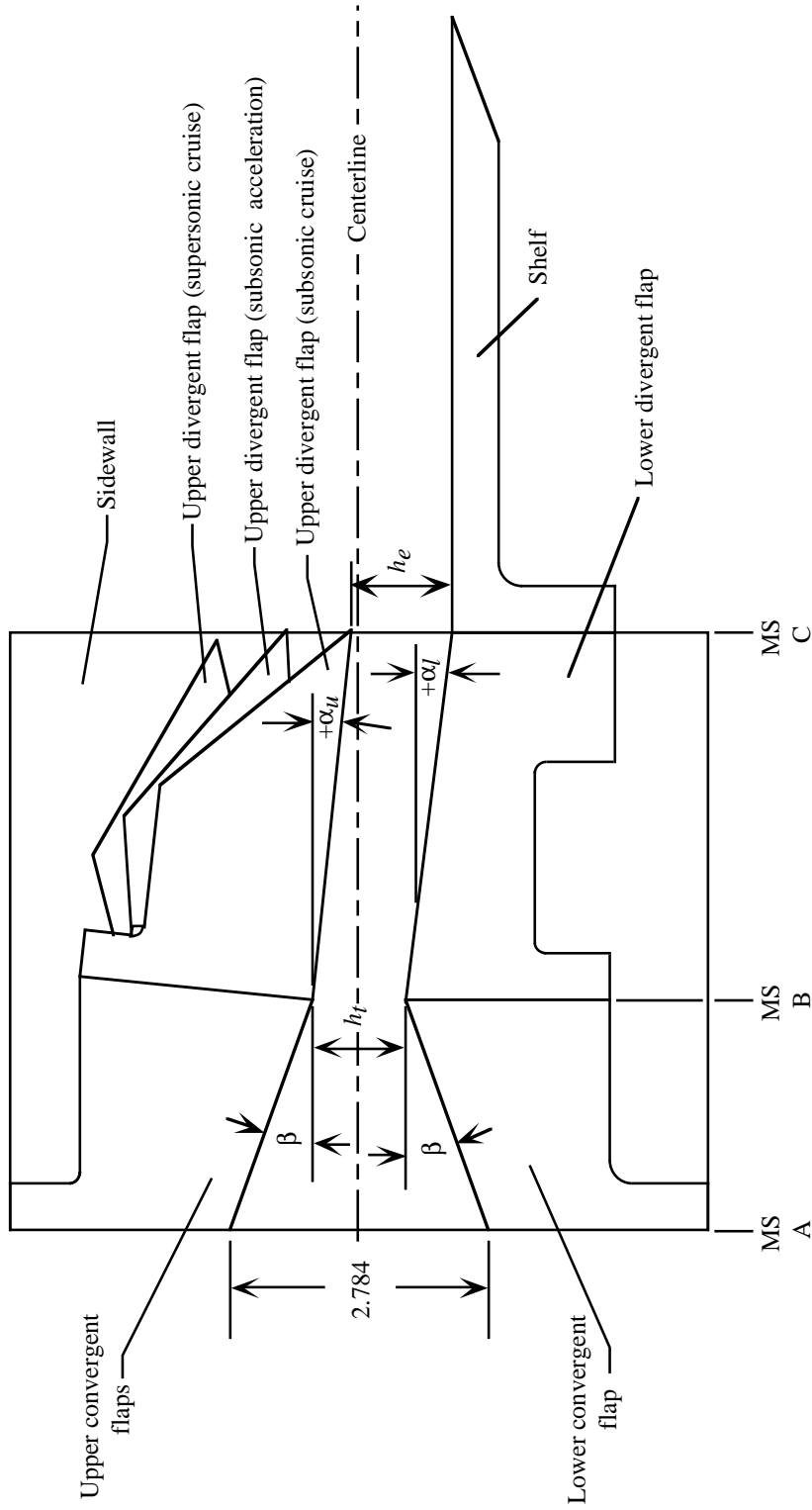
(b) Scarfed configurations (dry subsonic acceleration).

Figure 2. Continued.



(c) Sawtooth configurations (dry subsonic acceleration).

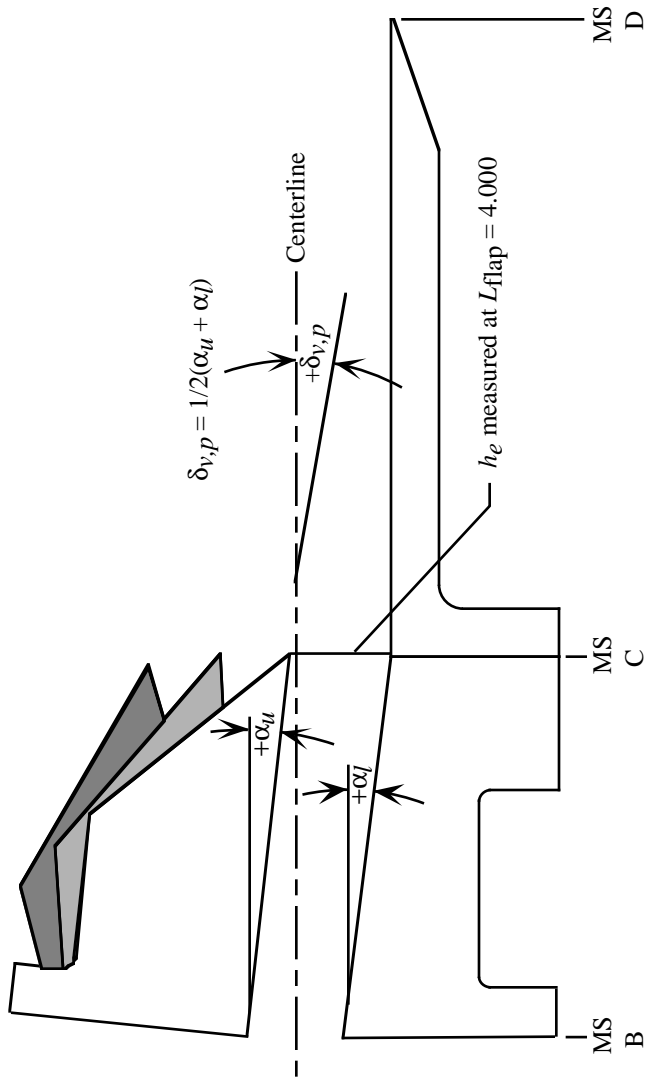
Figure 2. Concluded.



	Dry power			A/B power		
	Subsonic cruise	Subsonic acceleration	Supersonic cruise	Subsonic cruise	Subsonic acceleration	Supersonic cruise
MS A	41.845	41.845	41.845	41.845	41.845	41.845
MS B	44.296	44.296	44.296	44.330	44.330	44.330
MS C	48.265	48.265	48.265	48.285	48.285	48.285
h_t	1.000	1.000	1.000	1.200	1.200	1.200
h_e	1.100	1.750	2.500	1.320	2.100	3.000
β	20.00°	20.00°	20.00°	17.67°	17.67°	17.67°
α_l	7.18°	7.18°	7.18°	8.60°	8.60°	8.60°

(a) Parameters common to all configurations.

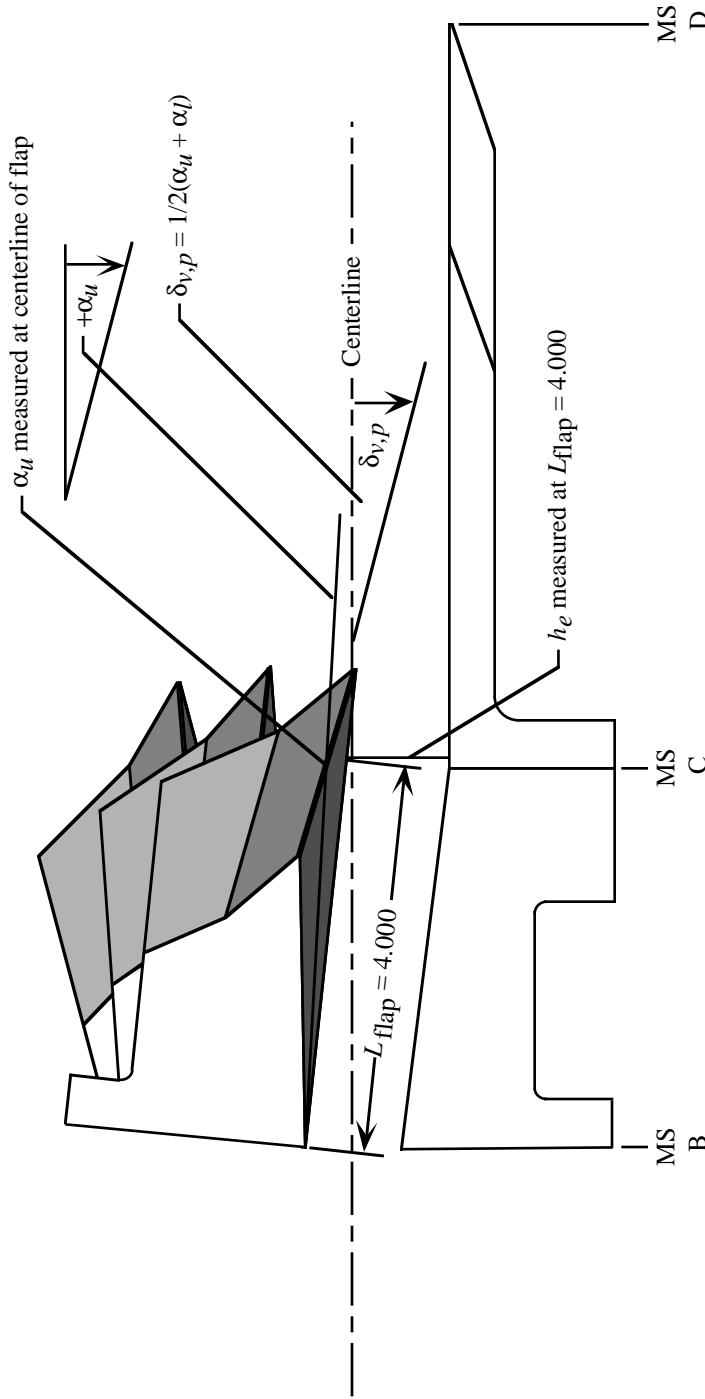
Figure 3. Shelf nozzle model parts and design parameters. Left sidewall removed; linear dimensions are in inches.



	Dry power			A/B power		
	Subsonic cruise	Subsonic acceleration Config 2	Supersonic cruise Config 3	Subsonic cruise Config 4	Subsonic acceleration Config 5	Supersonic cruise Config 6
MS B	44.296	44.296	44.296	44.330	44.330	44.330
MS C	48.265	48.265	48.265	48.285	48.285	48.285
MS D	54.865	54.865	54.865	54.885	54.885	54.885
α_u	5.76°	-3.54°	-14.66°	7.00°	-4.00°	-18.00°
α_l	7.18°	7.18°	7.18°	8.60°	8.60°	8.60°
$\delta_{v,p}$	6.47°	1.82°	-3.74°	7.80°	2.30°	-4.70°

(b) Parameters for baseline configurations.

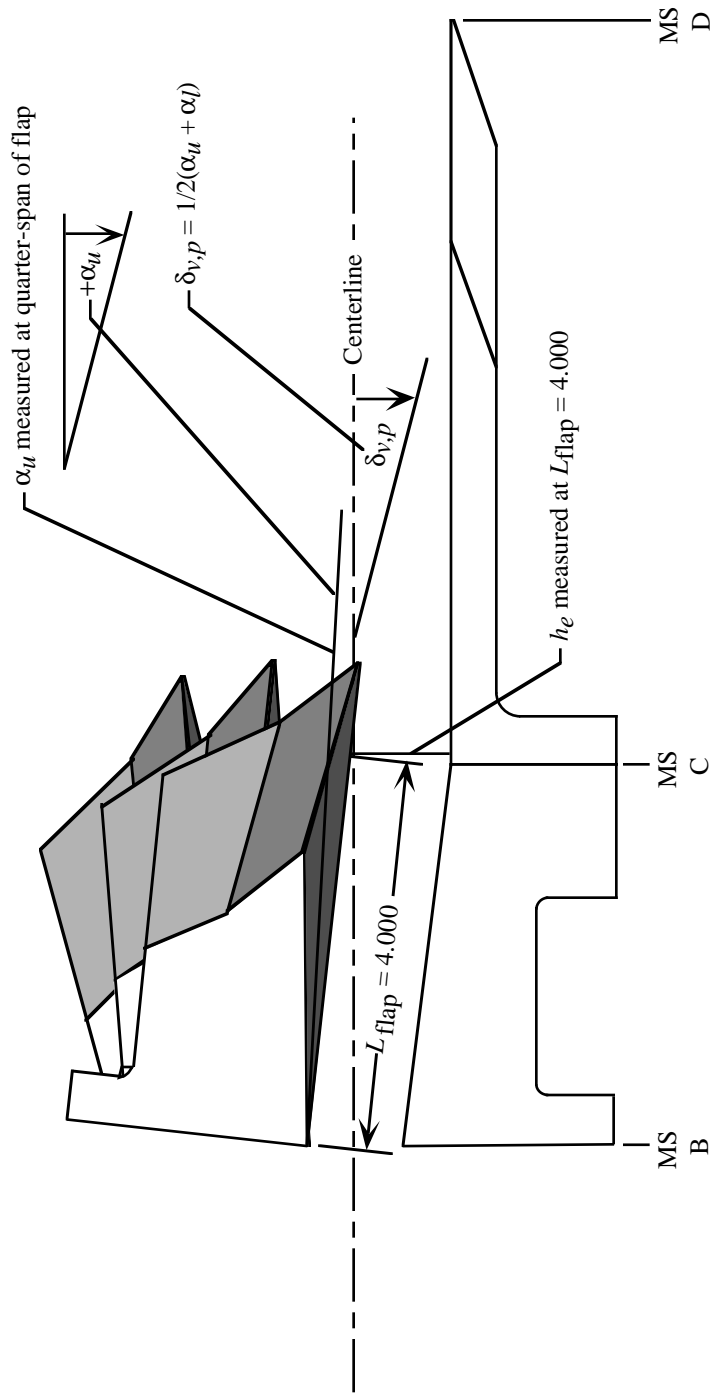
Figure 3. Continued.



	Dry power			A/B power		
	Subsonic cruise Config 7	Subsonic acceleration Config 8	Supersonic cruise Config 9	Subsonic cruise Config 10	Subsonic acceleration Config 11	Supersonic cruise Config 12
MS B	44.296	44.296	44.296	44.330	44.330	44.330
MS C	48.265	48.265	48.265	48.285	48.285	48.285
MS D	56.020	56.020	56.020	56.040	56.040	56.040
α_u	2.82°	-6.48°	-17.60°	4.06°	-6.94°	-20.94°
α_l	7.18°	7.18°	7.18°	8.60°	8.60°	8.60°
$\delta_{v,p}$	5.00°	0.35°	-5.21°	6.33°	0.83°	-6.17°

(c) Parameters for scarfed configurations.

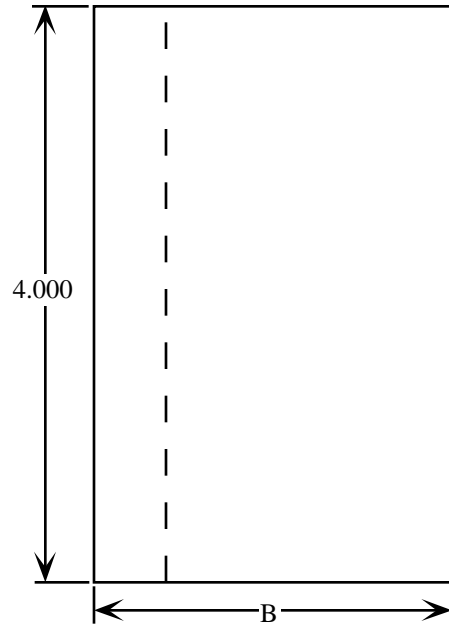
Figure 3. Continued.



	Dry power				A/B power			
	Subsonic cruise Config 13	Subsonic acceleration Config 14	Supersonic cruise Config 15	Subsonic cruise Config 16	Subsonic acceleration Config 17	Supersonic cruise Config 18		
MS B	44.296	44.296	44.296	44.330	44.330	44.330		
MS C	48.265	48.265	48.265	48.285	48.285	48.285		
MS D	55.865	55.865	55.865	55.885	55.885	55.885		
α_u	3.21°	-6.09°	-17.21°	4.45°	-6.55°	-20.55°		
α_l	7.18°	7.18°	7.18°	8.60°	8.60°	8.60°		
$\delta_{v,p}$	5.20°	0.55°	-5.02°	6.53°	1.03°	-5.98°		

(d) Parameters for sawtooth configurations.

Figure 3. Concluded.



Config	A	B	β
Dry	0.500	2.451	17.67
A/B	.600	2.485	20.00

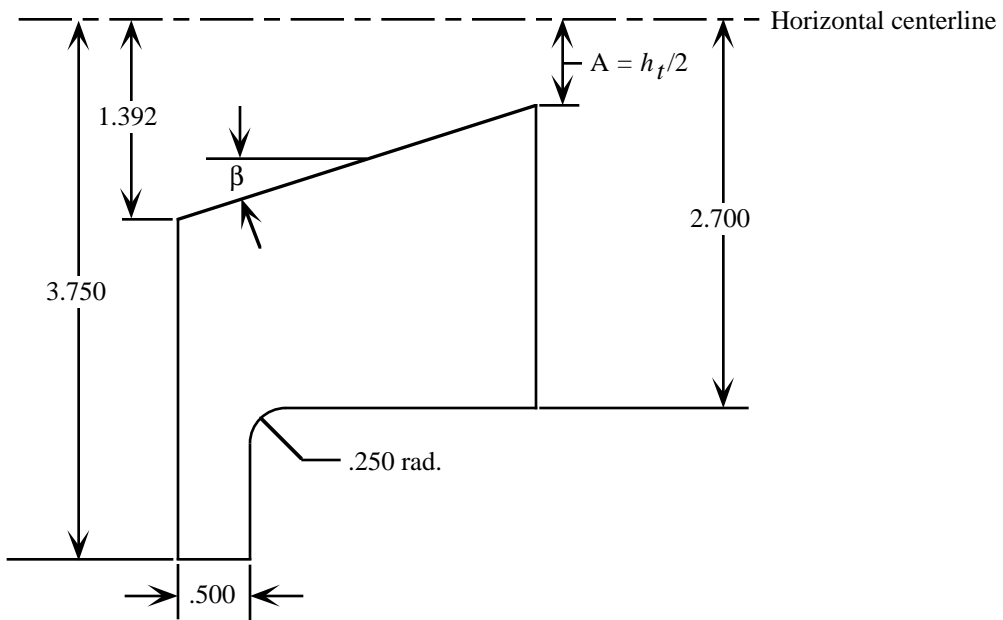


Figure 4. Details of lower convergent flaps. Linear dimensions are in inches.

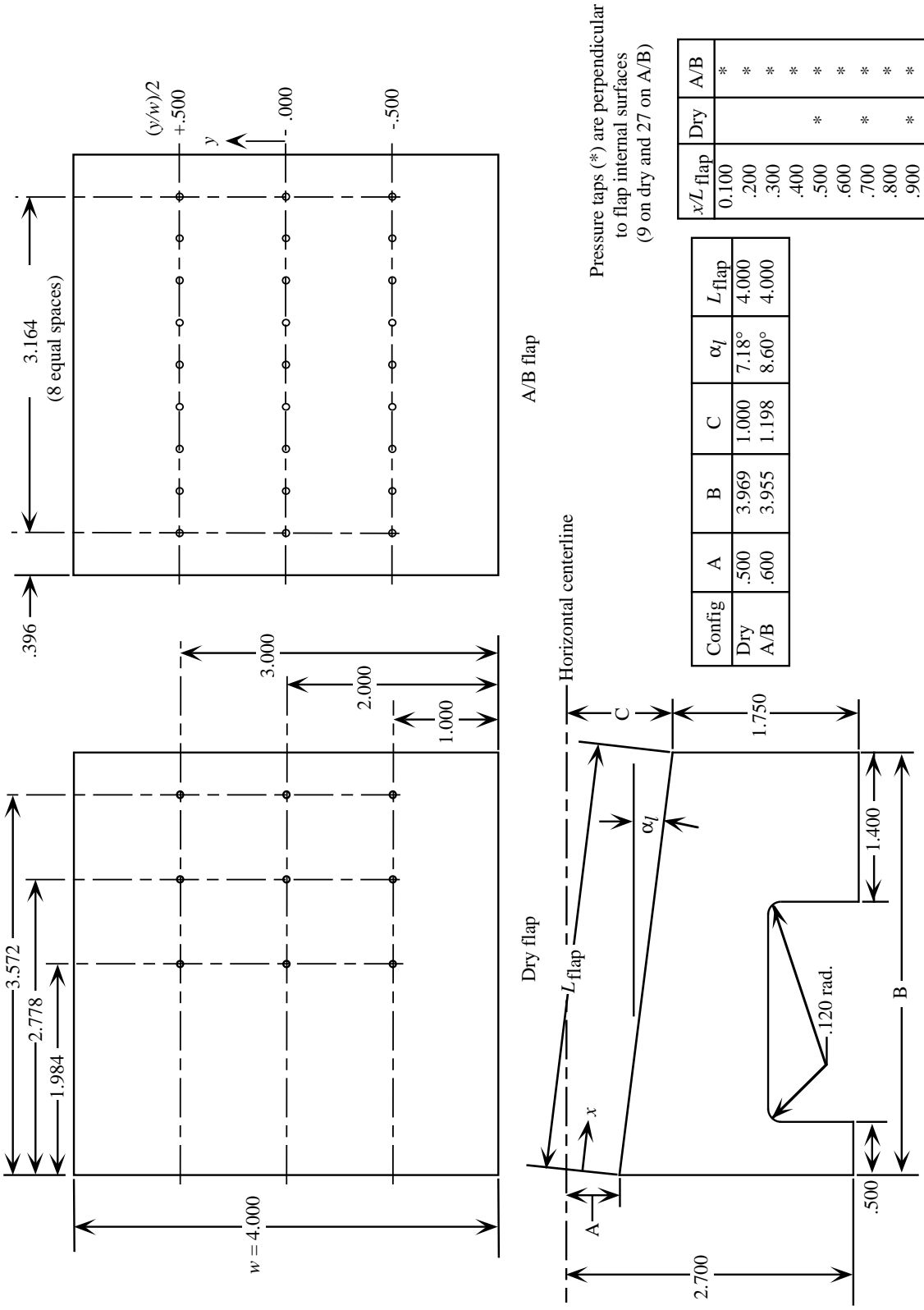
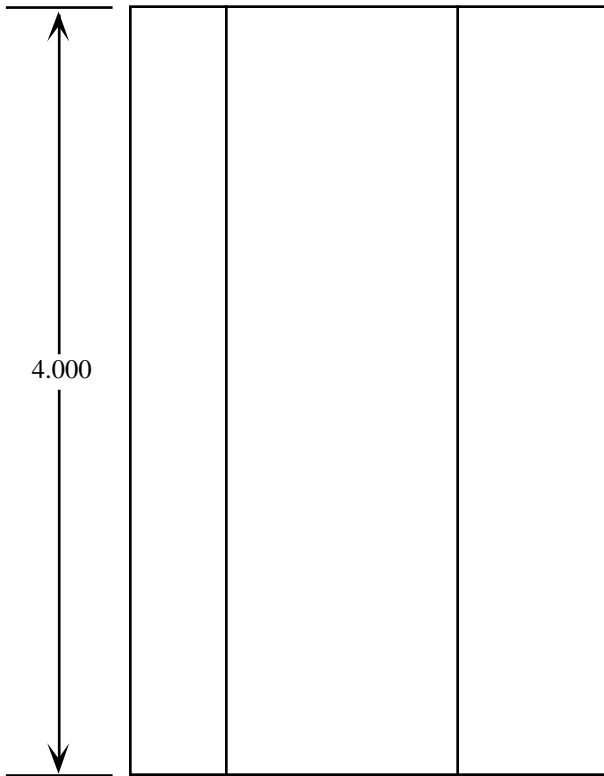


Figure 5. Details of lower divergent flaps including pressure tap locations. Some hidden lines excluded for clarity; linear dimensions are in inches.



Dry power			
	Config 1,7,13	Config 2,8,14	Config 3,9,15
A	0.500	0.500	0.500
B	2.419	2.495	2.487
C	2.451	2.451	2.451
D	1.818	2.297	2.702
β	20.00°	20.00°	20.00°
ϕ	-5.76°	3.54°	14.66°

Dry power			
	Config 4,10,16	Config 5,11,17	Config 6,12,18
A	0.600	0.600	0.600
B	2.378	2.494	2.481
C	2.485	2.485	2.485
D	1.712	2.312	2.790
β	17.67°	17.67°	17.67°
ϕ	-7.00°	4.00°	18.00°

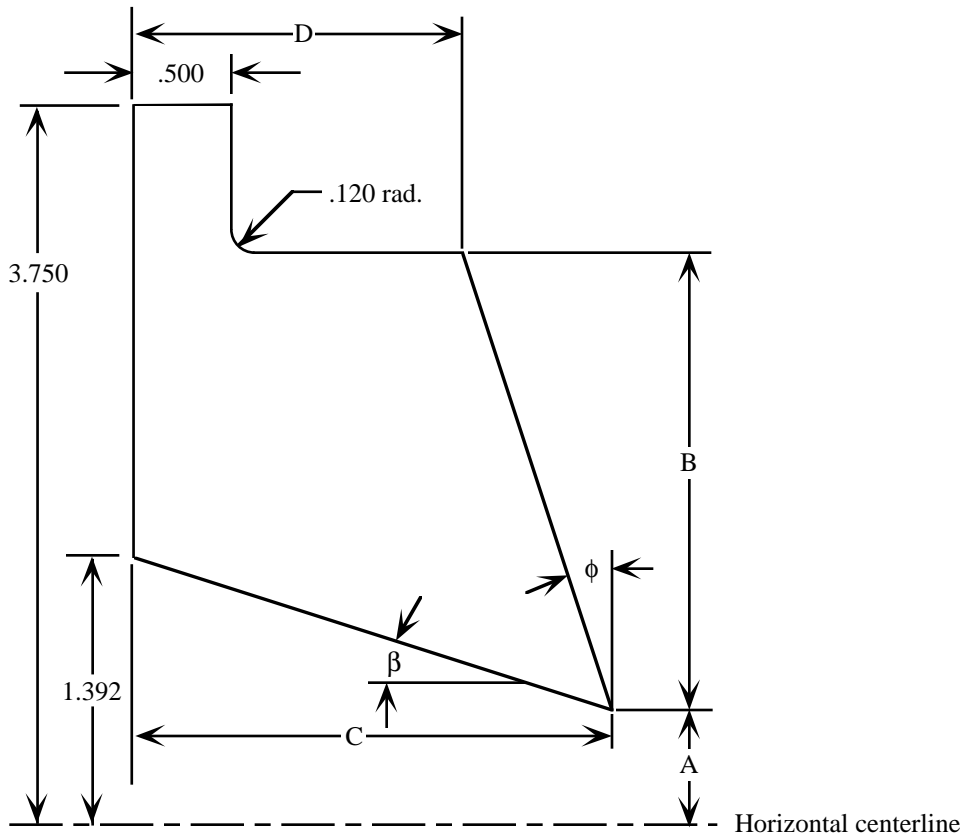
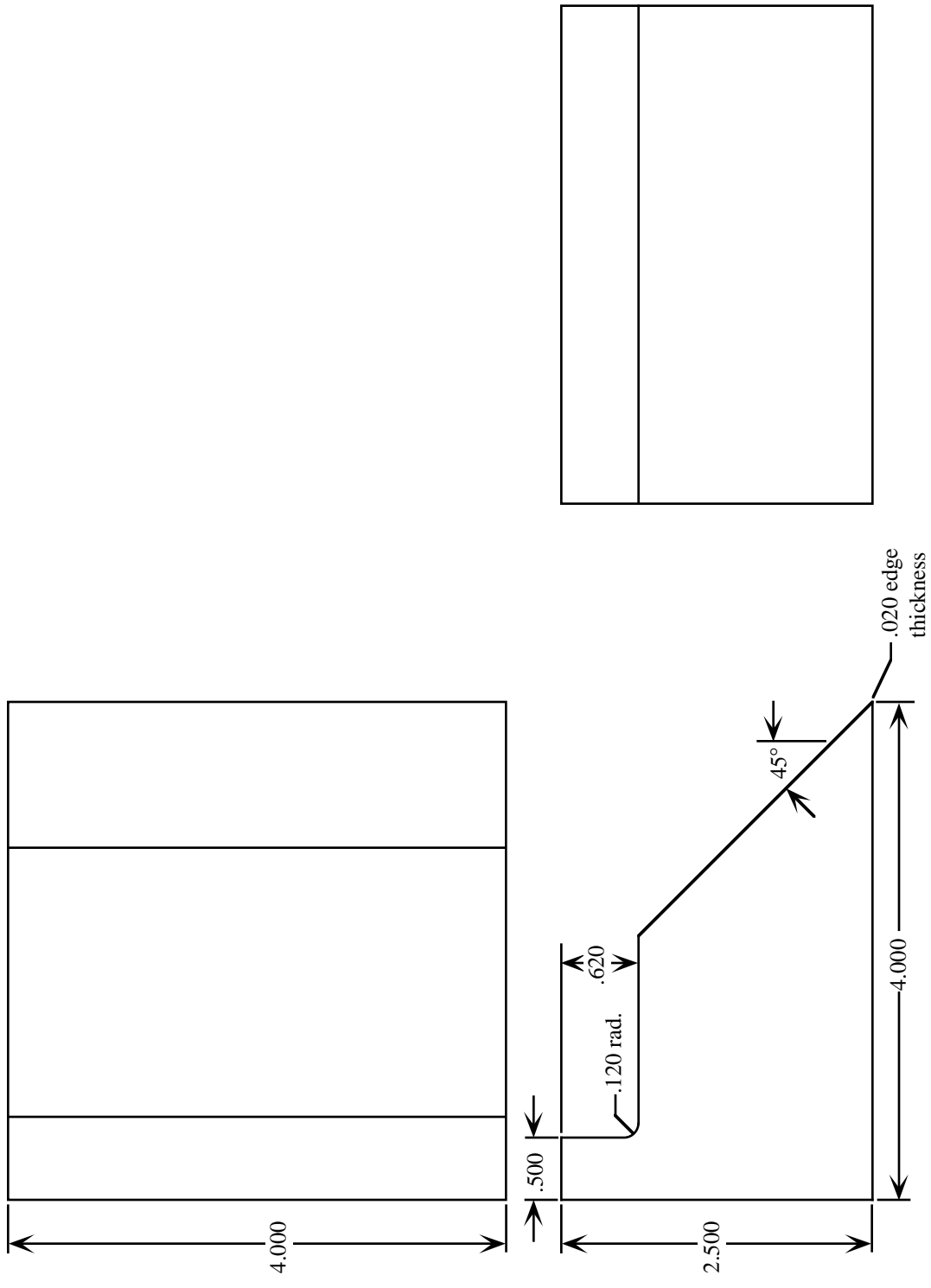
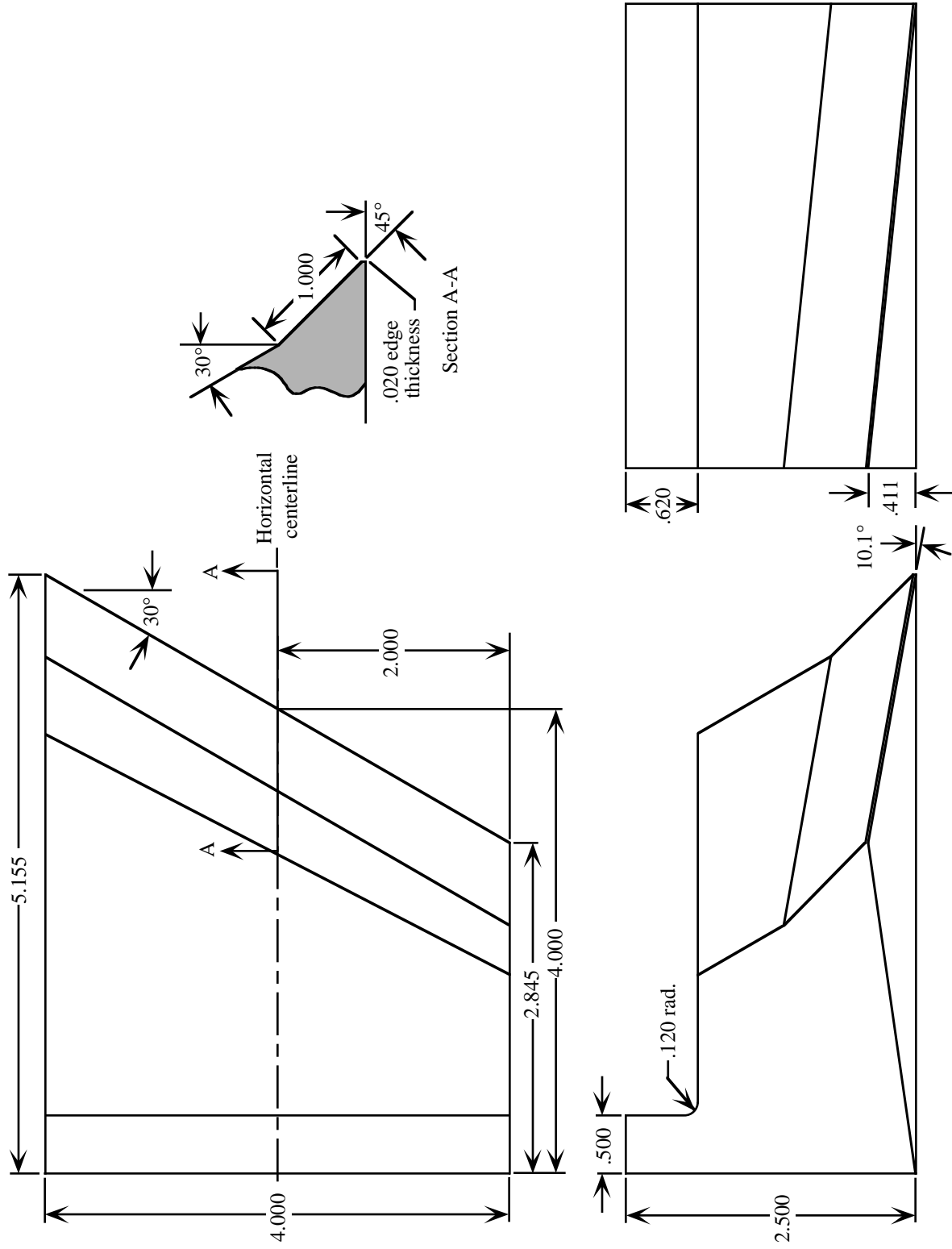


Figure 6. Details of upper convergent flaps. Linear dimensions are in inches.



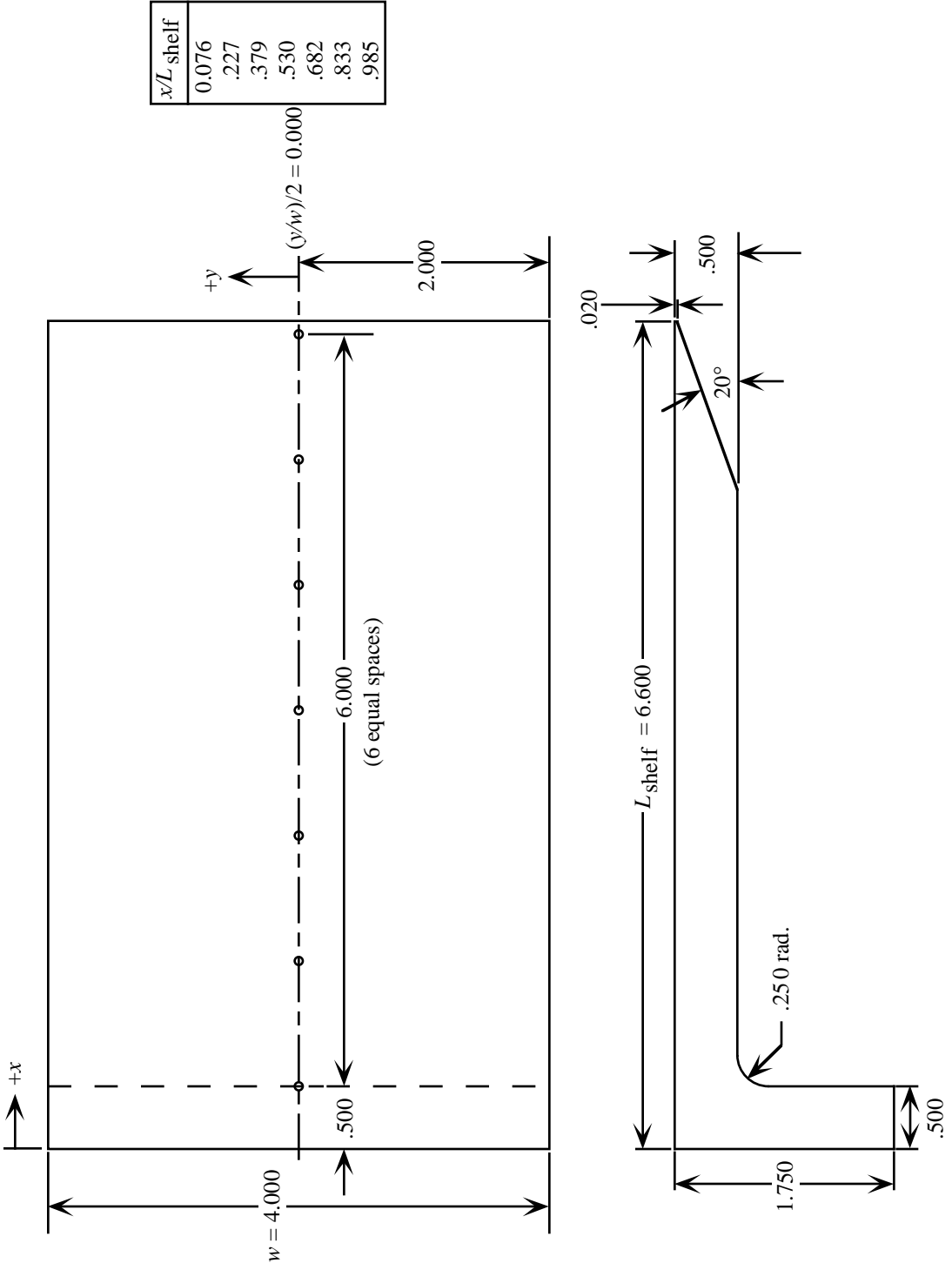
(a) Flap for baseline configurations.

Figure 7. Details of upper divergent flaps. All flaps have same planform area; linear dimensions are in inches; flaps are rotated to match angles on upper divergent flaps.



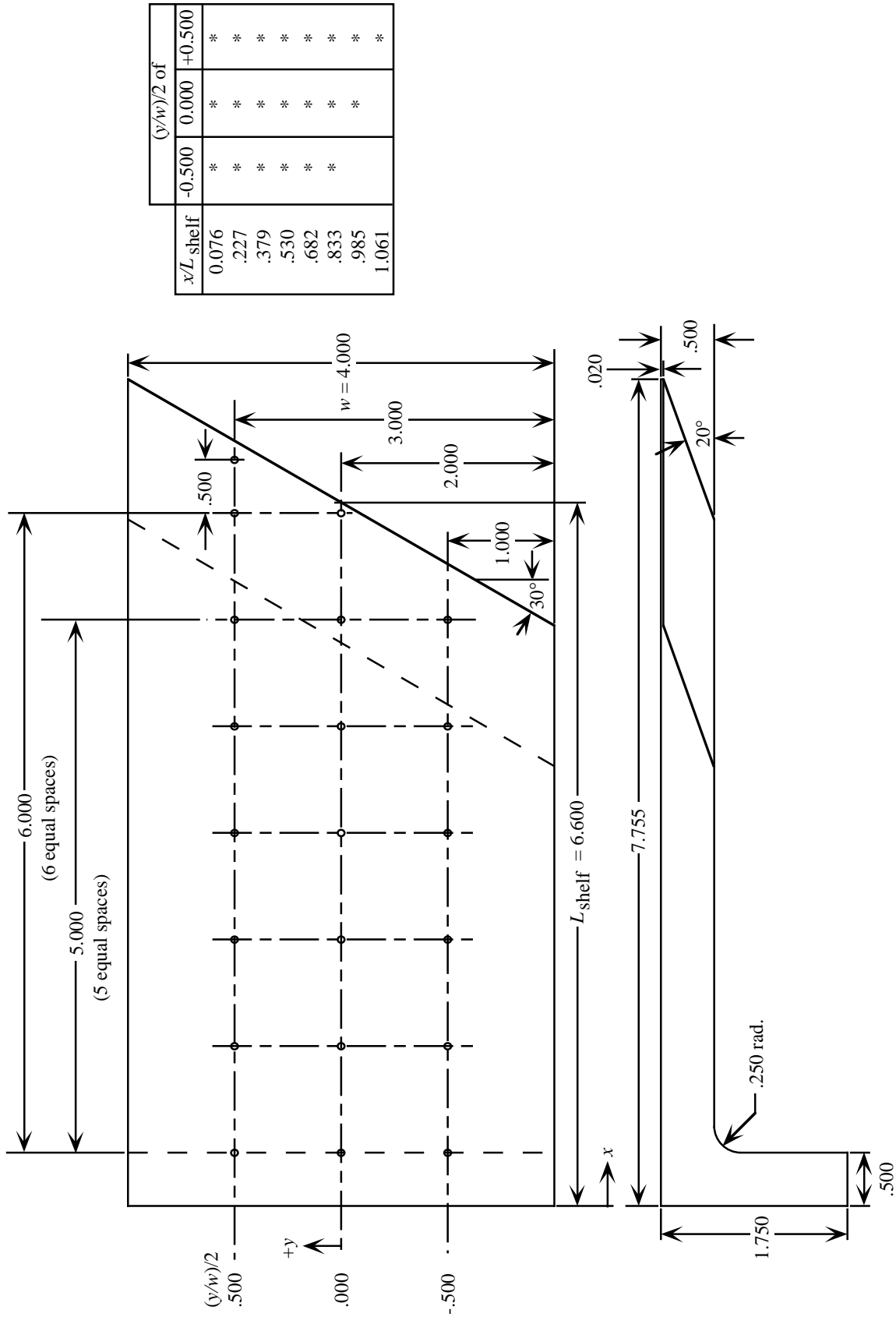
(b) Flap for scarfed configurations.

Figure 7. Continued.



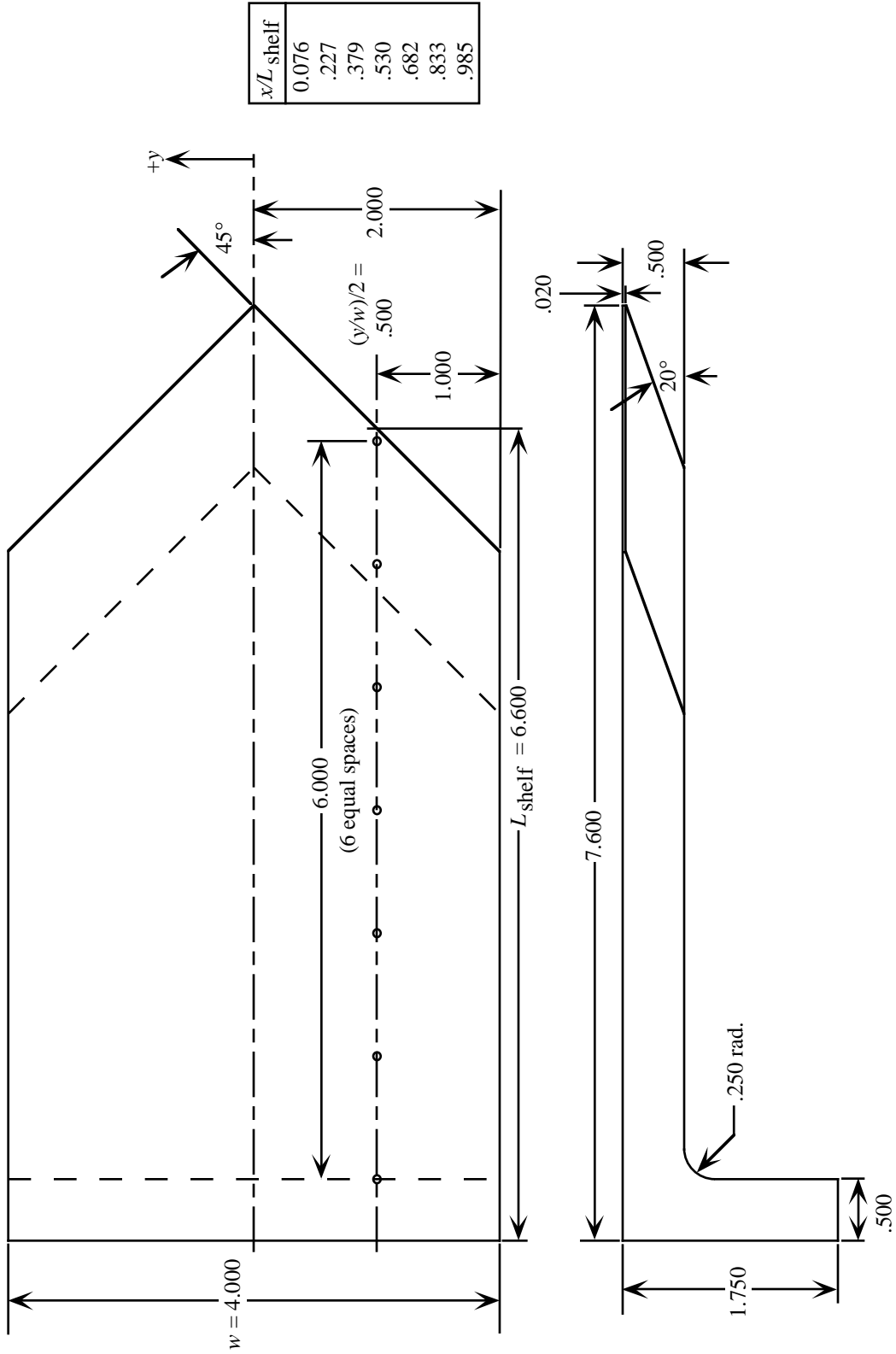
(a) Baseline shelf.

Figure 8. Details of shelves. Each shelf has same platform area; linear dimensions are in inches.



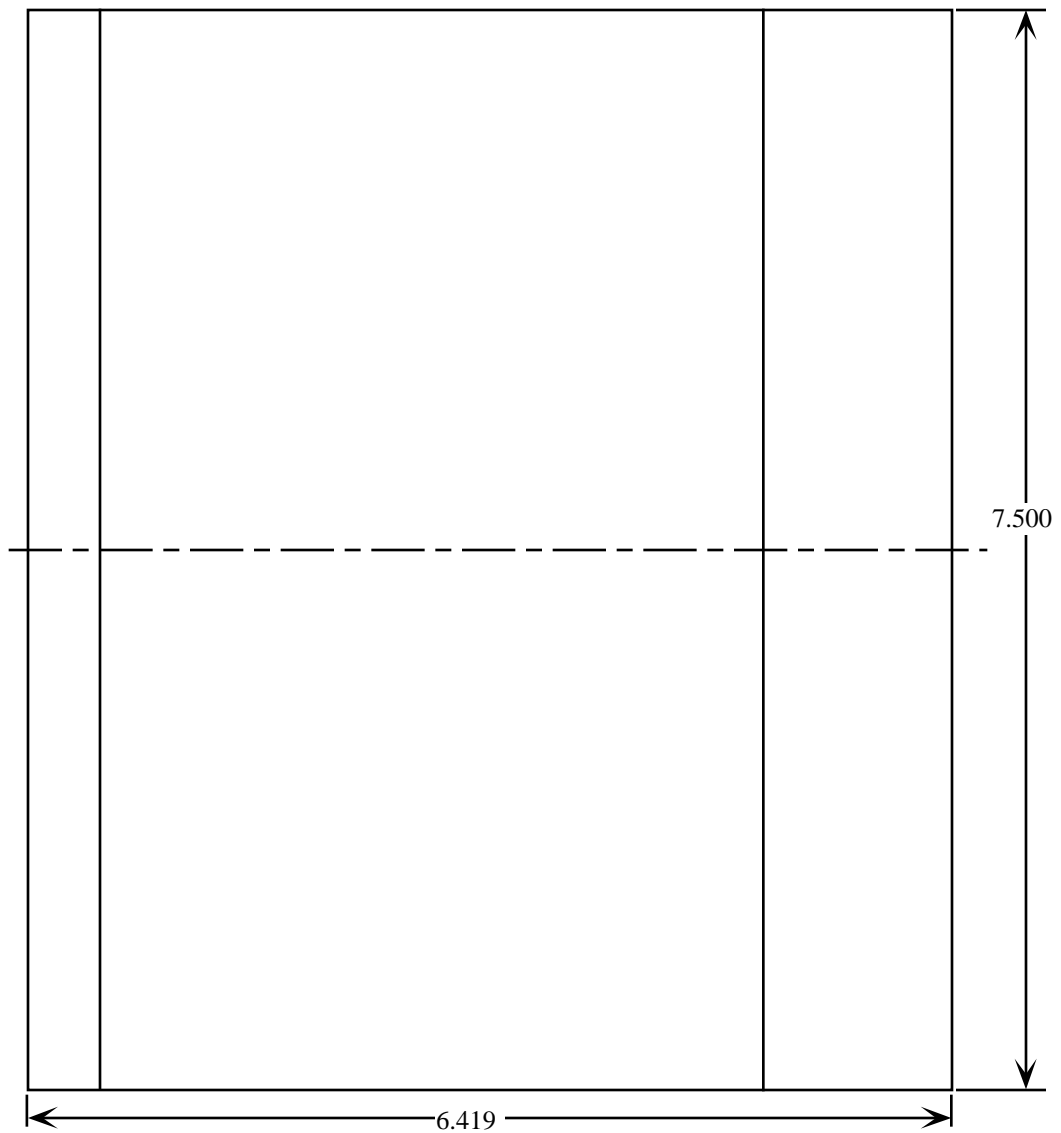
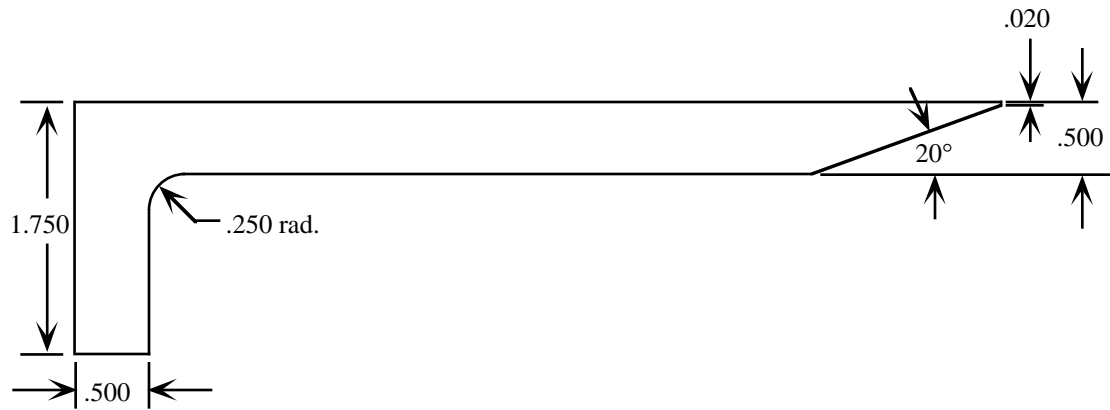
(b) Scarfed shelf.

Figure 8. Continued.



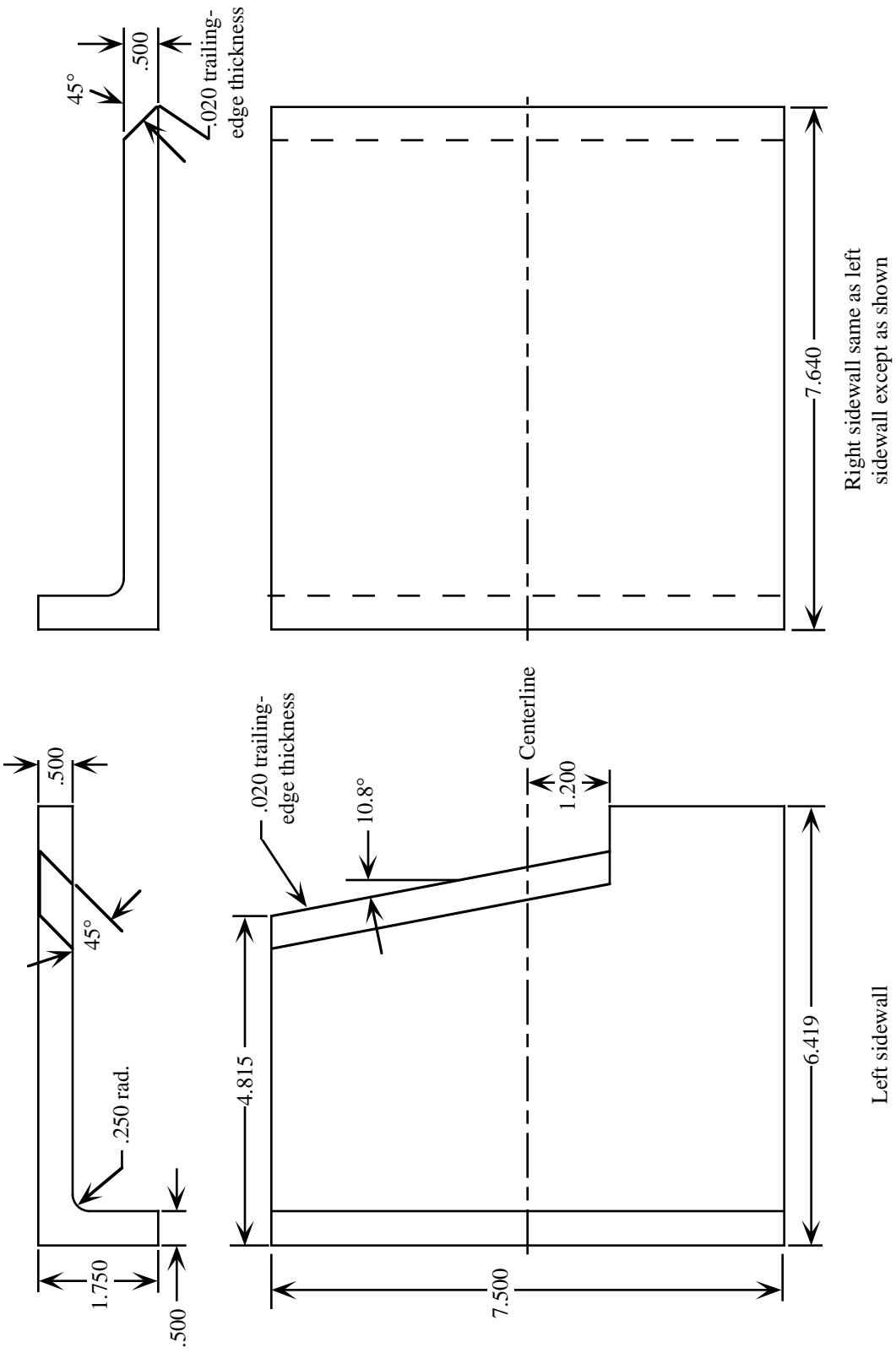
(c) Sawtooth shelf.

Figure 8. Concluded.



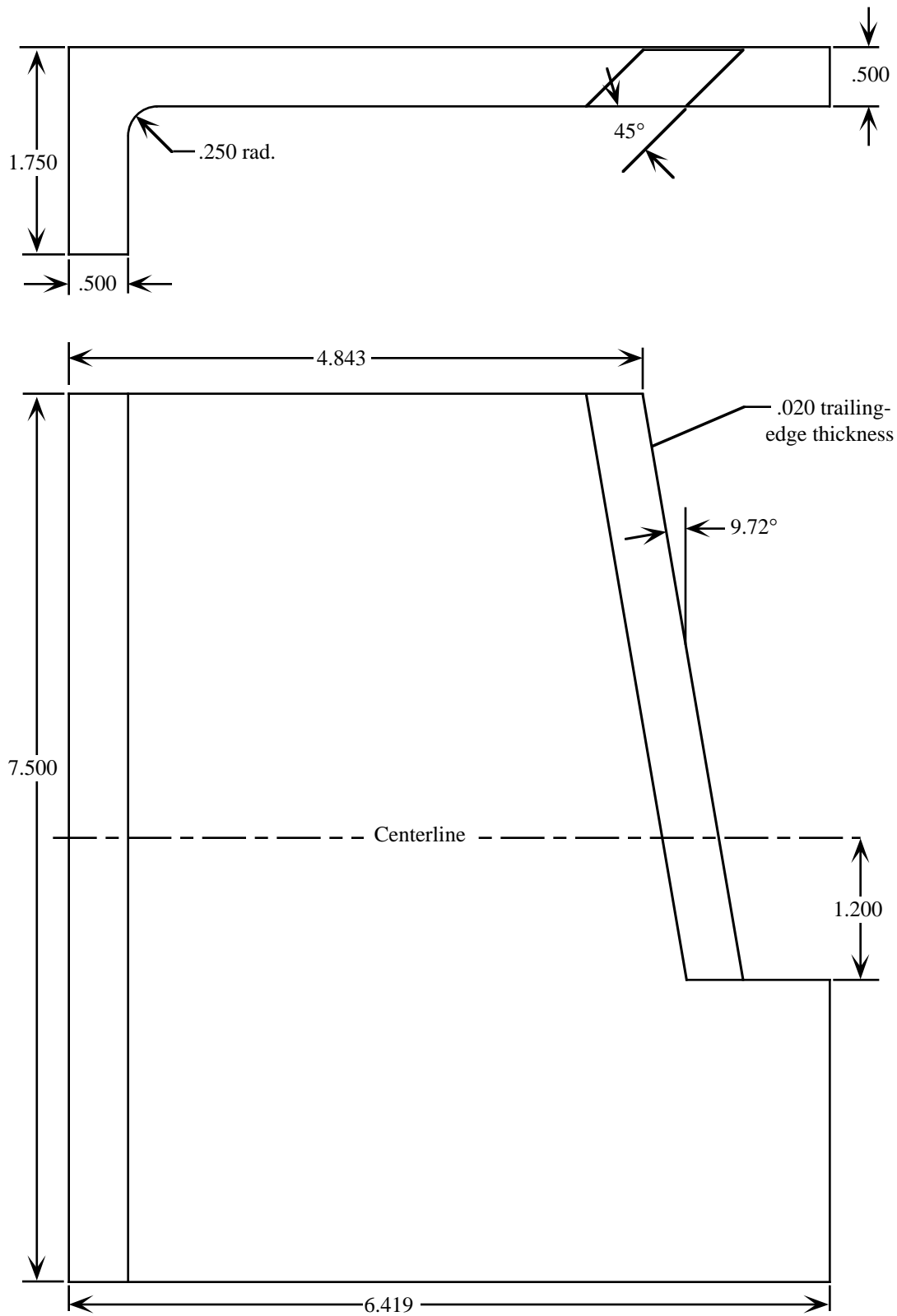
(a) Baseline sidewalls; right and left are identical.

Figure 9. Details of sidewalls. Linear dimensions are in inches.



(b) Sidewalls for scarf configurations.

Figure 9. Continued.



(c) Sidewalls for sawtooth configurations; right and left are identical.

Figure 9. Concluded.

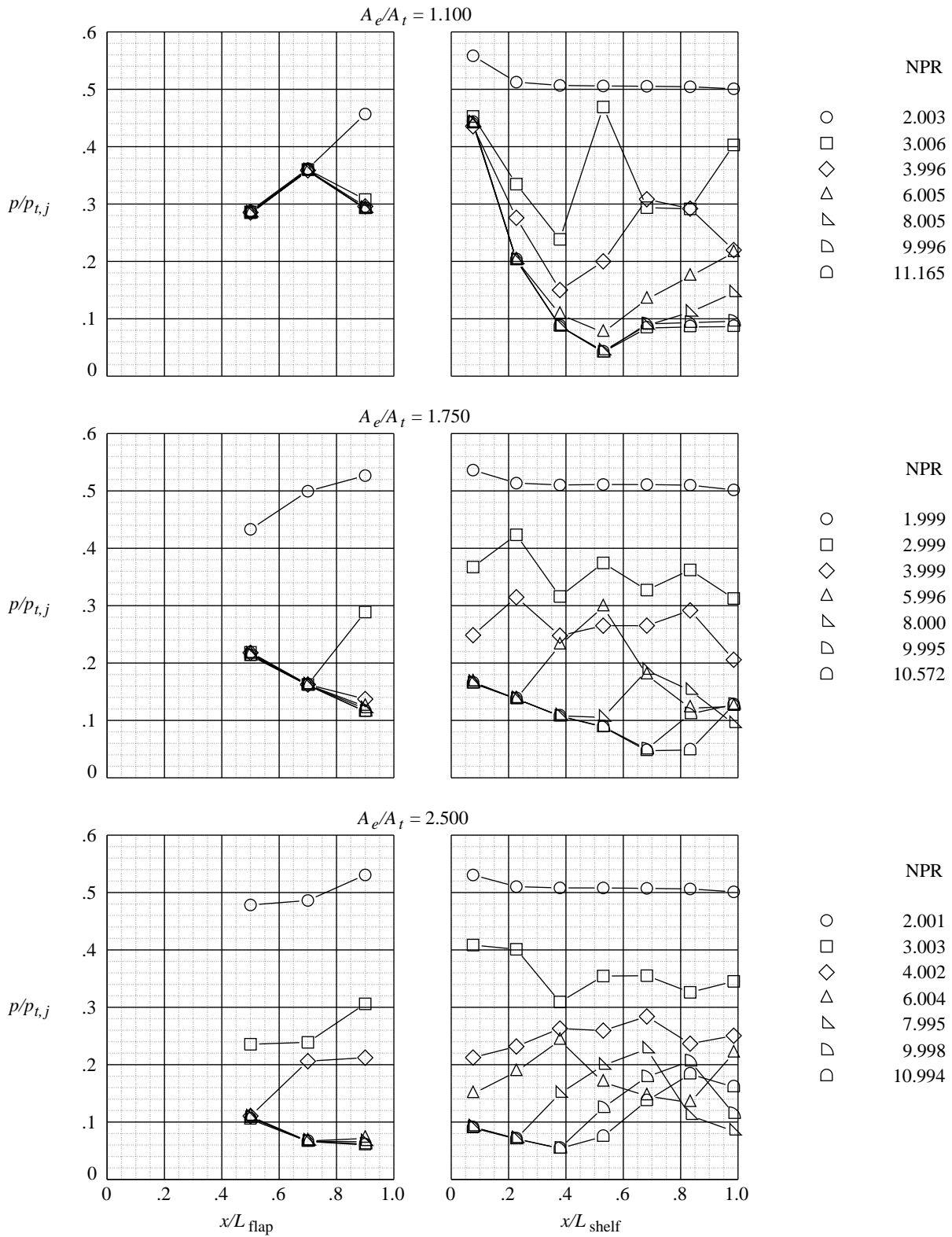


Figure 10. Static pressure ratio distributions along surface where $L_{shelf} = 6.600$ in.

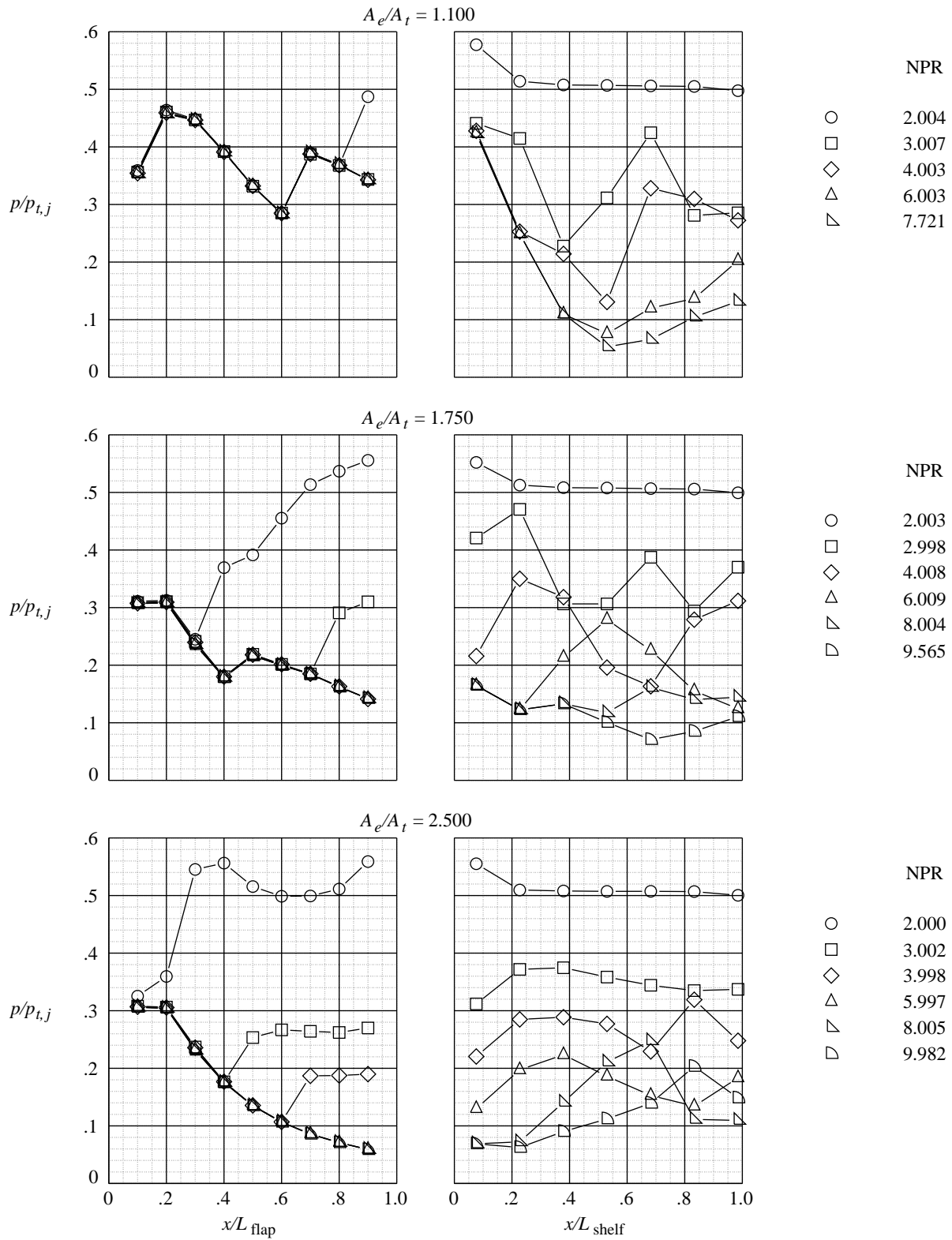
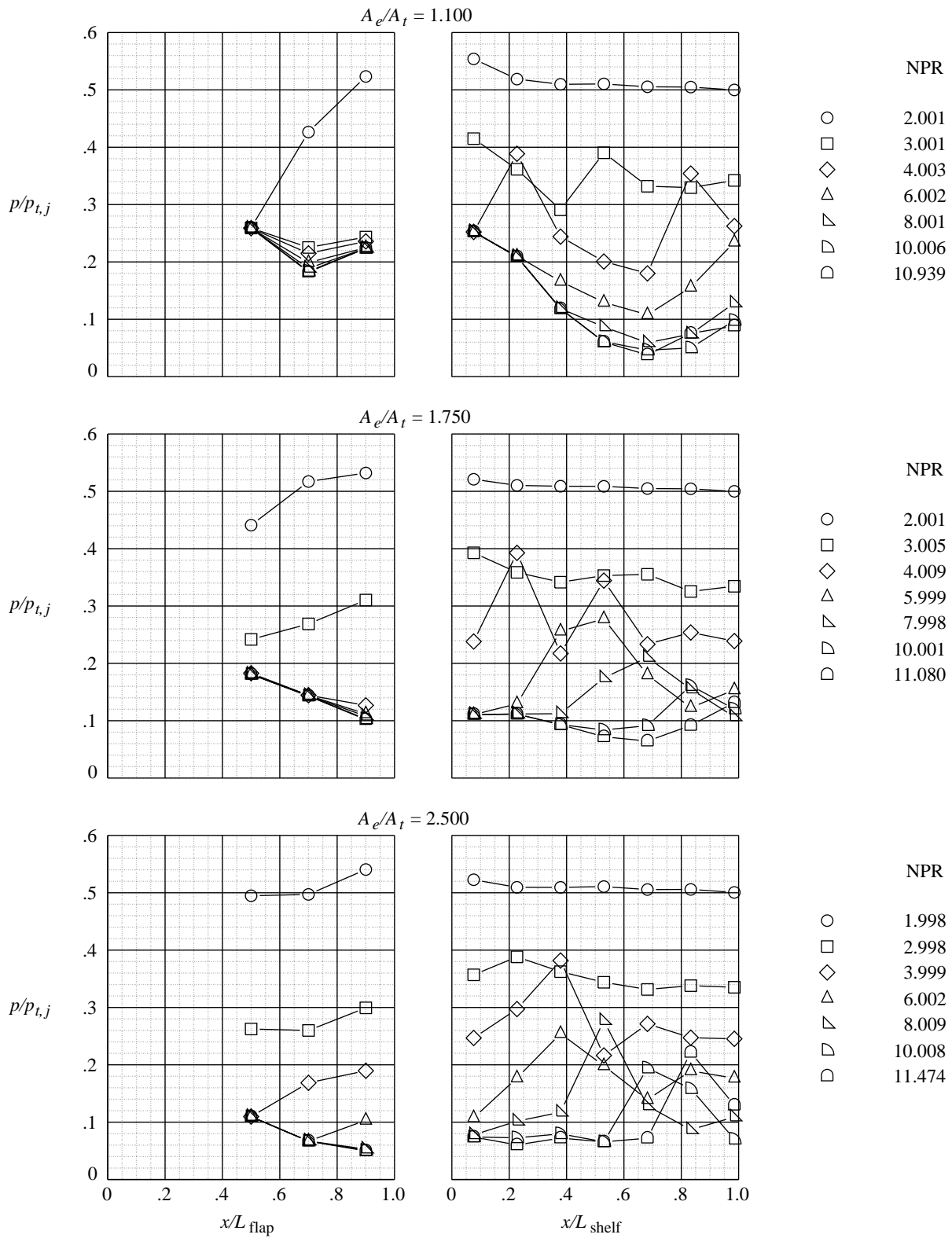
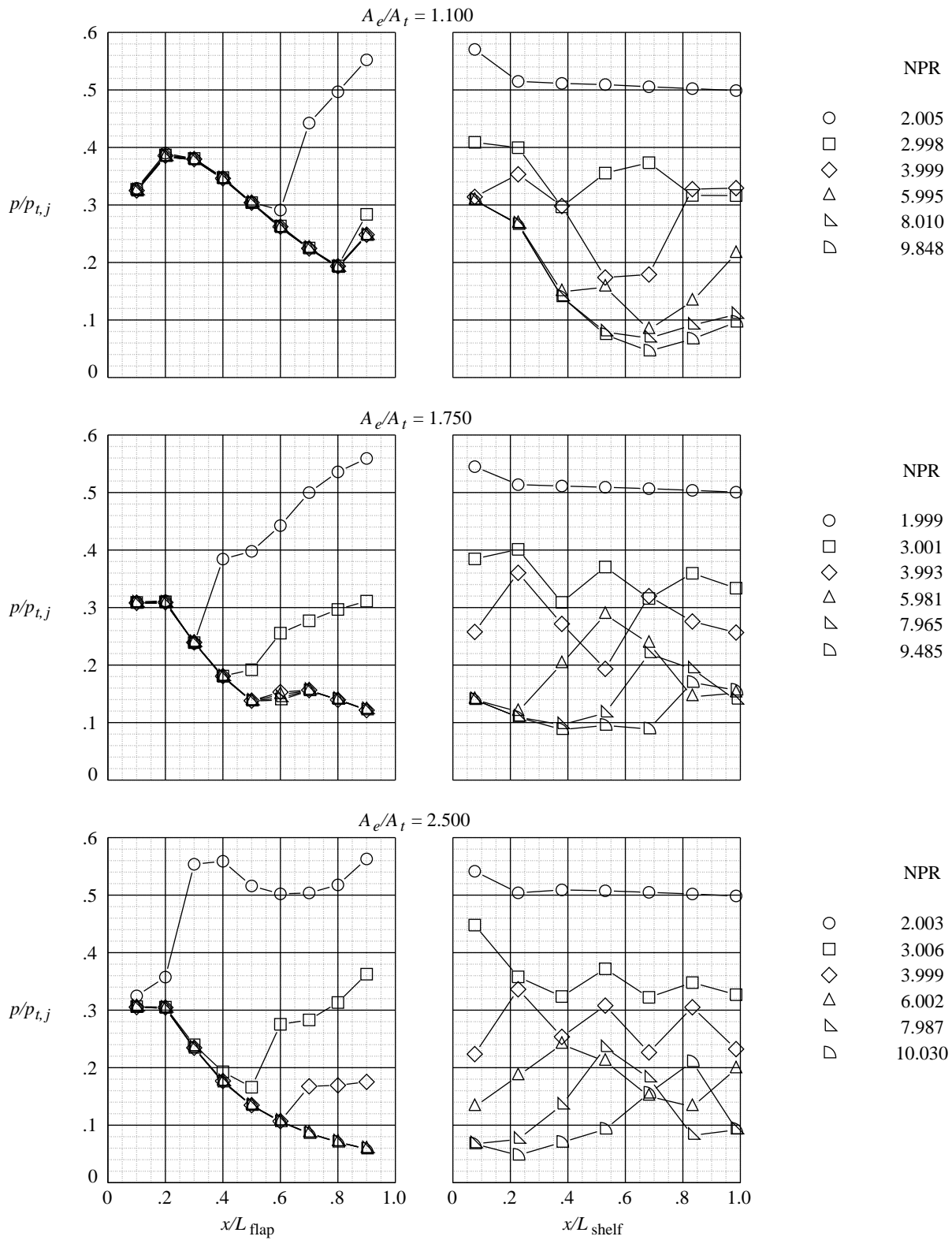


Figure 10. Continued.



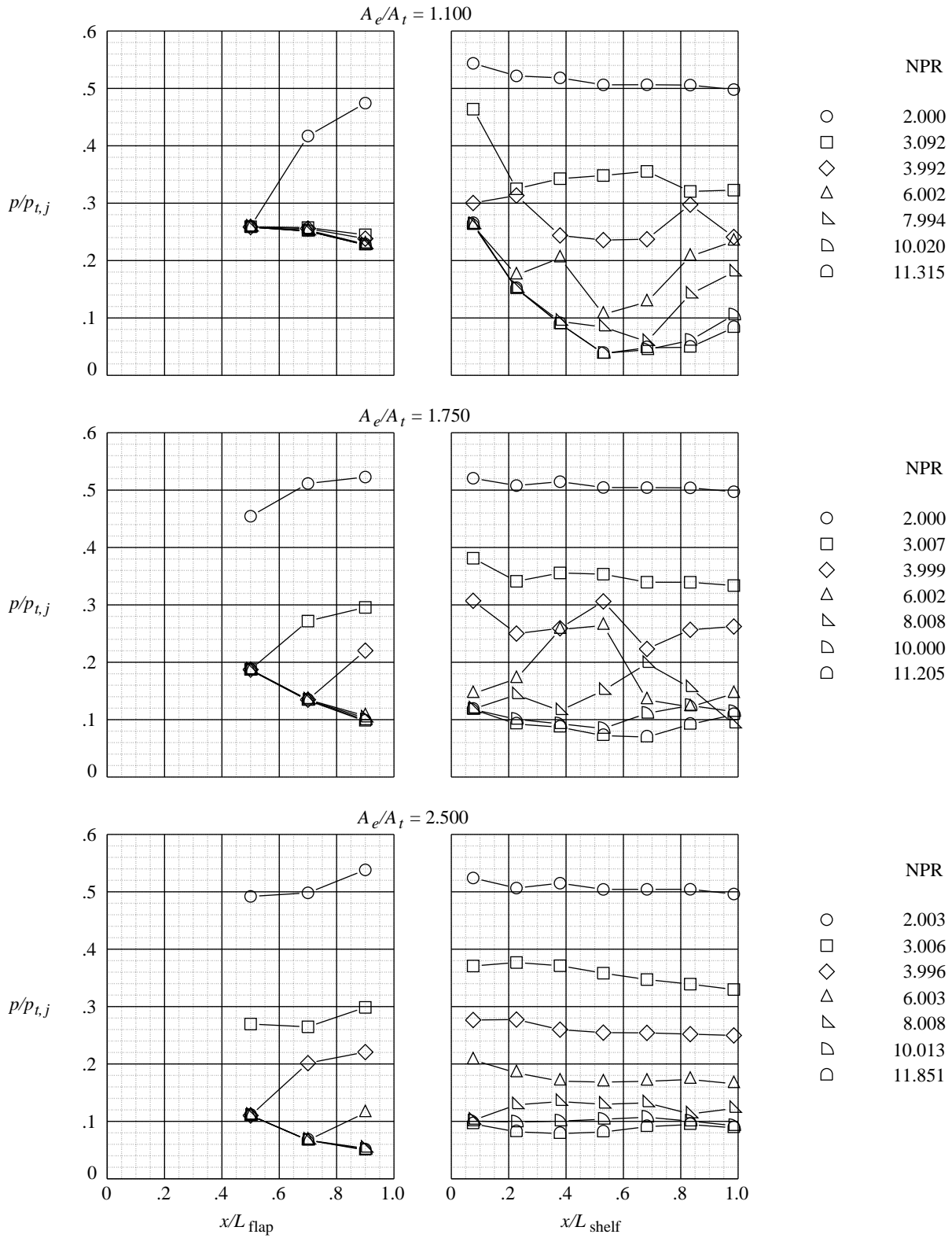
(c) Dry power scarfed configurations.

Figure 10. Continued.



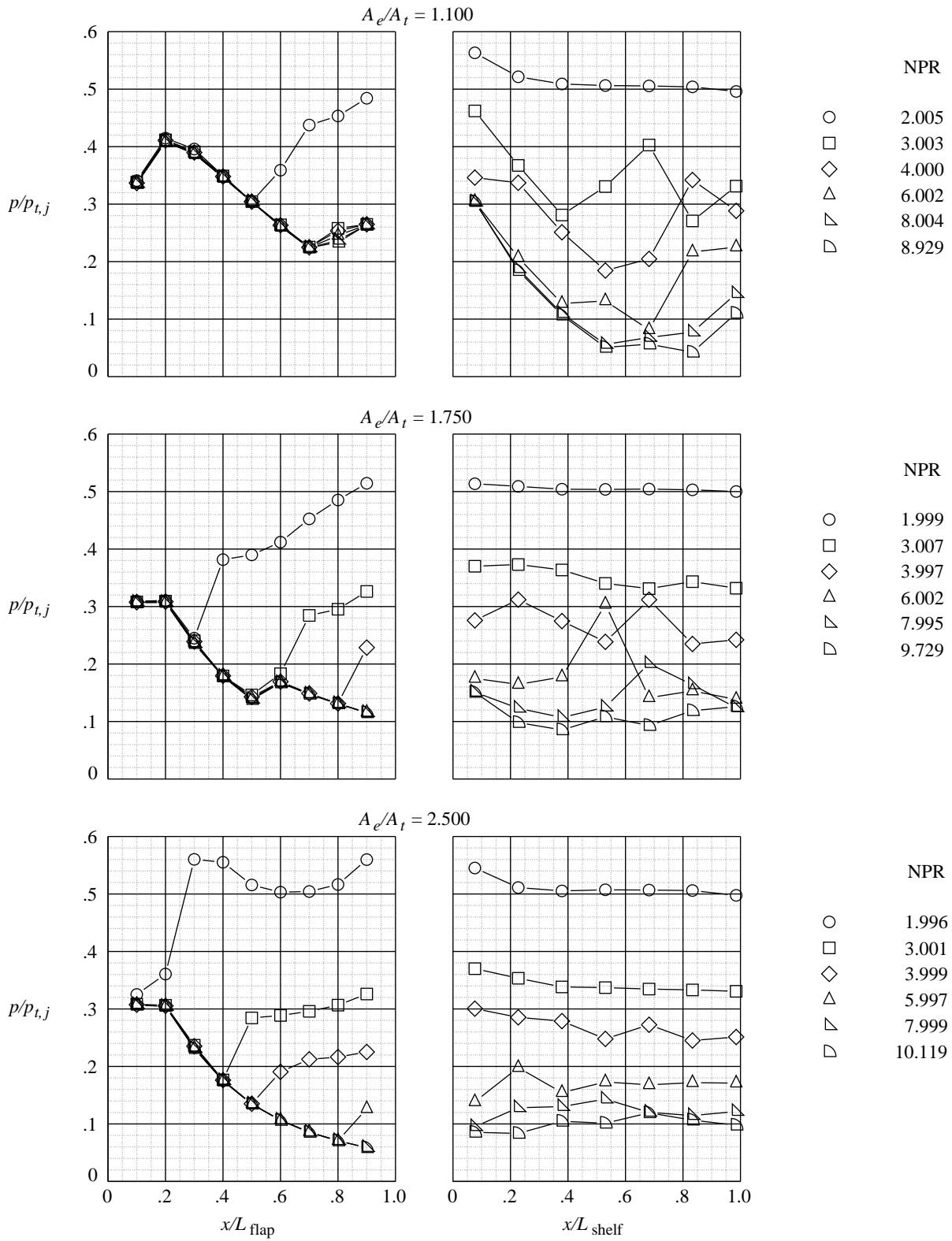
(d) A/B power scarfed configurations.

Figure 10. Continued.



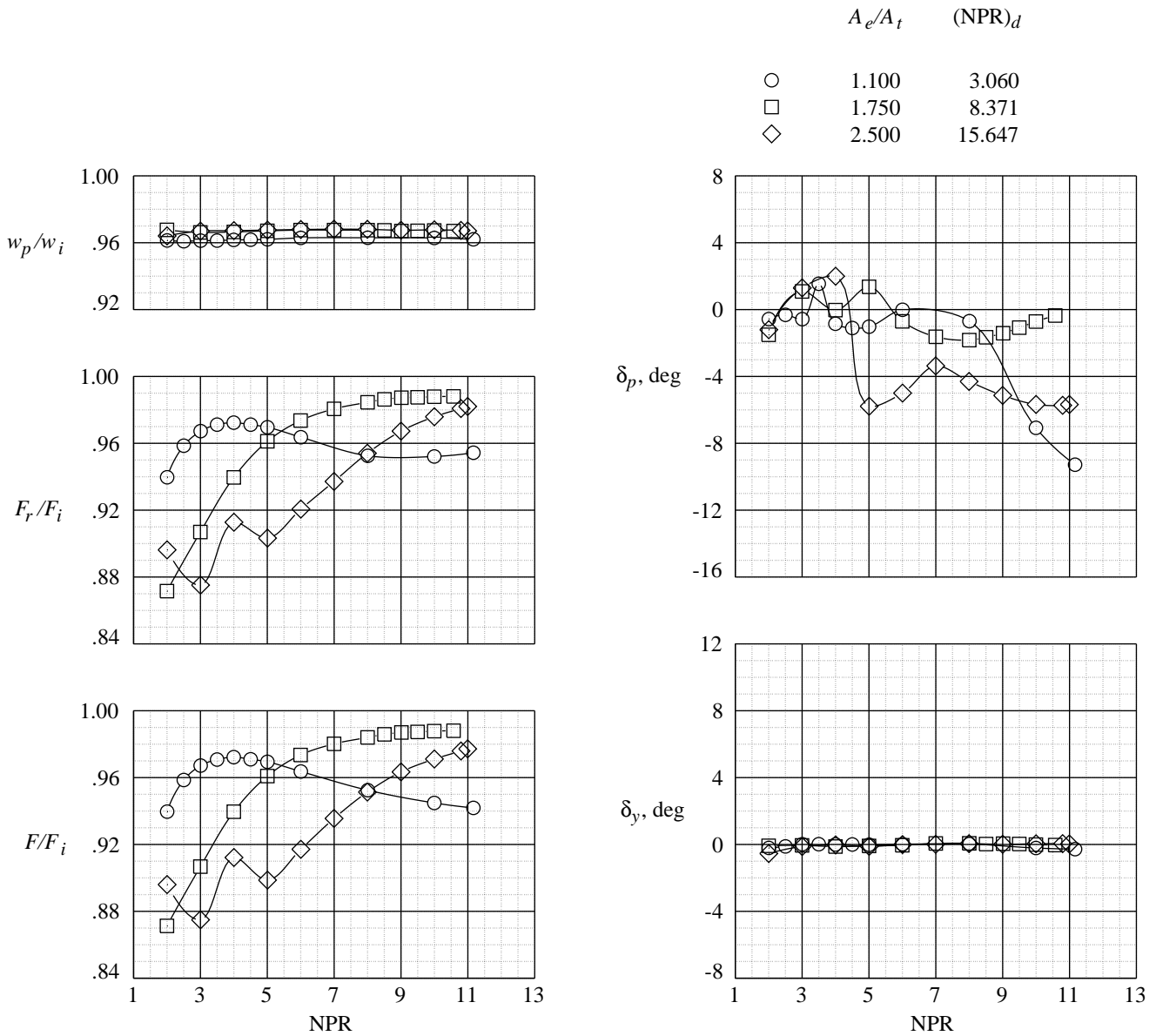
(e) Dry power sawtooth configurations.

Figure 10. Continued.



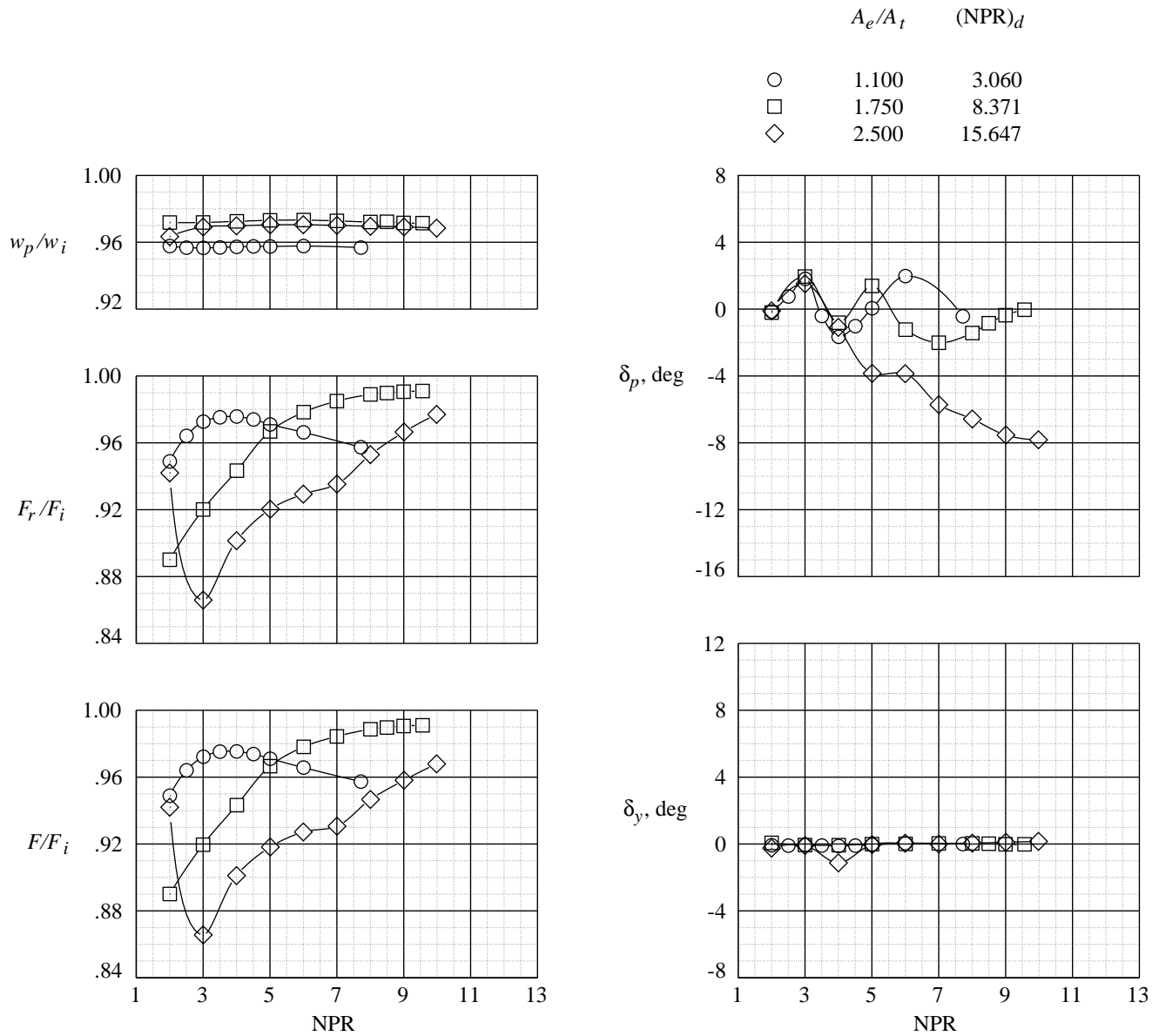
(f) A/B power sawtooth configurations.

Figure 10. Concluded.



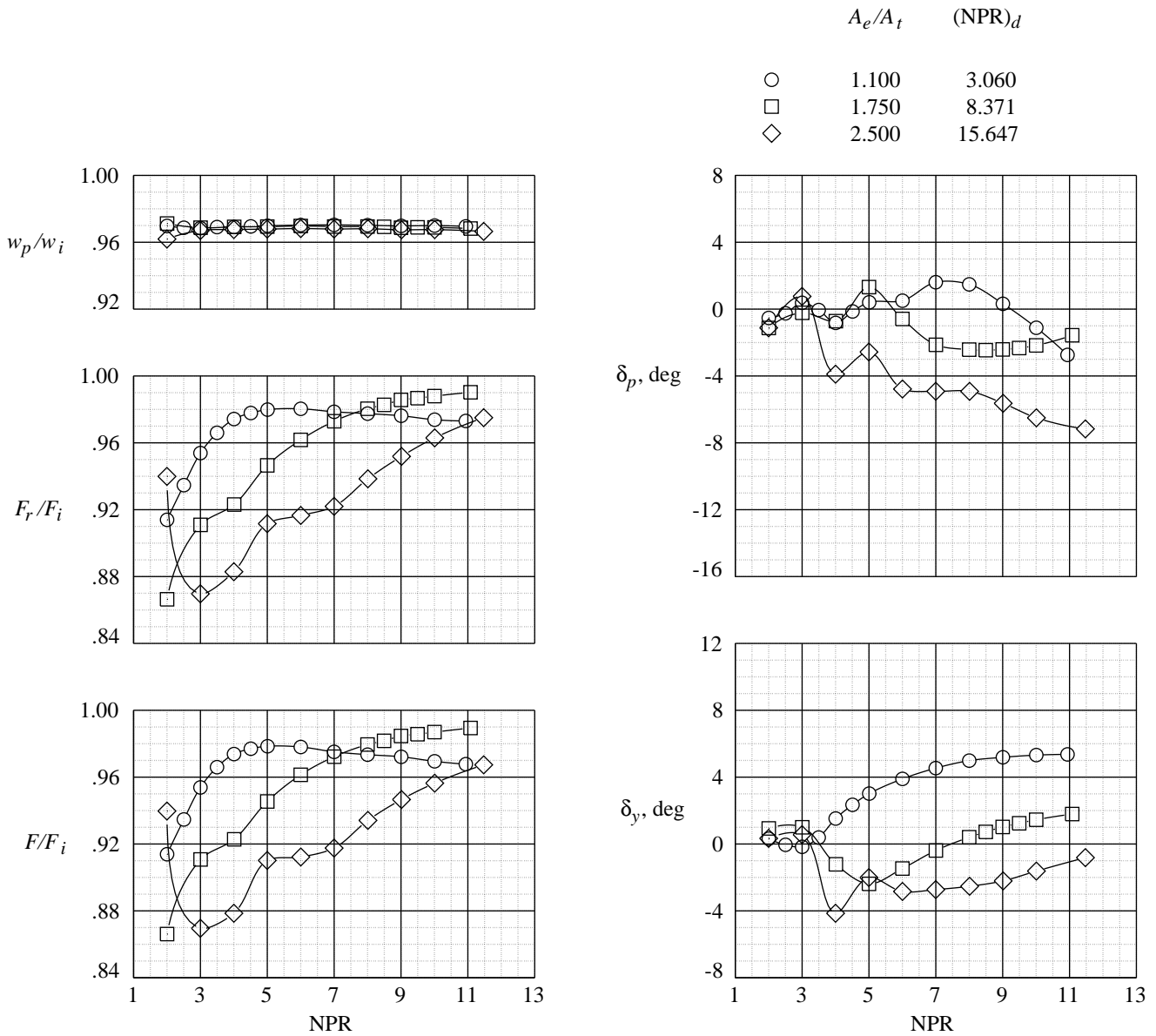
(a) Dry power.

Figure 11. Effect of expansion ratio on internal performance characteristics of baseline configurations.



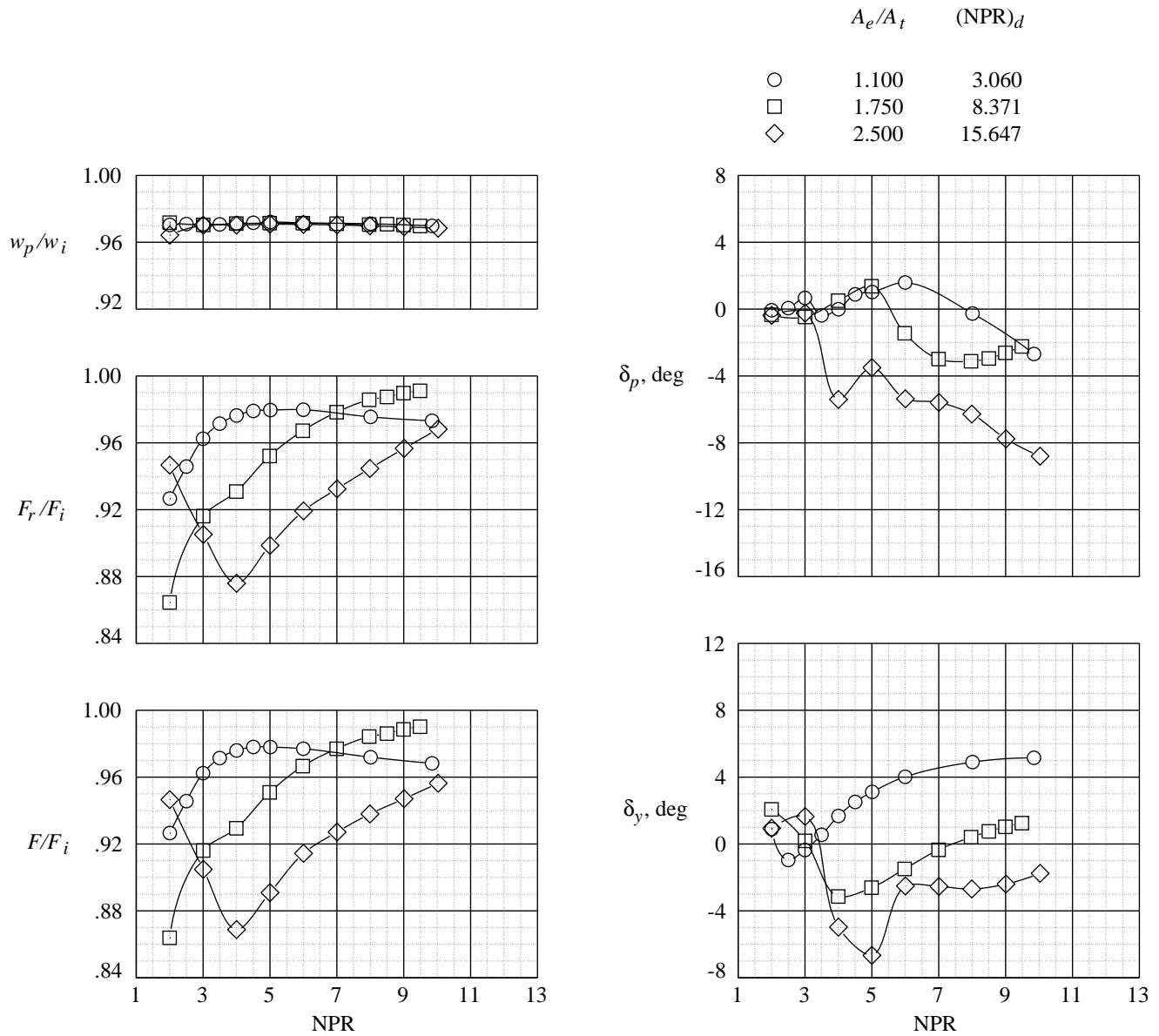
(b) A/B power.

Figure 11. Concluded.



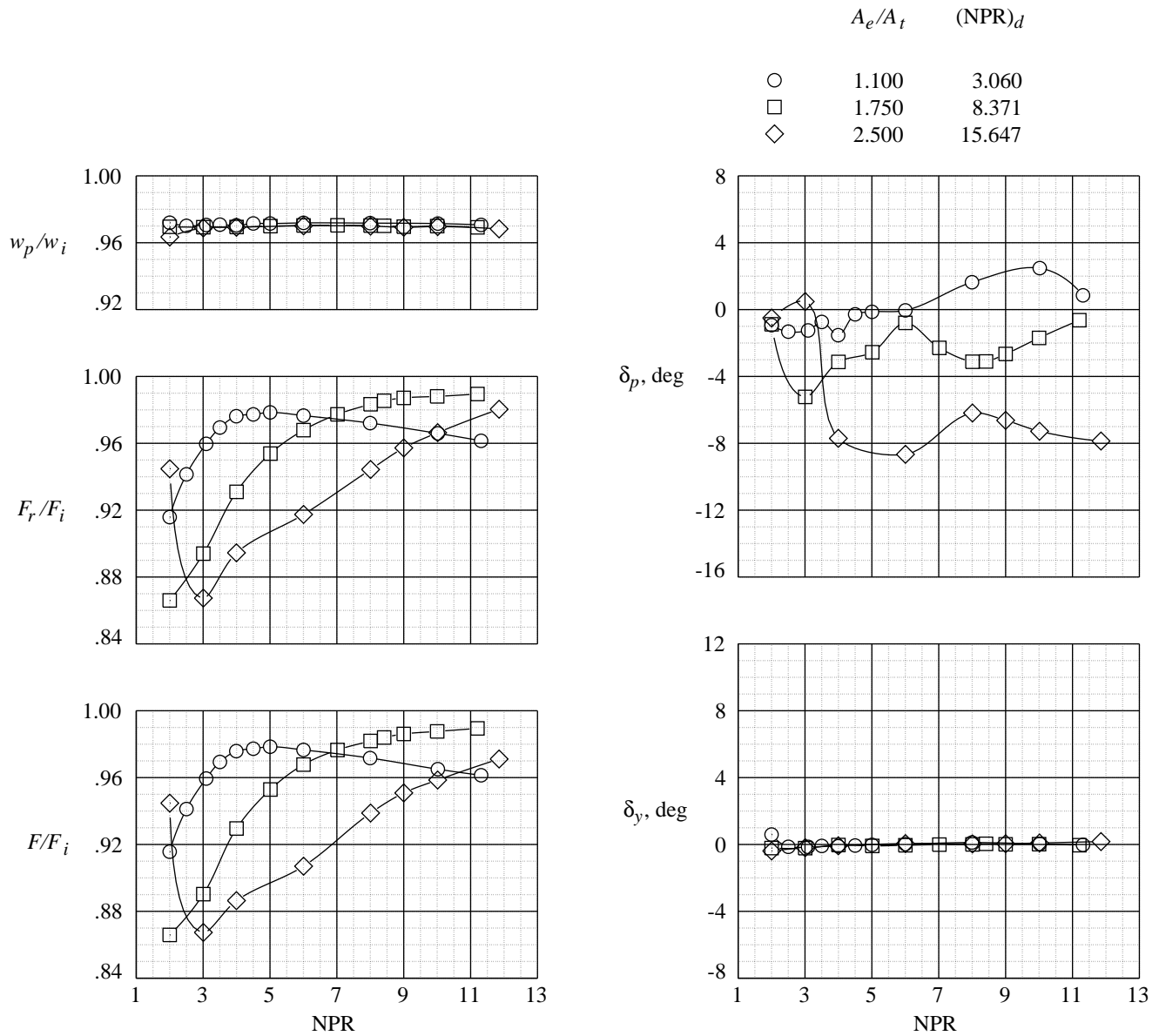
(a) Dry power.

Figure 12. Effect of expansion ratio on internal performance characteristics of scarfed configurations.



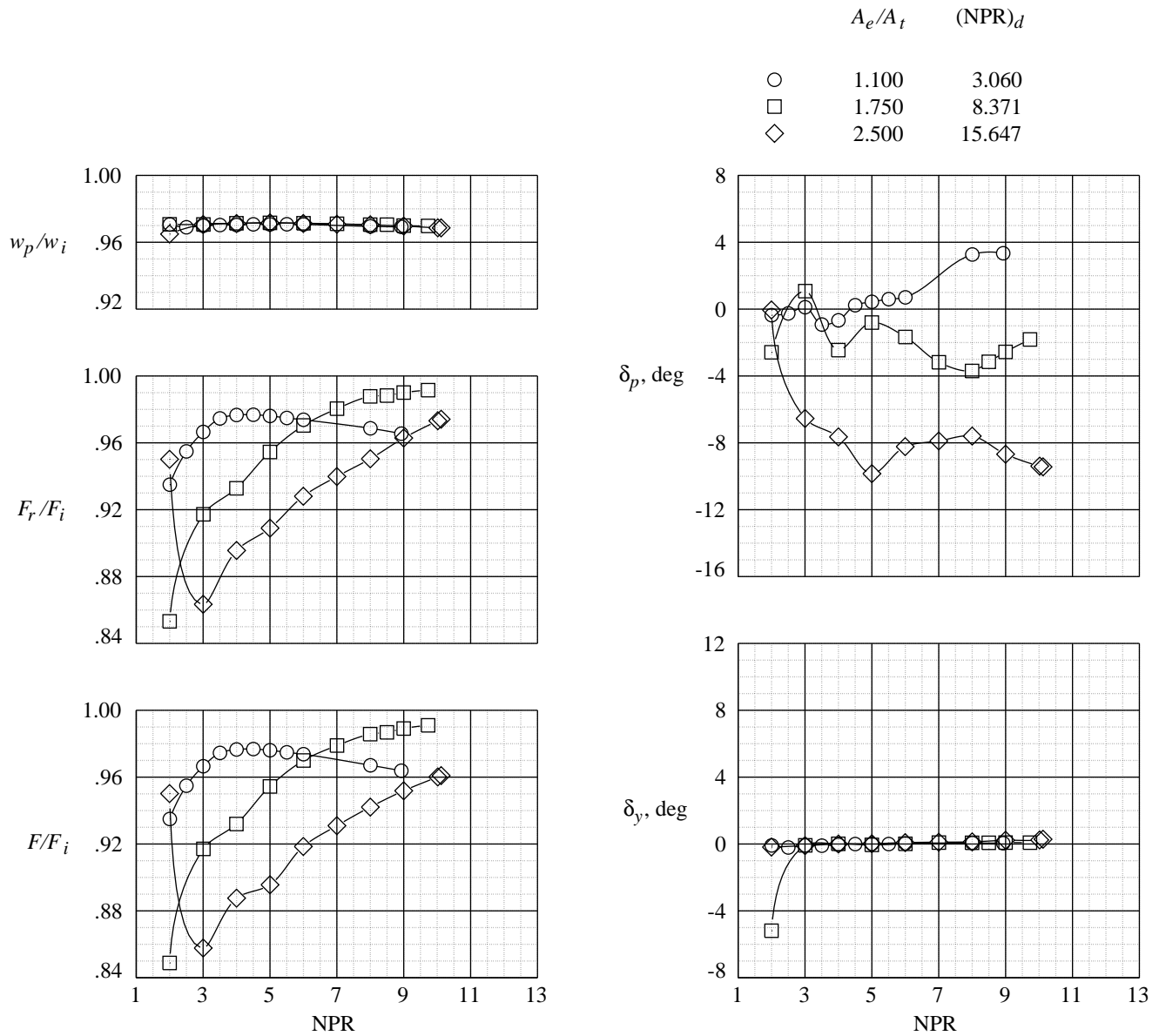
(b) A/B power.

Figure 12. Concluded.



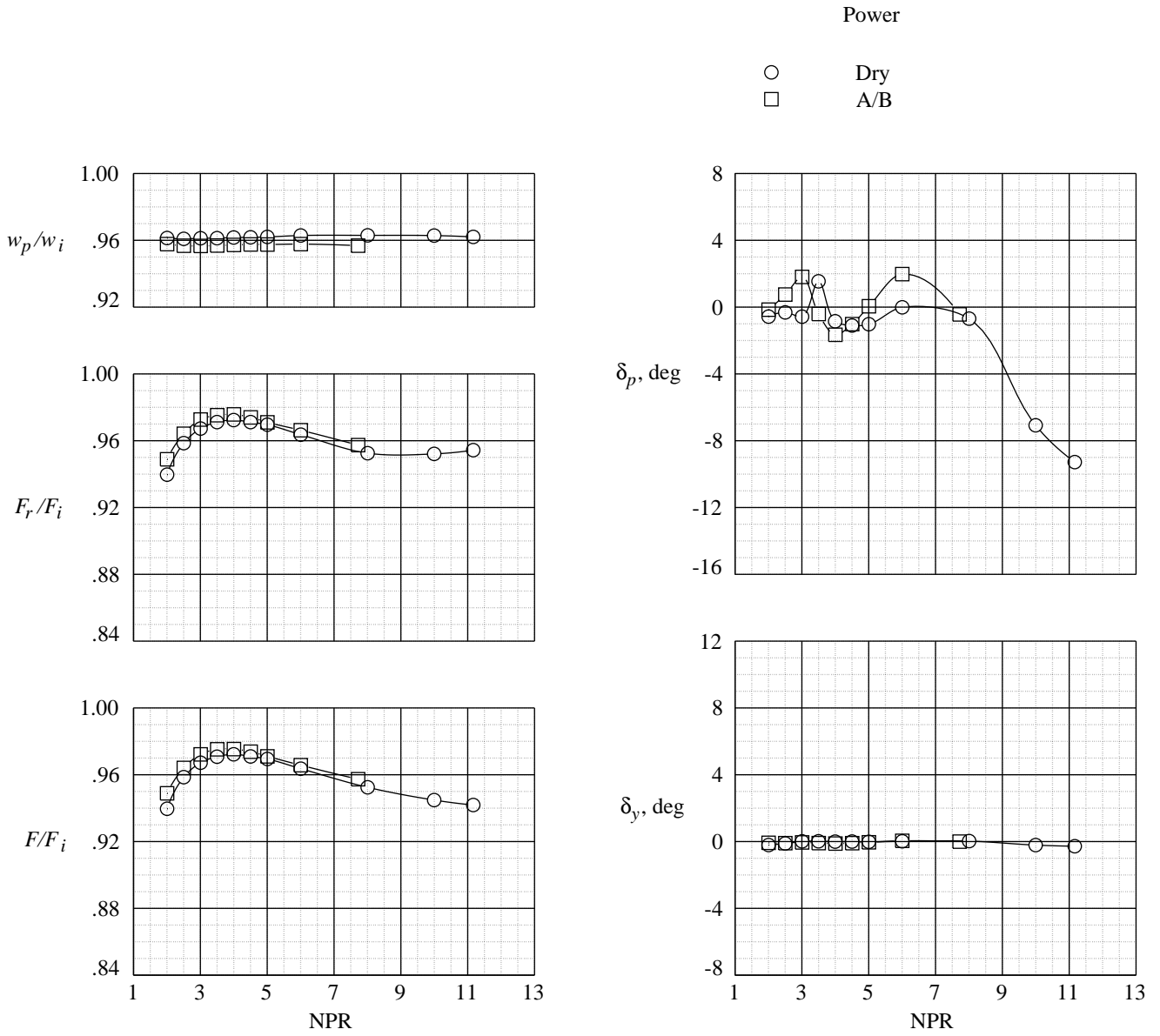
(a) Dry power.

Figure 13. Effect of expansion ratio on internal performance characteristics of sawtooth configurations.



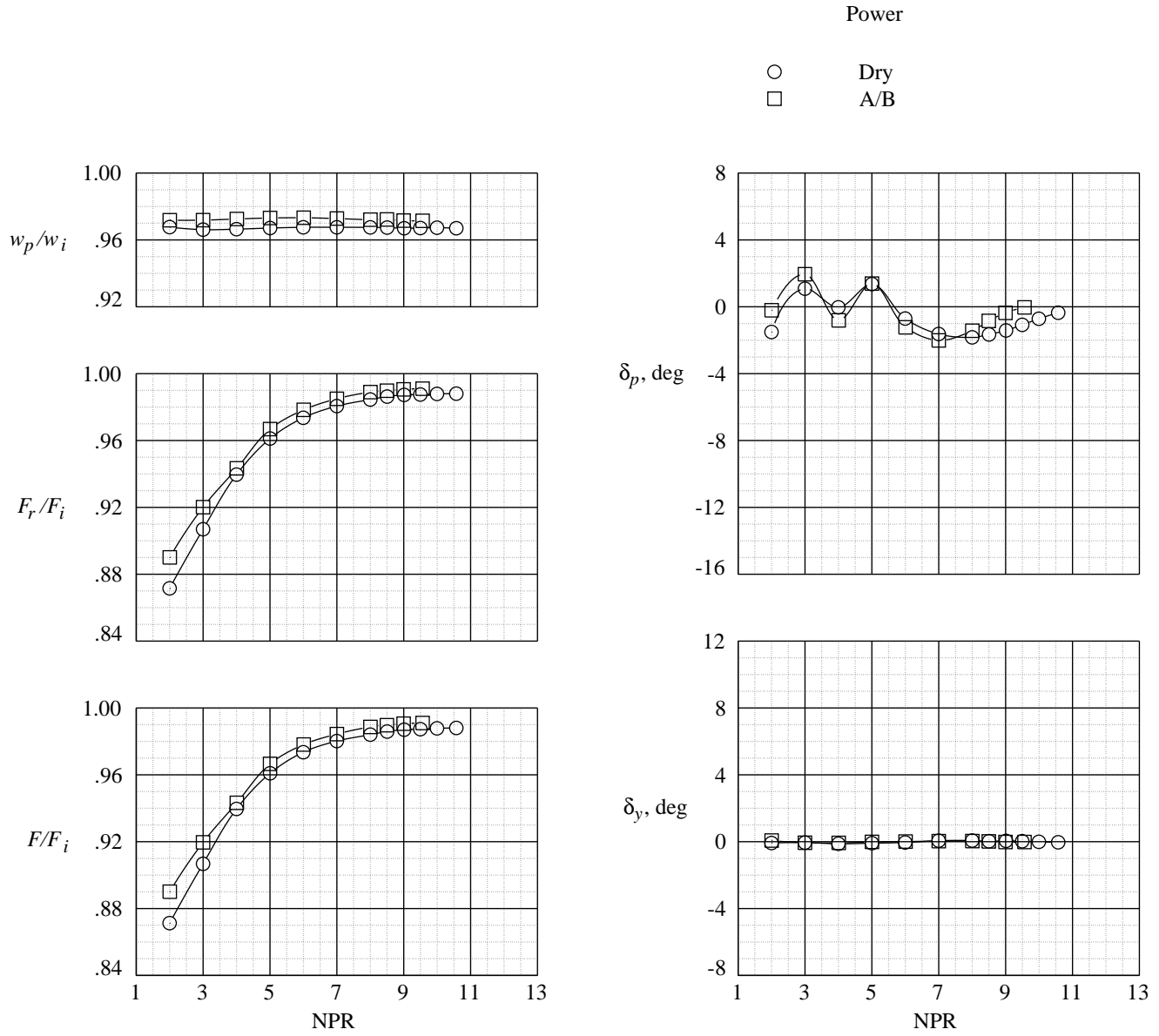
(b) A/B power.

Figure 13. Concluded.



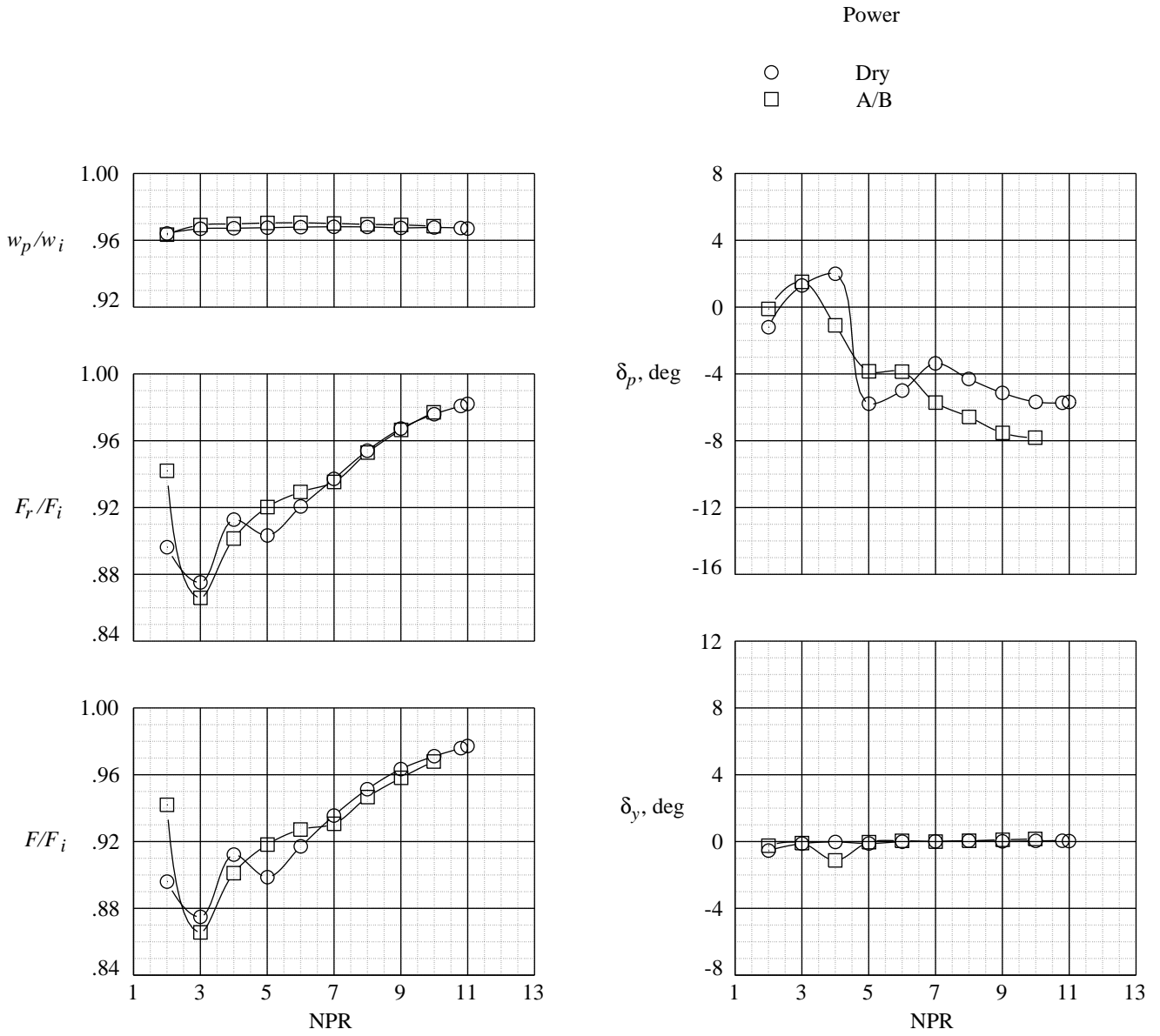
(a) $A_e/A_t = 1.100$; $(\text{NPR})_d = 3.060$.

Figure 14. Effect of power setting on internal performance characteristics of baseline configurations.



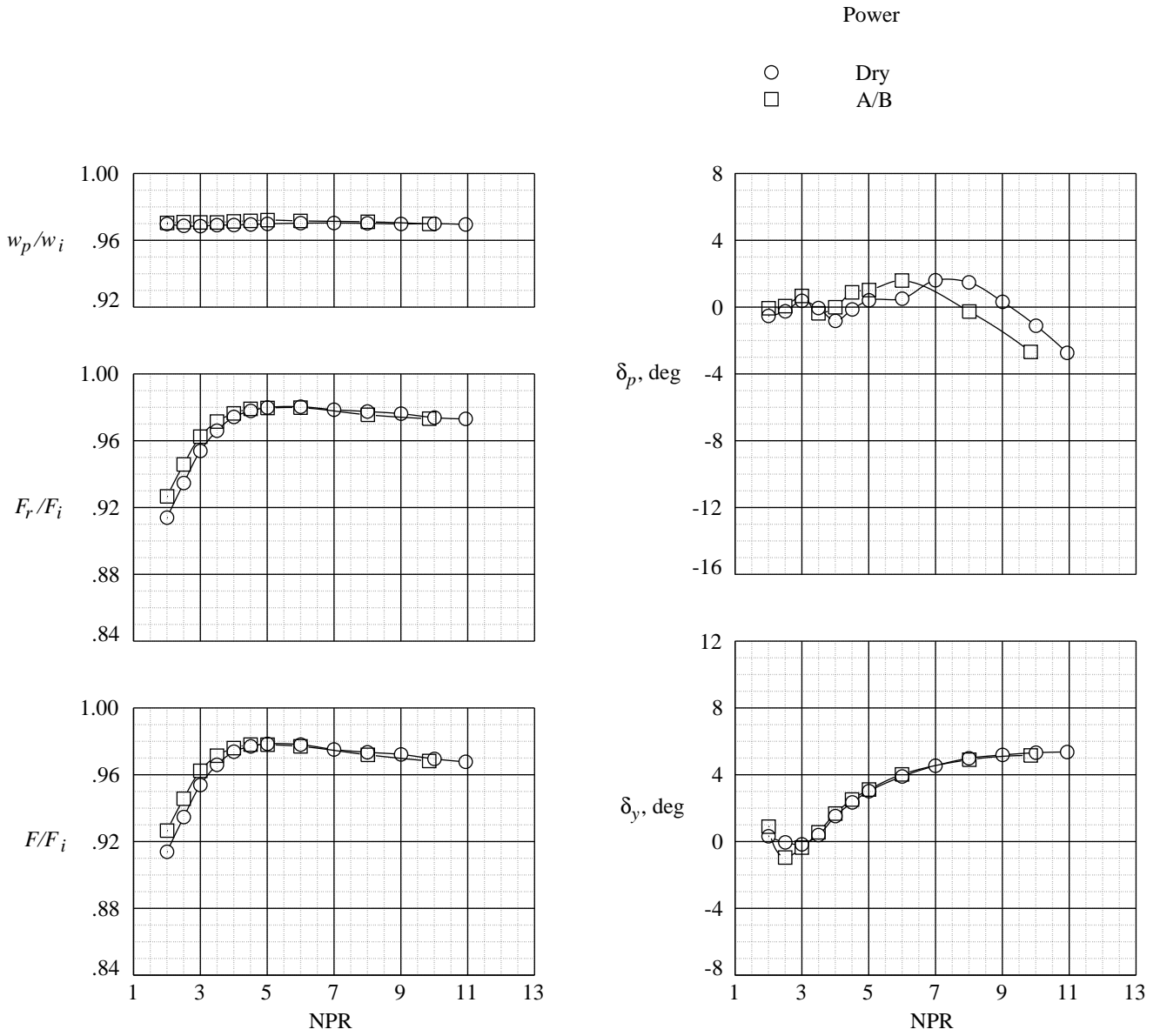
(b) $A_e/A_t = 1.750$; $(\text{NPR})_d = 8.371$.

Figure 14. Continued.



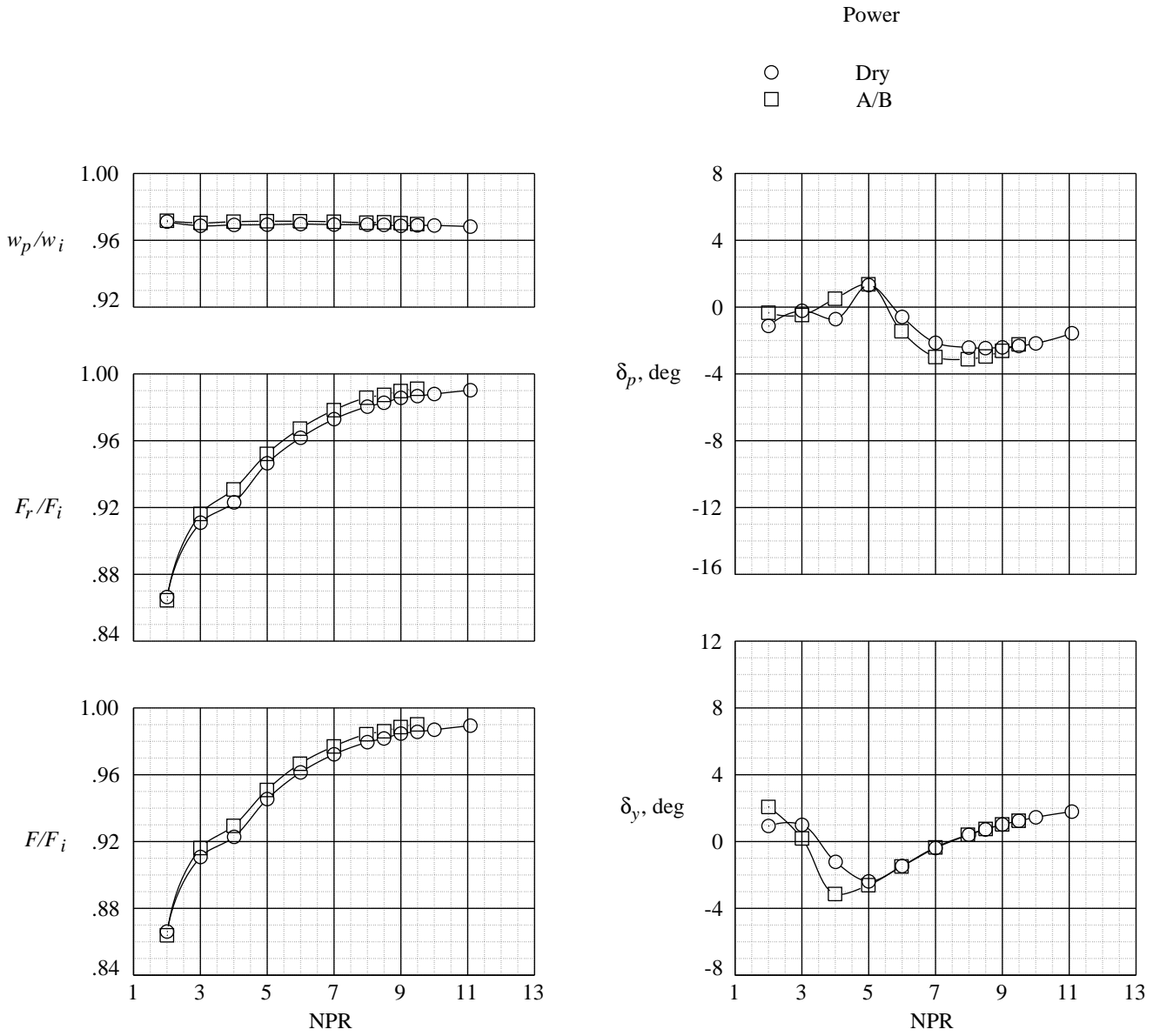
(c) $A_e/A_t = 2.500$; $(NPR)_d = 15.647$.

Figure 14. Concluded.



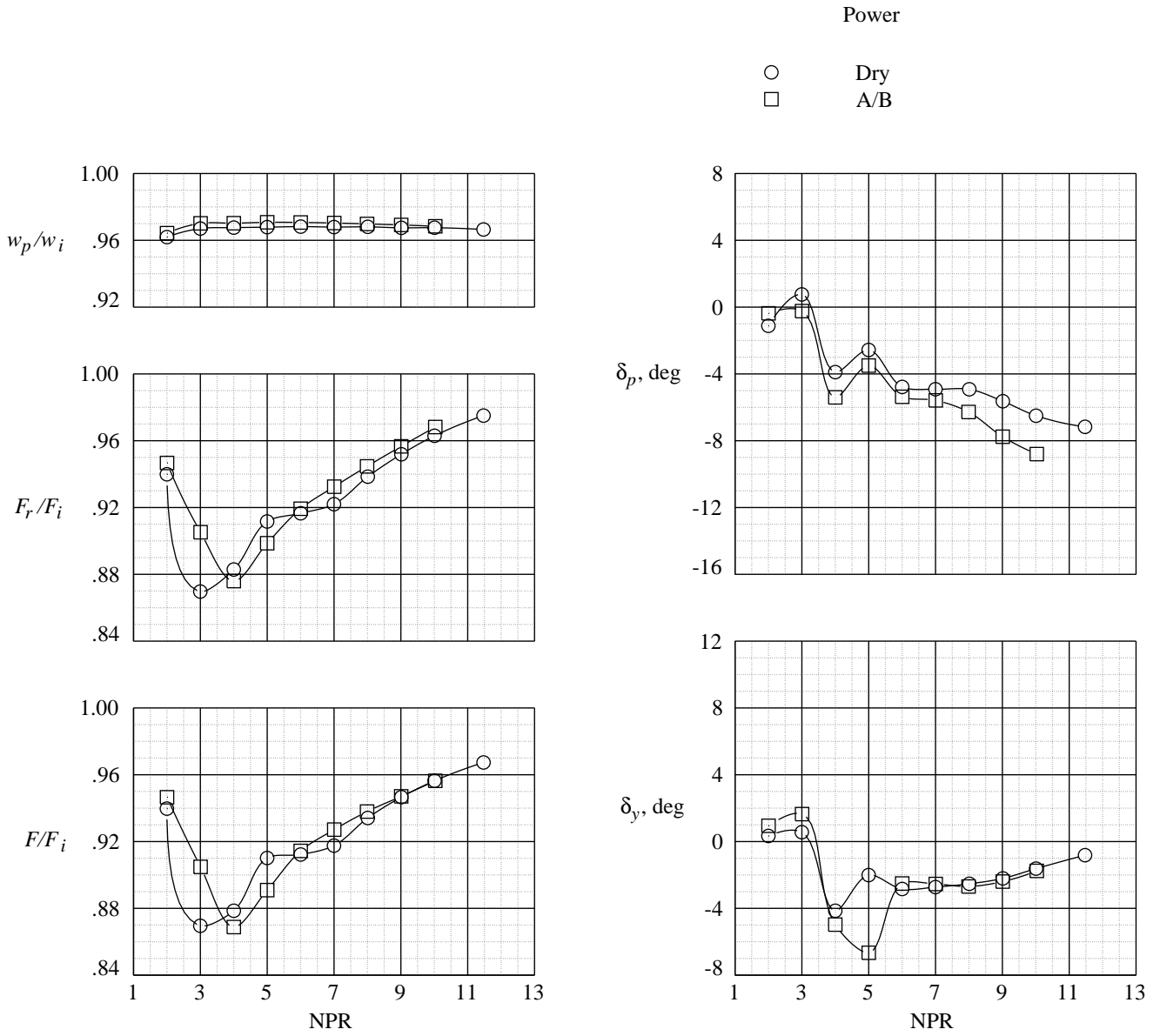
(a) $A_e/A_t = 1.100$; $(NPR)_d = 3.060$.

Figure 15. Effect of power setting on internal performance characteristics of scarfed configurations.



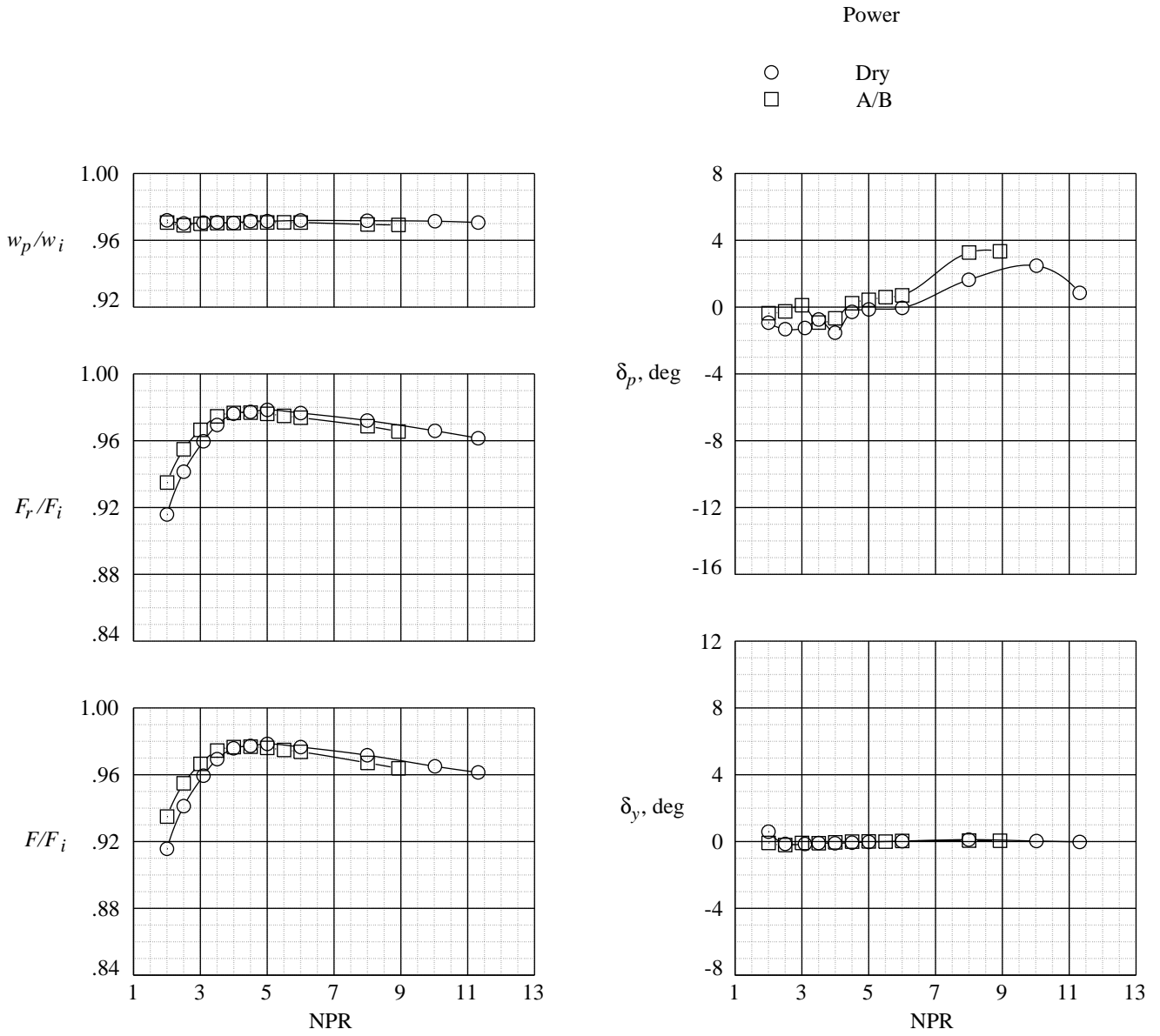
(b) $A_e/A_t = 1.750$; $(\text{NPR})_d = 8.371$.

Figure 15. Continued.



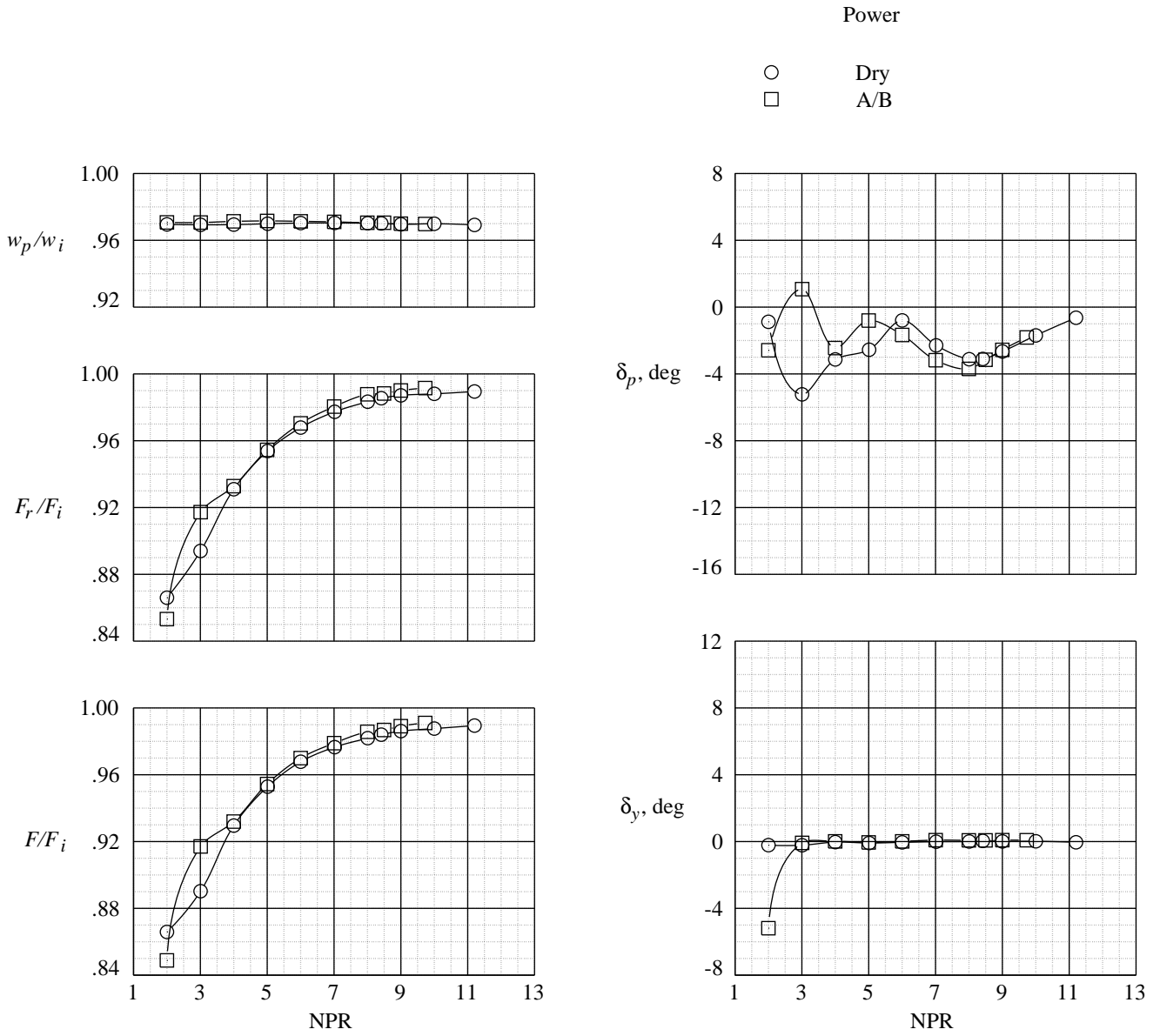
(c) $A_e/A_t = 2.500$; $(\text{NPR})_d = 15.647$.

Figure 15. Concluded.



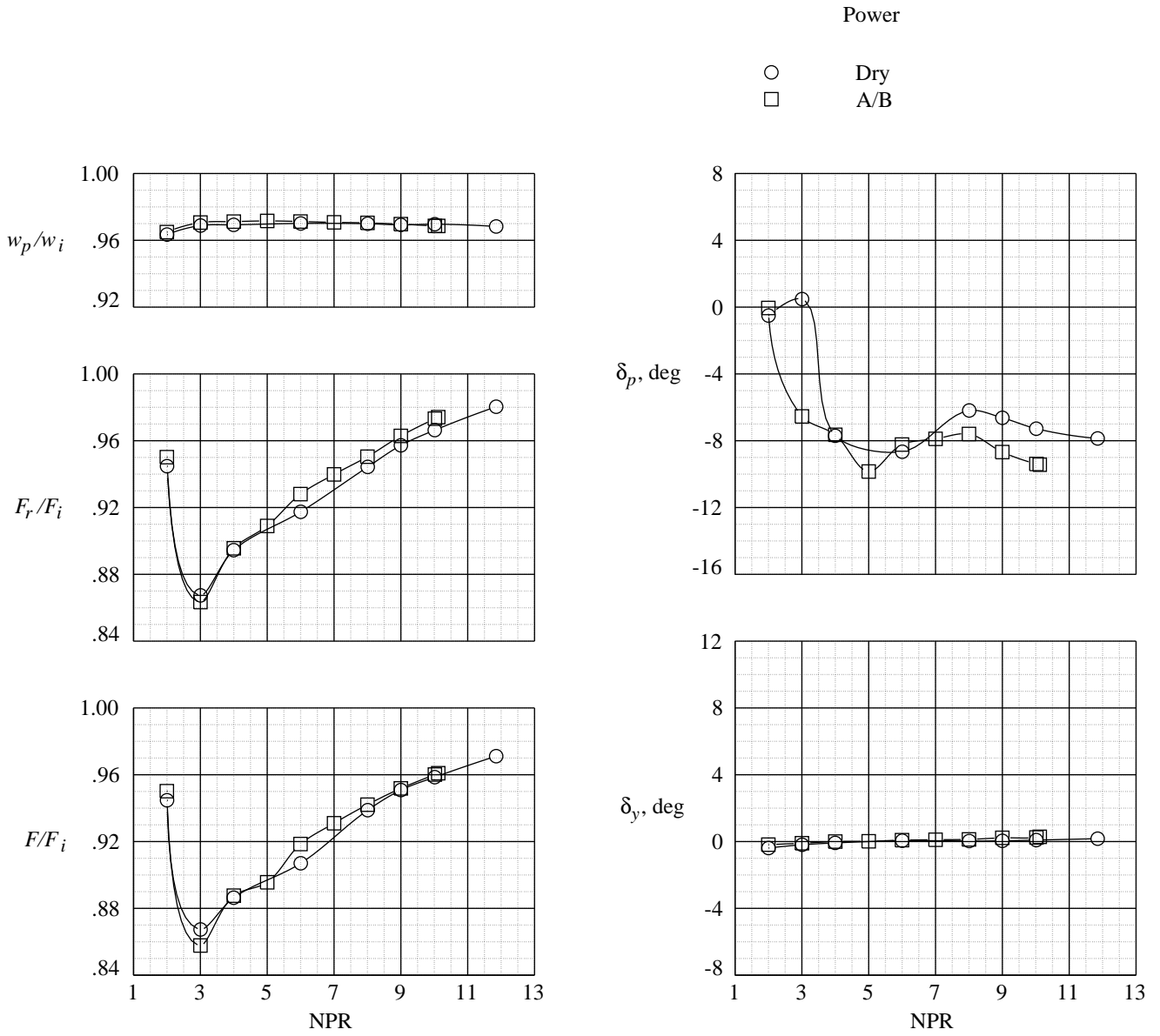
(a) $A_e/A_t = 1.100$; $(\text{NPR})_d = 3.060$.

Figure 16. Effect of power setting on internal performance characteristics of sawtooth configurations.



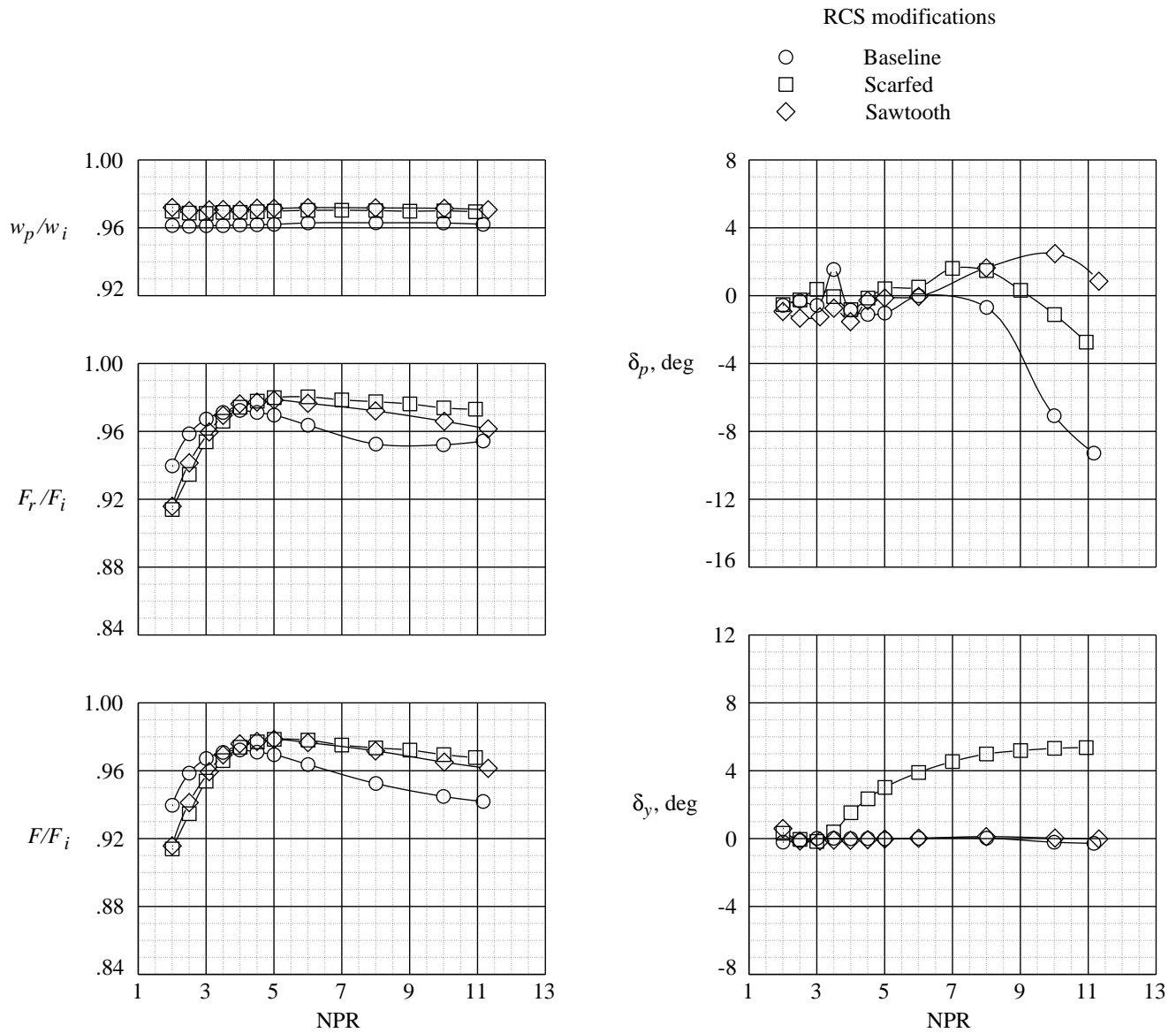
(b) $A_e/A_t = 1.750$; $(NPR)_d = 8.371$.

Figure 16. Continued.



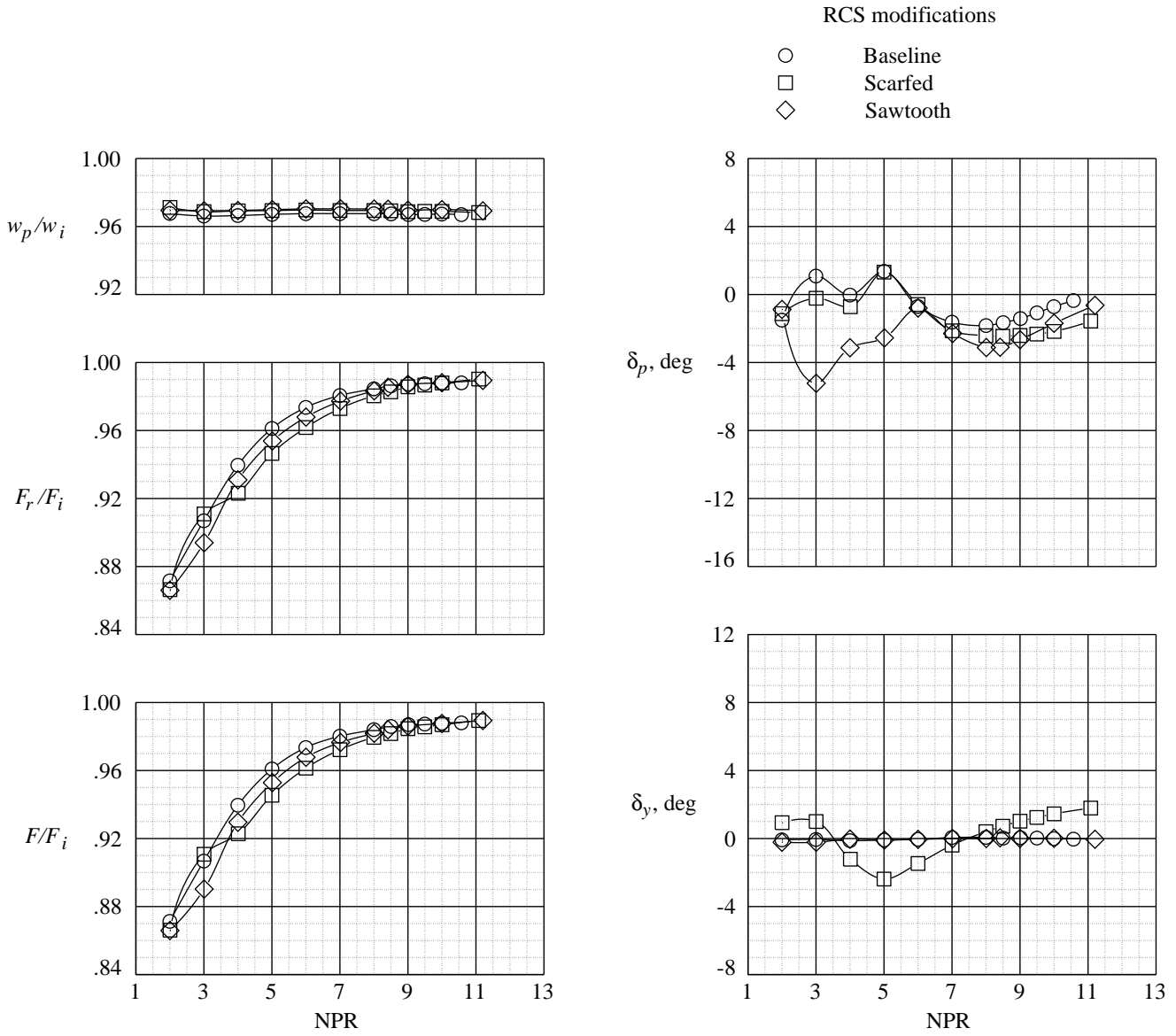
(c) $A_e/A_t = 2.500$; $(NPR)_d = 15.647$.

Figure 16. Concluded.



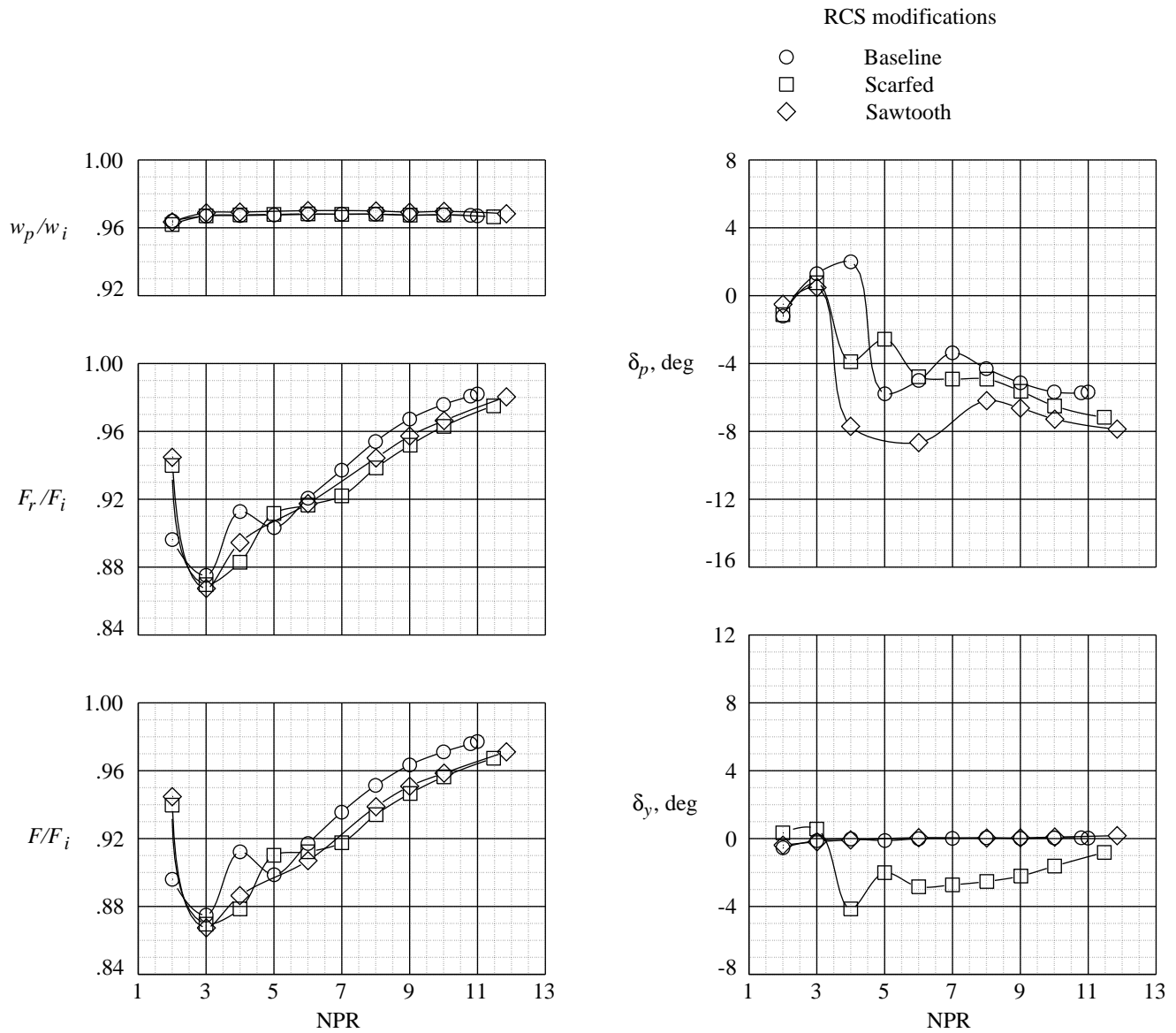
(a) $A_e/A_t = 1.100$; $(\text{NPR})_d = 3.060$.

Figure 17. Effect of RCS modifications on internal performance characteristics of dry power configurations.



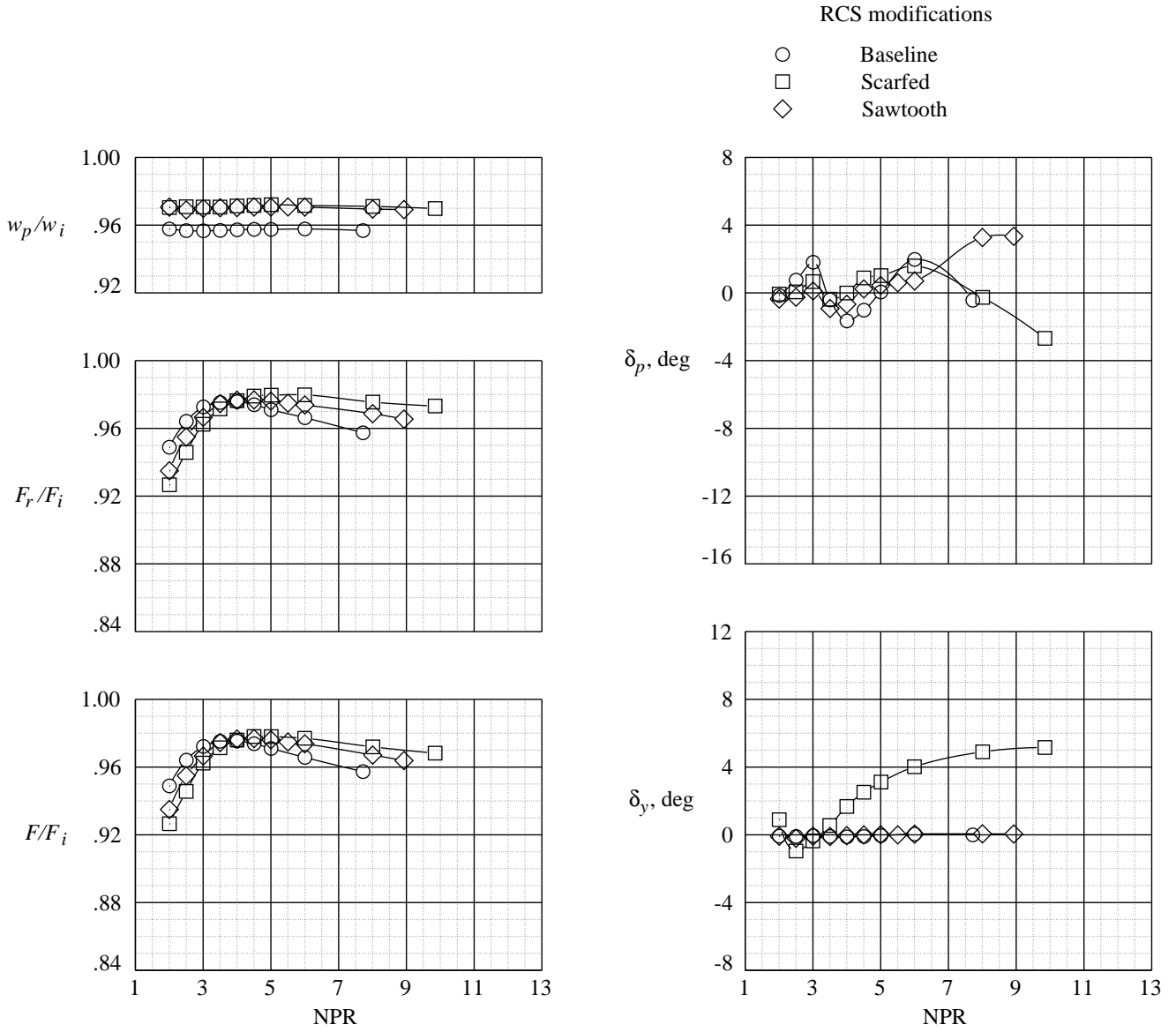
(b) $A_e/A_t = 1.750$; $(\text{NPR})_d = 8.371$.

Figure 17. Continued.



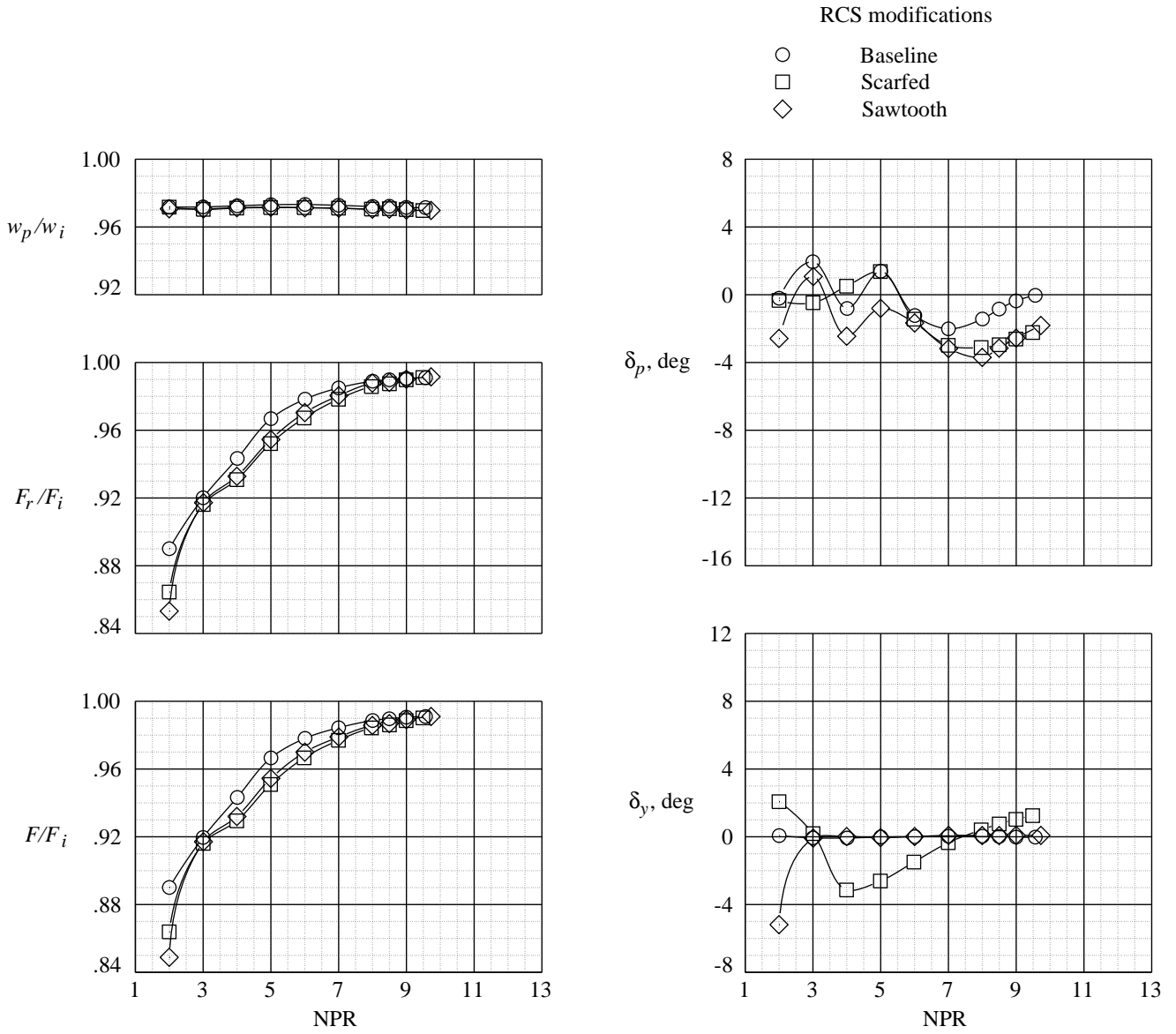
(c) $A_e/A_t = 2.500$; $(\text{NPR})_d = 15.647$.

Figure 17. Concluded.



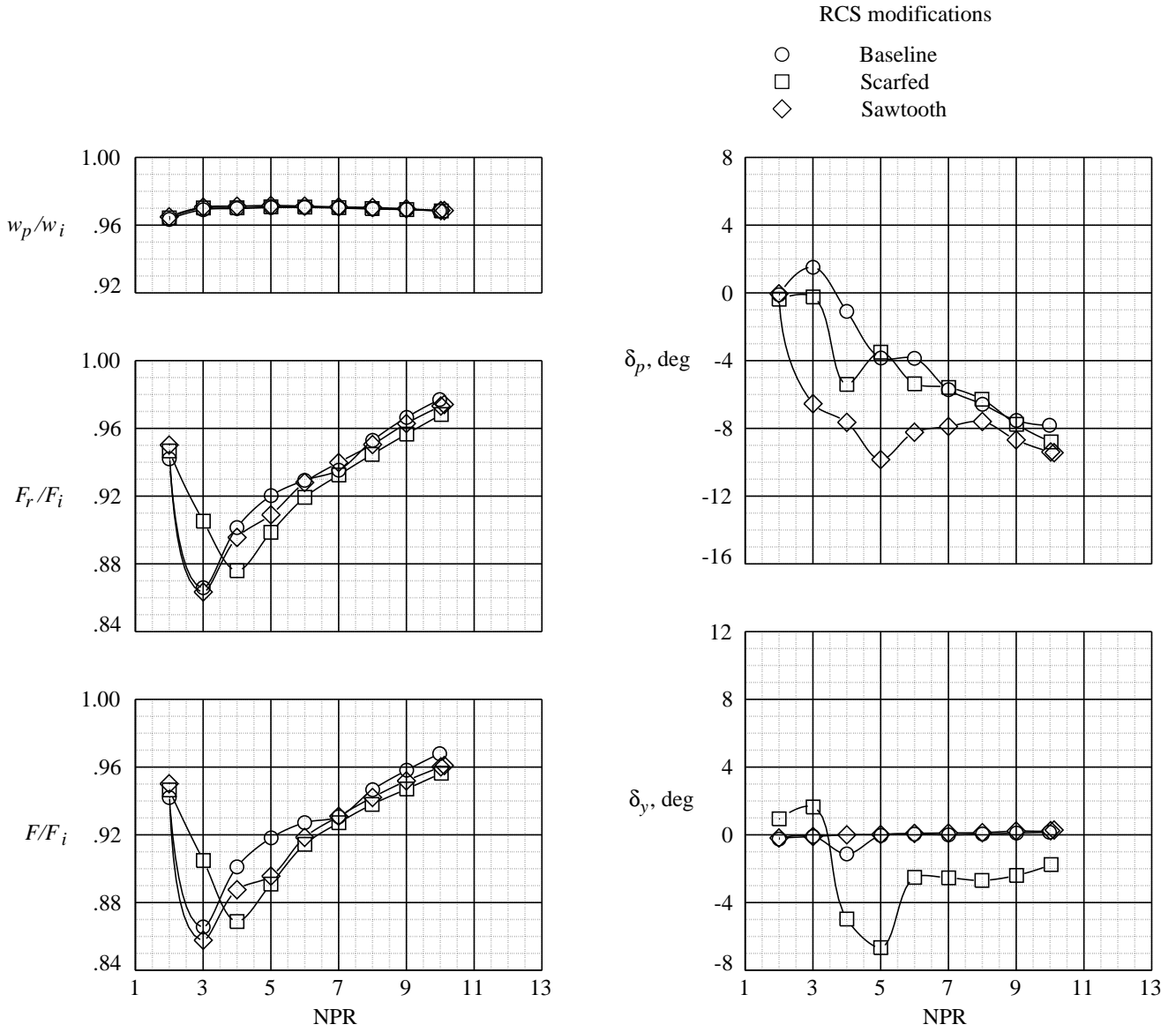
(a) $A_e/A_t = 1.100$; $(NPR)_d = 3.060$.

Figure 18. Effect of RCS modifications on internal performance characteristics of A/B power configurations.



(b) $A_e/A_t = 1.750$; $(NPR)_d = 8.371$.

Figure 18. Continued.



(c) $A_e/A_t = 2.500$; $(NPR)_d = 15.647$.

Figure 18. Concluded.



(a) Baseline configuration 1; NPR \approx 3.00.

Figure 19. Shelf surface oil flow visualization for dry power configurations. $A_e/A_t = 1.100$.



(b) Scarfed configuration 7; $\text{NPR} \approx 5.00$.

Figure 19. Continued.



(c) Sawtooth configuration 13; NPR \approx 5.00.

Figure 19. Concluded.

REPORT DOCUMENTATION PAGE

Form Approved
OMB No. 0704-0188

Public reporting burden for this collection of information is estimated to average 1 hour per response, including the time for reviewing instructions, searching existing data sources, gathering and maintaining the data needed, and completing and reviewing the collection of information. Send comments regarding this burden estimate or any other aspect of this collection of information, including suggestions for reducing this burden, to Washington Headquarters Services, Directorate for Information Operations and Reports, 1215 Jefferson Davis Highway, Suite 1204, Arlington, VA 22202-4302, and to the Office of Management and Budget, Paperwork Reduction Project (0704-0188), Washington, DC 20503.

1. AGENCY USE ONLY <i>(Leave blank)</i>	2. REPORT DATE September 1996	3. REPORT TYPE AND DATES COVERED Technical Memorandum	
4. TITLE AND SUBTITLE Static Internal Performance of a Two-Dimensional Convergent-Divergent Nozzle With External Shelf		5. FUNDING NUMBERS WU 505-59-70-04	
6. AUTHOR(S) Milton Lamb, John G. Taylor, and Mark C. Frassinelli			
7. PERFORMING ORGANIZATION NAME(S) AND ADDRESS(ES) NASA Langley Research Center Hampton, VA 23681-0001		8. PERFORMING ORGANIZATION REPORT NUMBER L-17478	
9. SPONSORING/MONITORING AGENCY NAME(S) AND ADDRESS(ES) National Aeronautics and Space Administration Washington, DC 20546-0001		10. SPONSORING/MONITORING AGENCY REPORT NUMBER NASA TM-4719	
11. SUPPLEMENTARY NOTES Lamb and Taylor: Langley Research Center, Hampton, VA; Frassinelli: Detailed to NASA from Air Force Wright Research and Development Center, Wright-Patterson Air Force Base, OH.			
12a. DISTRIBUTION/AVAILABILITY STATEMENT Unclassified-Unlimited Subject Category 02 Availability: NASA CASI (301) 621-0390		12b. DISTRIBUTION CODE	
13. ABSTRACT <i>(Maximum 200 words)</i> An investigation was conducted in the static test facility of the Langley 16-Foot Transonic Tunnel to determine the internal performance of a two-dimensional convergent-divergent nozzle. The nozzle design was tested with dry and afterburning throat areas, which represent different power settings and three expansion ratios. For each of these configurations, three trailing-edge geometries were tested. The baseline geometry had a straight trailing edge. Two different shaping techniques were applied to the baseline nozzle design to reduce radar observables: the scarfed design and the sawtooth design. A flat plate extended downstream of the lower divergent flap trailing edge parallel to the model centerline to form a shelflike expansion surface. This shelf was designed to shield the plume from ground observation (infrared radiation (IR) signature suppression). The shelf represents the part of the aircraft structure that might be present in an installed configuration. These configurations were tested at nozzle pressure ratios from 2.0 to 12.0.			
14. SUBJECT TERMS Two-dimensional; Convergent-divergent shelf nozzles; Static internal performance; Pressure distributions		15. NUMBER OF PAGES 106	
		16. PRICE CODE A06	
17. SECURITY CLASSIFICATION OF REPORT Unclassified	18. SECURITY CLASSIFICATION OF THIS PAGE Unclassified	19. SECURITY CLASSIFICATION OF ABSTRACT Unclassified	20. LIMITATION OF ABSTRACT